UNIVERSIDADE ESTADUAL DE CAMPINAS
Faculdade de Engenharia Elétrica e de Computação

DANILO FANTON RIBEIRO DA SILVA

HYBRID ENERGY STORAGE SYSTEM AND CONTROL STRATEGY FOR AN ELECTRIC URBAN BUS

SISTEMA DE ARMAZENAMENTO DE ENERGIA HÍBRIDO E ESTRATÉGIA DE CONTROLE PARA UM ÔNIBUS ELÉTRICO URBANO

CAMPINAS
2019

DANILO FANTON RIBEIRO DA SILVA

HYBRID ENERGY STORAGE SYSTEM AND CONTROL STRATEGY FOR AN ELECTRIC URBAN BUS

SISTEMA DE ARMAZENAMENTO DE ENERGIA HÍBRIDO E ESTRATÉGIA DE CONTROLE PARA UM ÔNIBUS ELÉTRICO URBANO

Dissertation presented to the School of Electrical and Computer Engineering of the University of Campinas in partial fulfillment of the requirements for the degree of Master, in the area of Electrical Energy.

Dissertação apresentada à Faculdade de Engenharia Elétrica e de Computação da Universidade Estadual de Campinas como parte dos requisitos exigidos para a obtenção do título de Mestre em Engenharia Elétrica, na área de Energia Elétrica.

Supervisor/*Orientador*: MARCELO GRADELLA VILLALVA

ESTE EXEMPLAR CORRESPONDE À VERSÃO FINAL DISSERTAÇÃO DEFENDIDA PELO ALUNO DANILO FANTON RIBEIRO DA SILVA, E ORIENTADA PELO PROF. DR. MARCELO GRADELLA VILLALVA

CAMPINAS
2019

Ficha catalográfica
Universidade Estadual de Campinas
Biblioteca da Área de Engenharia e Arquitetura
Rose Meire da Silva - CRB 8/5974

	Silva, Danilo Fanton Ribeiro da, 1979-
Si38h	Hybrid energy storage system and control strategy for an electric urban bus / Danilo Fanton Ribeiro da Silva. – Campinas, SP : [s.n.], 2019.
	Orientador: Marcelo Gradella Villalva.
	Dissertação (mestrado) – Universidade Estadual de Campinas, Faculdade de Engenharia Elétrica e de Computação.
	1. Veículos elétricos. 2. Eletrônica de potência. 3. Baterias. 4. Supercapacitores. 5. Conversores de energia elétrica. I. Villalva, Marcelo Gradella, 1978-. II. Universidade Estadual de Campinas. Faculdade de Engenharia Elétrica e de Computação. III. Título.

Informações para Biblioteca Digital

Título em outro idioma: Sistema de armazenamento de energia híbrida e estratégia de controle para um ônibus elétrico urbano
Palavras-chave em inglês:
Electrical vehicles
Power electronics
Batteries
Supercapacitors
Electrical energy converters
Área de concentração: Energia Elétrica
Titulação: Mestre em Engenharia Elétrica
Banca examinadora:
Marcelo Gradella Villalva [Orientador]
Jose Antenor Pomílio
Tárcio André dos Santos Barros
Data de defesa: 08-03-2019
Programa de Pós-Graduação: Engenharia Elétrica

Identificação e informações acadêmicas do(a) aluno(a)
- ORCID do autor: https://orcid.org/0000-0002-3750-7775
- Currículo Lattes do autor: http://lattes.cnpq.br/2404752753364057

COMISSÃO JULGADORA - DISSERTAÇÃO DE MESTRADO

Candidato: Danilo Fanton Ribeiro da Silva RA: 970515

Data da Defesa: 08 de março de 2019

Título da Tese: " HYBRID ENERGY STORAGE SYSTEM AND CONTROL STRATEGY FOR AN ELECTRIC URBAN BUS” (SISTEMA DE ARMAZENAMENTO DE ENERGIA HÍBRIDO E ESTRATÉGIA DE CONTROLE PARA UM ÔNIBUS ELÉTRICO URBANO).

Prof. Dr. Marcelo Gradella Villalva (Presidente)
Prof. Dr. Tárcio André dos Santos Barros
Prof. Dr. José Antenor Pomílio

A ata de defesa, com as respectivas assinaturas dos membros da Comissão Julgadora, encontra-se no SIGA (Sistema de Fluxo de Dissertação/Tese) e na Secretaria de Pós-Graduação da Faculdade de Engenharia Elétrica e de Computação.

To my wife Tatiana and my son Gustavo.
To my parents João and Joanina.
To my brother Hugo.

ACKNOWLEDGMENTS

I would like to thank professor Marcelo Gradella Villalva, who made possible my return to university, offering his support, knowledge and the laboratory for my work.

I am also thankful to professor José Antenor Pomilio, who guided me in several issues and doubts to reach this accomplishment.

To Bosch and specially to my past managers, Erwin Franieck and Marcos Araújo, who supported and allowed me to work on this study even when it was necessary to leave the office earlier or arrive later, due to classes taken in the university.

I am most grateful to my wife, my love, Tatiana, who encouraged me to go for this master, who supported me and had patience to let me work over the weekends, who pushed me when I was lazy and comforted me when I was stressed.

To my son, who was born almost when this project started and was patient with my absence, allowing me to work and giving me all his love when I was back to him.

ABSTRACT

This master thesis describes the use of a hybrid energy storage system (HESS) composed of battery and an electrochemical capacitor[1] (EC) as energy sources and a multi-input bi-directional interleaved DC-DC converter to provide energy to an electric urban bus. Using a control strategy with different cutoff frequencies, when each power source is going to provide the energy required by the engine, it is possible to use the EC for rapid changes on the load demands, while the battery is used as a constant source.

The Manhattan cycle from SAE J2711 was used as a standard cycle in order to define a speed profile, which was used to create an engine load profile that was used to simulate the HESS. From this load profile it was possible to determine the current load. In the simulation a current source is used as load, instead of an electric engine and its inverter, because the target was to study the DC-DC converter. After defining the current load, the power consumption was determined and the battery and EC dimensioning was determined. It was then defined the switching frequency and a thermal analysis was calculated in order to evaluate the transistor application. The defined switching frequency was 20kHz and it was possible to determine the amount of transistors required to support the load demand working accordingly.

The FFT analysis of the power consumption was done and the cutoff frequency of the range where the battery should work as almost a constant energy source was determined.

A bi-directional Boost DC-DC converter was modelled with state space equations. The converter controllers were designed from the Bode plots obtained from the state space equations. A switched simulation model of the converter and controllers was implemented with the PSIM software. In a first moment, a simple two transistor bi-directional boost DC-DC converter was simulated, which allowed to observe that the amount of current drawn in one single transistor was too high. Then a three-phase interleaved DC-DC converter was applied for the battery and for the EC, reducing the current demand for each transistor.

It was possible to observe the function of the interleaved strategy to reduce current ripple and the HESS was able to manage the best of each power source, allowing the EC to quickly react to load variations and the battery would work as a main energy source, but running with low variation, assuring the best compromise for lifetime and driving range.

[1] Electrochemical capacitor (EC), supercapacitor (SC) and ultracapacitor (UC) are synonyms. In this work it is used EC as a generic name, which is going to be better explained in section 2.3.

RESUMO

Esta tese de mestrado descreve o uso de um sistema híbrido de energia (HESS), composto de um banco de baterias e de capacitores eletroquímico[2] (EC) como principais fontes de energia e um conversor DC-DC bidirecional entrelaçado de múltiplas entradas para fornecer energia a um ônibus elétrico urbano. Com uma estratégia de controle que divide em frequências de corte diferentes, quando cada fonte de energia irá atuar de acordo com a demanda da carga do motor, é possível utilizar o EC para rápidas variações na demanda da carga, enquanto a bateria é usada como uma fonte de potência média.

Foi utilizado um ciclo de perfil de velocidade padrão da norma SAE J2711, o ciclo Manhattan, que foi utilizado para definir o perfil de carga a ser utilizado para a simulação do HESS. Com o perfil de carga, foi possível determinar a corrente de carga. Na simulação, foi definido utilizar como carga uma fonte de corrente, ao invés de um motor elétrico e seu inversor, porque o objetivo é o estudo do conversor DC-DC. Após a definição da corrente da carga, determinou-se o consumo de potência e o dimensionamento da bateria e do EC foi realizado. Então a frequência de chaveamento foi determinada e o cálculo térmico dos transistores foi feito para assegurar sua possibilidade de aplicação. A frequência de chaveamento definida foi de 20kHz e com isso foi possível de se definir a quantidade de transistores necessária para se trabalhar adequadamente.

A análise FFT da potência de consumo foi realizada e a frequência de corte abaixo da qual a bateria deveria atuar como praticamente uma fonte de potência constante foi determinada.

O conversor DC-DC bidirecional elevador de tensão foi modelado, as equações de estado foram determinadas, os gráficos de Bode analisados e os controladores para o conversor foram definidos. O circuito foi implementado no software de simulação PSIM. Em um primeiro momento foi simulado o conversor DC-DC bidirecional com o sistema simples de dois transistores e foi observado que a corrente era muito alta. Então sistemas entrelaçados de três fases foram implementados para a bateria e para o EC, reduzindo o esforço de corrente para cada transistor.

Foi possível observar a função da estratégia de entrelaçamento para reduzir a flutuação de corrente e o HESS foi capaz de gerenciar quando cada fonte atuar, de modo a deixar o EC reagir rapidamente às variações de demanda e a bateria a trabalhar como a fonte principal de energia, mas rodando com baixa variação, assegurando o melhor compromisso em vida útil e autonomia veicular.

[2] Capacitor eletroquímico (EC), supercapacitor (SC) e ultracapacitor (UC) são sinônimos. Neste trabalho será utilizado a palavra EC por ser o nome genérico, que será melhor explicado na seção 2.3.

LIST OF FIGURES

LIST OF TABLES

ABBREVIATION’S LIST

AC – alternate current
AEC – asymmetric electrochemical capacitor
CCM – Continuous conduction mode
DC – direct current
DCM – discontinuous conduction mode
EC – electrochemical capacitor
EDR – equivalent distributed resistance
ESR – equivalent series resistor
ESRL – equivalent series resistor for inductor
ESRC – equivalent series resistor for capacitor
EV – electric vehicle
FC – fuel cell
FFT – fast Fourier transform
HESS – hybrid energy storage system
SC – Supercapacitor
SEC – symmetric electrochemical capacitor
SOC – state of charge
UC – Ultracapacitor

SYMBOL'S LIST

A – metallic material
a – constant
AB – reaction product of A and B
A_f – front area
B – metallic material
b – constant
bm – bus distance to the ground
C – capacitor / capacitance
C_o – output capacitor
C_d – aerodynamic drag coefficient
C_{EC} – electrochemical capacitor capacitance
C_f – fast term capacitance
C_{in} – capacitive filter
C_i – capacitive filter capacitance
C_m – medium-term capacitance
cm – bus length
C_s – long-term capacitance
d – duty cycle
e^- – negatively charged electrons
E – energy
Energy – energy contained in an electrochemical system
E_{ON} – energy loss at transistor switching ON time
E_{OFF} – energy loss at transistor switching OFF time
f – switching frequency
f_z – zero frequency
f_p – pole frequency
g – gravity
$G_{ci\text{-}uc}$ – plant model controller
$G_{c\text{-}vo}$ – output voltage controller
$G_{c\text{-}vuc}$ – electrochemical capacitor voltage controller
$G_{i\text{-}uc}$ – plant model
hm – bus height
i – current density
i_{Ci} – capacitive filter current
I_D – drain current
i_e – electronic current
i_i – internal current
I_i – input current
$I_{i\text{-}bt}$ – battery current
I_L – inductor current
i_L – inductor current
I_o – output current

i_{out} – output current
K – battery capacity
k – controller gain
L – inductor
life – battery lifetime
lm – bus width
L_{min} – minimal inductance
M_v – vehicle mass
P – power
P_{max} – the maximum instantaneous power
P_{ON} – power conduction losses
$P_{t\text{-}ON}$ – power loss at switching ON time
$P_{t\text{-}OFF}$ – power loss at switching OFF time
P_{TOTAL} – total power loss at transistor
Q – available amount of active material in coulombs
q – charge capacity
R_{bat} – battery internal resistance
R_{Ci} – capacitive filter internal resistance
R_e – electronic resistance
R_f – fast term resistance
R_i – internal resistance
R_L – inductor internal resistance
R_m – medium-term resistance
rm – bus front and rear radius
rmm – bus lateral radius
R_s – long-term resistance
S – the accessible capacitor surface
sm – bus tire thickness
t – time
T – controller time constant
T_j – junction temperature
T_a – environmental temperature
V – potential difference
v – instant speed
V_a, V_b – voltage range from a capacitor
V_{appl} – applied voltage
V_{bat} – battery voltage
v_{co} – output capacitor voltage
v_{ci} – capacitive filter voltage
V_{DS} – voltage between drain and source
V_i – input voltage
V_o – output voltage
V_{out} – externally measurable cell voltage
V_{peak} – voltage peak

V_s – no-load voltage
V_{th} – Thevenin voltage
V_{uc} – electrochemical capacitor voltage
W – the energy stored within an electrochemical capacitor
x – effective thickness of the double layer
α, β = empirical constants
δ – duty cycle
ε_r – dielectric constant of the electrolyte
ε_0 – the dielectric constant of the vacuum
γ – polarization coefficient
ρ – air density
τ – period

TABLE OF CONTENTS

1 Introduction

Pollution problems and their consequences, especially the global warming effect, have become one of the major concerns around the globe due to possible catastrophic results for future generations. Due to this fact, governments are creating stricter environmental regulations in relation to vehicle emissions. Car makers, therefore, are developing solutions to meet those new regulations.

The automotive industry is investing in electric vehicles (EV) in order to meet the emission regulations. Most of current EVs are powered by batteries, but the limited driving range, battery lifetime and maintenance costs have been the barrier to increase their popularity until the present day.

Another power source option is the use of fuel cells (FC), producing electrical energy directly by the use of hydrogen as fuel. Although FC systems exhibit good power capability during steady-state operation, the dynamic response of FCs during transient and instantaneous peak power demands is relatively slow. On the other hand, batteries release the storage energy when requested. Their response time is better than FC, but such demand reduces the battery lifetime.

According to acceleration and breaking behavior from vehicle/driver the load requirement changes rapidly. These demands require that the energy source should be able to respond to fast changing loads. Fuel cells do not have the capacity to respond to fast changing loads with response time of 10's of second (mainly because of its auxiliaries) [1] and batteries are not going to work for long periods when working in such conditions. Thus, there is a need for secondary energy storage which can respond to the increased load instantly.

To improve the performance of the EV system during transient and instantaneous peak power demands in electric vehicle application, the FC or battery system is always associated with hybrid electrical storage system (HESS).

Hybrid electrical storage systems have the advantages of compensating the low dynamics of the FC, absorbing the braking energy into the system, compensating the power difference between main energy source and system load, reducing weight and volume of the electrical system. They usually consist of one or more energy sources (FC and/or battery) as well as one or more power sources (battery and/or electrochemical capacitor[3]) which are able to deliver or absorb the energy of the electrical system.

The use of electrochemical capacitors (ECs) [1] as a storage system in DC hybrid sources, with FC and/or batteries, is a good option due to several advantages like high power density, long lifecycle and very good charge/discharge efficiency [2].

The objective of this work is to develop a HESS and its control for an urban electric bus. This HESS consists of a battery pack, as the energy source; the EC, as the power source and a multi-input bi-directional interleaved DC-DC converter to manage the required power for the bus powertrain. A high-power DC-DC converter is a key element that interfaces the HESS with the DC bus in the powertrain of the EVs. Thus, the design of high-power DC-DC converter and its controller play an important role to manage the power regulation and they are the main purpose of this work.

[3] Electrochemical capacitor (EC), supercapacitor (SC) and ultracapacitor (UC) are synonyms. In this work it is used EC as a generic name, which is going to be better explained in section 2.3.

For the HESS development, firstly it is necessary to determine the vehicle power demand, based on a speed profile, its mass and basic dimensions. Once the vehicle power demand is defined, it is possible to calculate the electric engine required power as well as the power sources dimensioning, in this work is the dimensioning of the battery and the electrochemical capacitor. After that, with the definition of the DC-DC converter to be used, it is possible to understand the current draw demanded by the transistors thus define the switching frequency and perform a thermal analysis for the basic circuit. With the thermal analysis available, it is possible to evaluate if the maximal junction temperature at the transistor is acceptable or if the circuit shall be revised in regards to the topology of transistors (parallel transistor, or interleaved topology) or even the switching frequency could be reduced. Once the thermal analysis is acceptable, the next step is the circuit calculation for the controller's definition. The diagram in Figure 1 shows this development process.

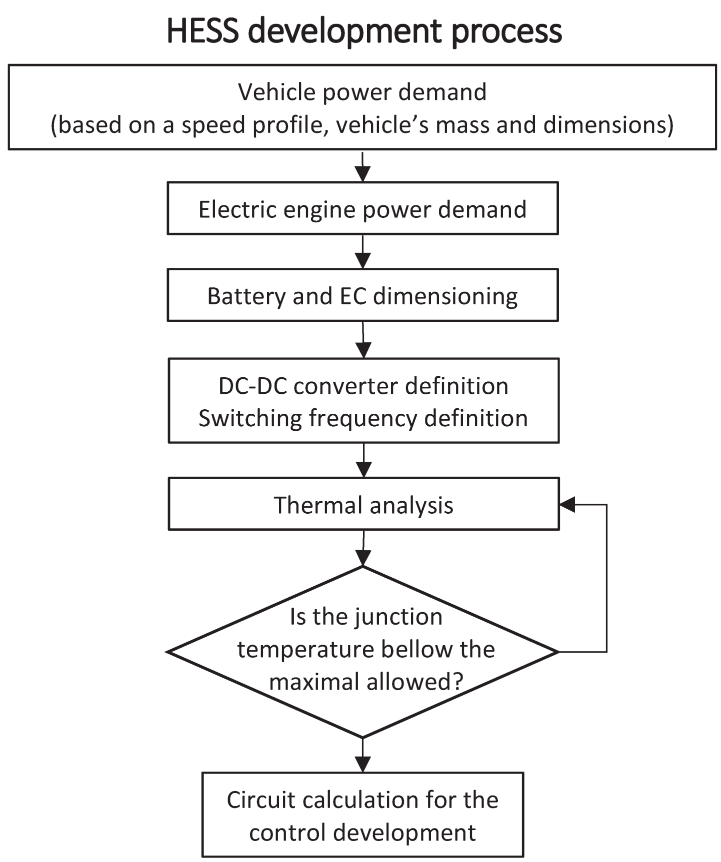

Figure 1 – HESS development process

In order to get the most efficiency from the different power sources, as described in [3], [4], the control strategy shall define a way that the battery works almost as a constant power source, while the EC provides the power variations. For this control strategy the vehicle power demand is analyzed in frequency domain and a cutoff frequency is defined, which is the boundary about when the battery or EC shall actuate.

This work is divided in five sections, the first one is the introduction, then in chapter 0 presents the basic HESS topologies, the chosen circuit to use, a brief analysis about the battery and the EC and their circuit models and then the explanation about the control strategy used. After that, in chapter 3, the whole dimensioning is done: the vehicle and the electrical engine power demand, battery and EC dimensioning, the thermal analysis is done, the inductors and capacitors are determined; then, the circuit is calculated and the transfer functions created and the controls determined. In chapter 4 the simulation results are presented, showing the model validation, and the circuit results based on the speed profile. Lastly, in chapter 5, the conclusions about this work and the future studies are shown.

2 Circuit topology and control strategy

2.1 Electrical circuit

In order to create an electric powertrain vehicle, with the limitations that either batteries and ECs have, hybrid energy storage systems (HESS) have been proposed [5]. The basic idea of a HESS is to combine electrochemical capacitors and batteries to achieve a better overall performance.

Several configurations for HESS have been proposed, which range from simple to complex circuits. Based on the use of power electronic converters in the configurations, HESS can be classified into two types: passive or active. Conventional active methods use one or multiple full-size DC-DC converters to interface the energy storage device to the DC link. In this case, full size refers to the fact that the DC-DC converter forms the sole path for the flow of energy in the device.

In the most widely used conventional HESS designs, the battery pack is directly connected to the DC link while a half-bridge converter is placed between the EC bank and the DC link. However, in order to utilize the power density advantage of the EC, the half-bridge converter must match the power level of the EC. In most cases, the half-bridge converter is a significant portion of the cost. Although this design solves the problem of the peak power demands, the battery still suffers from frequent charge and discharge operations.

2.1.1 Basic Passive Parallel

Passive paralleling is the simplest method of combining battery and EC bank together because the two energy sources are hybridized without any power electronic converters/inverters. Figure 2 shows the basic topology of the passive parallel method. In this method, since the two sources are always paralleled, $V_{Batt} = V_{EC} = V_{DC}$. The EC essentially acts as a low-pass filter.

Advantages of this method include ease of implementation and no requirements for control or expensive power electronic converters, thus the cost is low. The major problem with this topology is that it cannot effectively utilize the EC stored energy. The terminal voltages of the two power sources are forced to be equal, and the lack of flexibility because the actual output power of battery and EC is only decided by the own characteristics of the two power sources [5].

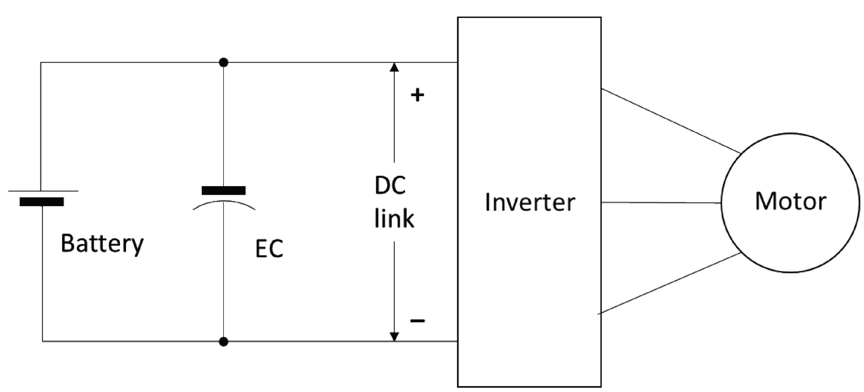

Figure 2 – Basic passive parallel hybrid configuration [5]

2.1.2 EC/Battery Configuration

The EC/battery configuration is the most studied and researched HESS. Figure 3 shows the diagram of the HESS configuration. By using a bidirectional DC-DC converter to interface the EC, the voltage of EC can be used in a wide range. However, the bidirectional converter needs to be of a larger size in order to handle the power of the EC (higher costs). In addition, the nominal voltage of the EC bank can be lower. The battery is connected directly to the DC link; as a result, the DC-link voltage cannot be varied.

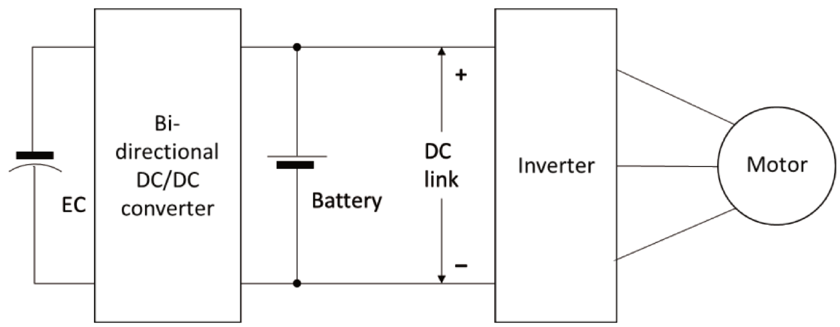

Figure 3 – EC/baterry configuration [5]

2.1.3 Battery/EC Configuration

By swapping the positions of the battery and EC in the EC/battery configuration, we get the battery/EC configuration as shown in Figure 4. In this configuration, the voltage of the battery can be maintained lower or higher than the EC voltage. The EC is connected to the DC link directly working as a low-pass filter. The control strategy applied to this topology allows the DC-link voltage to vary within a range so that the EC energy can be more effectively used.

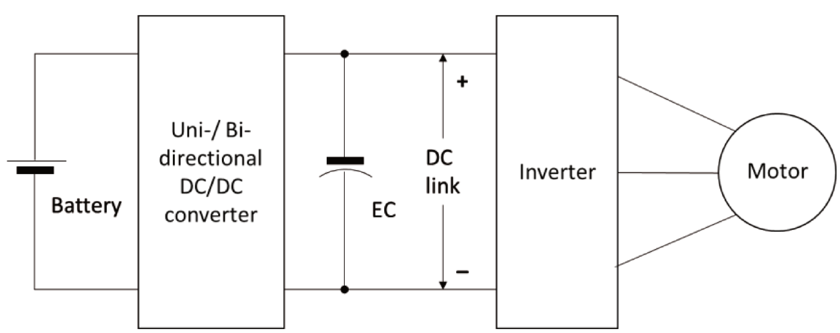

Figure 4 – Battery/EC configuration [5]

2.1.4 Cascaded Configuration

To make a better working range of the EC of the battery/EC configuration, another bidirectional DC-DC converter was added between the EC bank and the DC link. This forms a cascaded converter topology as can be seen in Figure 5.

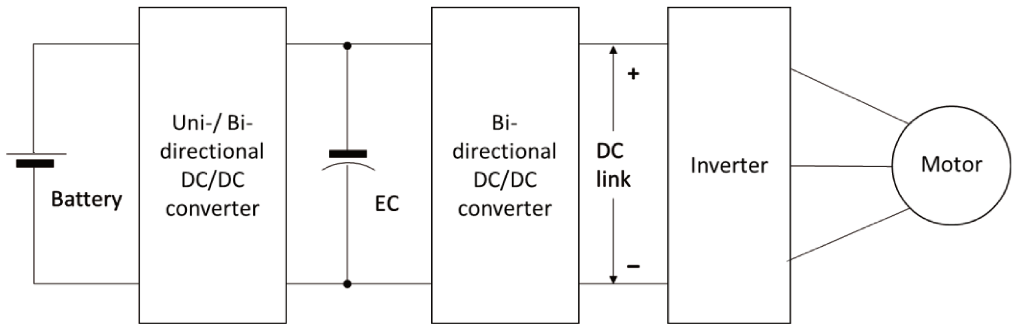

Figure 5 – Cascaded configuration [5]

2.1.5 Multiple Converter Configuration

Instead of cascaded connection of the two converters, the multiple converter method parallels the output of the two converters. Figure 6 shows the diagram of the multiple converter topology. The outputs of the two converters are the same as the DC-link voltage. Voltages of both the battery and the EC can be maintained lower than the DC-link voltage, less balancing problem so as incurred. The voltage of the EC can vary in a wide range so the capacitor is fully used. The disadvantage of this method is that two full-size converters are necessary.

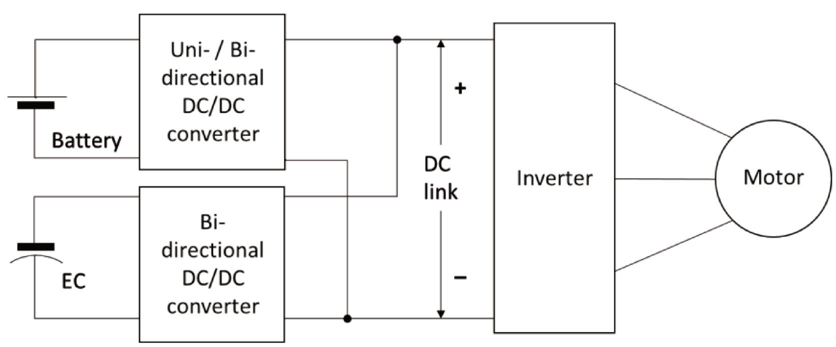

Figure 6 – Multiple converter configuration [5]

2.1.6 Multiple Input Converter Configuration

The cost of multiple converter configuration is expensive because it requires two full-size bidirectional converters to interface both battery and EC. Multiple input converter topologies are proposed in order to reduce the cost of the overall system. The system diagram of the multiple input converters method is shown in Figure 7.

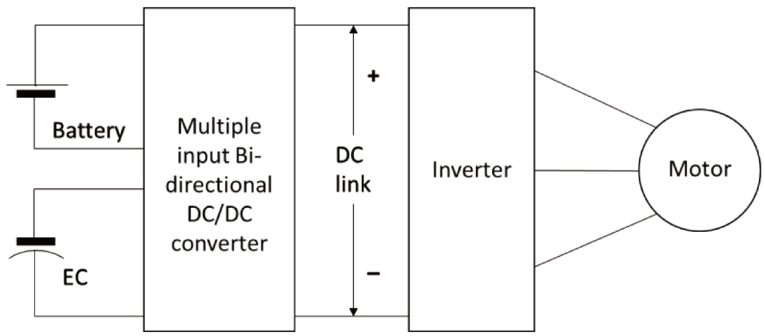

Figure 7 – Multiple input converter configuration [5]

In this work, the configuration of multiple converter configuration, as described in 2.1.5 was applied using the maximal of each power source and full bi-directional converters.

2.1.7 Bi-directional step-up DC-DC converter

A standard step-up converter can be observed in Figure 8.

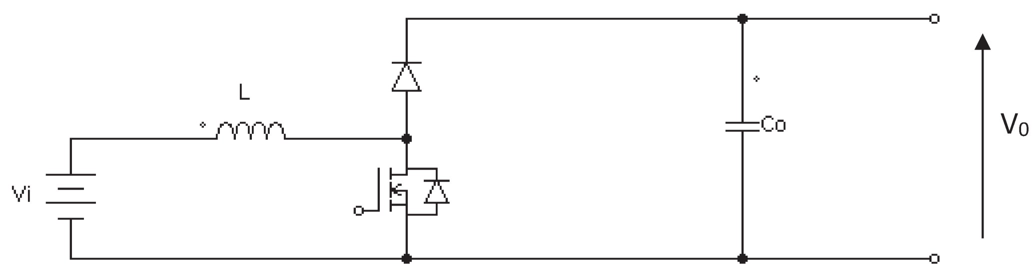

Figure 8 – Step-up basic circuit

As described in the literature ([6], [7]) it can be proven that in steady state condition the relation between output voltage V_0 and input voltage V_i can be defined as

$$\frac{V_0}{V_i} = \frac{1}{1-\delta} \tag{2-1}$$

Where δ is the converter duty cycle, which defines the transistor ON time in a determined switching frequency.

A step-down DC-DC converter is defined according to the Figure 9.

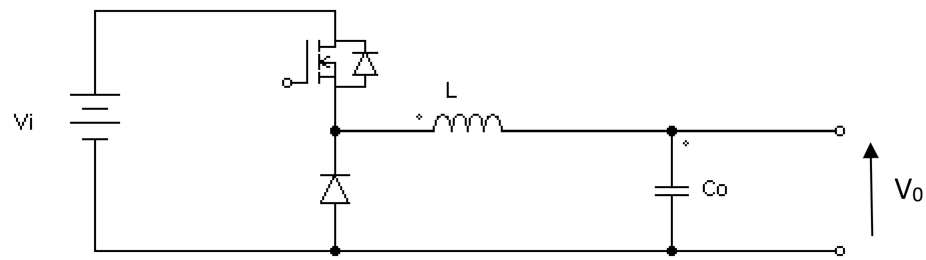

Figure 9 – Step-down basic circuit

In the step-down converter the relationship between V_0 and V_i in steady state condition is

$$\frac{V_0}{V_i} = \delta \tag{2-2}$$

The bi-directional converter is an arrangement in such a way that the step-up and step-down converters are together with the step-up voltage from one voltage source (V_i in the Figure 10) to the other (V_0) and the step-down is the opposite direction (from V_0 to V_i)

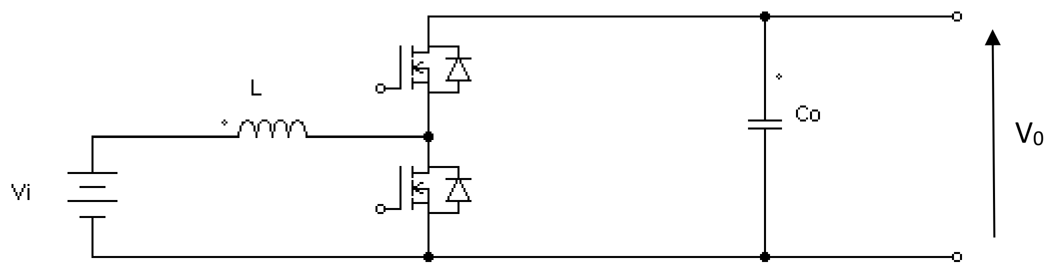

Figure 10 – Bi-directional DC-DC converter basic circuit

As described in [8], the bi-directional DC-DC converter is going to work in continuous conduction mode (CCM) because it presents lower current ripple at the input voltage source, minimizing the losses with a lower RMS current, increasing the battery and EC lifetime. Besides that, it is important to have a bi-directional system, in order to recover energy from regenerative braking system and also while the vehicle motor is acting as a generator, such as in downhill condition.

Another option commonly used in bi-directional converter is to use an interleaved architecture [9], to minimize the current ripple in the input source improving even further the battery and EC lifetime. A three-phase interleaved structure can be seen in Figure 11.

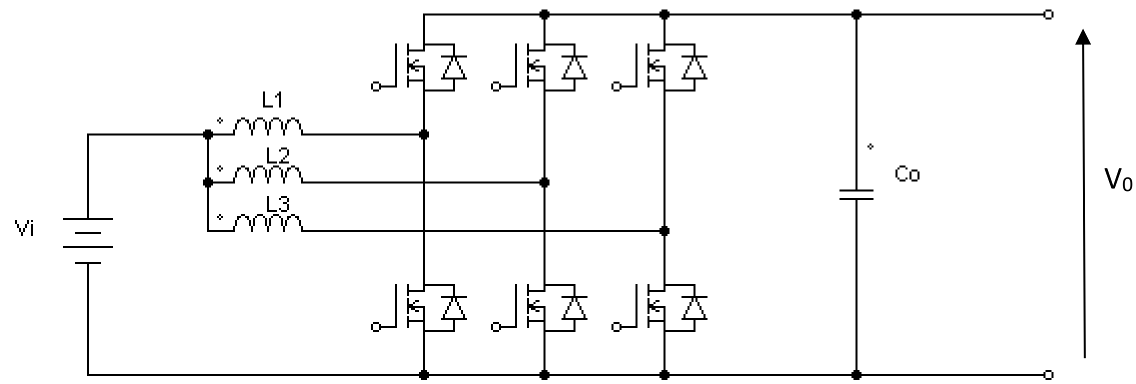

Figure 11 – Interleaved bi-directional DC-DC converter

For the switching controlling calculation, it was described in [10] that for a 2-phase interleaved converter, there is a change of $\sqrt{2}$ in the natural frequency (higher) and damping factor (lower). However, in this work this value was neglected for the circuit dynamics controlling calculation. Thus, it is going to be calculated considering a simple bi-directional converter, but when implementing the interleaved portion, the switching frequency for each phase will be shifted in this case by 120^o (360^o divided into 3 phases).

Another important aspect for controlling the bi-directional converter is that the boost and buck transistor shall be working complementary. It means that while the boost transistor is ON, the buck transistor is OFF and vice-versa. In this way it is assured that the circuit is always converging, avoiding the converter to go into the discontinuous conduction mode (DCM).

2.2 Battery modelling

As described in [11], there are a number of different ways in which the storage of energy can be done. One way is to convert two different types of energy: chemical and electrical energy. This involves the use of electrochemical devices that act as *transducers*, for they convert between electrical and chemical quantities – energies, potentials, and fluxes. Such electrochemical transduction systems are often called *galvanic cells*, or commonly, *batteries*.

For an electrical vehicle, in order to provide sufficient range, as well as adequate acceleration, relatively large amounts of energy must be available. Thus, the amount of energy per unit weight, defined as specific energy, is an important parameter to be considered.

As a general rule of thumb, the useful range of a battery-propelled vehicle, in kilometers, is approximately two times the specific energy of its battery system, in Wh/kg [11].

Another important consideration is, of course, the cost. Unfortunately, the least expensive currently available batteries, based upon the Pb/PbO_2 system, have a relatively low value of specific energy, some 30–40 Wh/kg [11]. Thus, electric vehicles using such batteries have useful ranges of only 60 – 80 km under normal conditions.

Although there is a great deal of activity aimed at their improvement, alternative electrochemical systems with greater specific energies are presently much more expensive.

Even though there has been a considerable amount of interest in the development of such battery-driven vehicles for some years, it has become obvious that the current state of battery technology is not sufficiently advanced for such all-electric vehicles to be price- and performance-competitive. As a result, such vehicles have found only a rather limited market to date.

This has led to a lot of research and development activity, and there have been a number of important technological changes in recent years. A number of these have not been just incremental improvements in already-known areas, but involve the use of new concepts, new materials, and new approaches.

An important reason for this progress has been the fact that such things as the discovery of fast ionic conduction in solids and the possibility of solid electrolytes, the concept of the use of materials with insertion reactions as high-capacity electrodes, and the discovery of materials that can produce lithium-based batteries with unusually high voltages have caused a number of people with backgrounds in other areas of science and technology to be drawn into this area. The result has been the infusion of new materials, concepts, and techniques into battery research and development, which used to be considered only as a part of electrochemistry.

Here is a short partial list of recent developments:

- Metal hydrides
- Lithium-carbon alloys
- Intermetallic alloys
- Lithium-transition metal oxides
- Polymeric components, in both electrolytes and electrodes
- Liquid electrodes
- Both crystalline and amorphous solid electrolytes
- Organic solvent electrolytes
- Mixed-conductor matrices
- Protective solid electrolyte interfaces in organic electrolyte systems
- Use of soft chemistry to produce nonequilibrium electrode compositions
- New fabrication methods, and new cell shapes and sizes
- Fabrication of lithium batteries in the discharged state

A number of battery's manufacturing technologies are suitable to equip an electric vehicle, technologies that today, are widely accepted by the companies in the manufacturing industry [12]:

- <u>Lead acid (Pb-acid)</u> – this is the oldest type of batteries used worldwide. They have the major disadvantages associated with handling acid substances, the presence of lead in their construction, a low stored energy/weight ratio and low stored energy/volume ratio. Because of their inexpensive manufacturing technology and a high ratio electric power/weight ratio they are a cheap solution to equip electric vehicles.
- <u>Nickel-Cadmium (NiCd)</u> – of all batteries they have the highest lifespan expressed through the number of cycles of charge and discharge (about 1500 cycles). Their biggest disadvantage is the use of a heavy metal (Cadmium) in the construction, with harmful effects on the environment and human and animal health. EU directives limit the use of this type of battery.
- <u>Nickel-Metal-Hydride (NiMH)</u> – NiMH battery manufacturing technology and operation resembles that of NiCd battery. The main advantage of NiMH batteries is the lack of memory effect, which affects the maximum load capacity of the battery. Compared to the

Li-ion, NiMH batteries have lower energy storage capacity and also a high self-discharge coefficient.

- Lithium-ion (Li-ion) – this type of battery is characterized by a large power storage capacity with very good energy density/ weight ratio. However, the limitations in the way of massive use of this type of battery are given by: high costs, a potential for overheating and a limited lifecycle.
- Lithium-ion Polymer – provides a greater lifecycle than the classical Li-ion batteries, but it presents a functional instability both in the case of an overload and in the case of battery discharges below a certain value.
- Sodium Nickel Chloride (NaNiCl) – is also known as the “Zebra battery” and it uses a molten salt electrolyte with an operating temperature of 270–350^{o}C. It offers the advantage of having a high stored energy density. The major disadvantages are related to its operational safety and its storage for longer periods.

In Figure 12, it is possible to see the differences between the battery types in relation to energy density and volume.

For applications that aim to power electric motors that equip electric vehicles, the batteries that offer the highest coefficient of stored energy density are preferred. The higher the value of this coefficient, the higher the autonomy of the electric vehicle will be. Thus, the need for further research to increase the energy density of batteries that equip electric vehicles is of immediate importance, and also an important external factor in increasing the penetration of the contemporary auto market by electric vehicles.

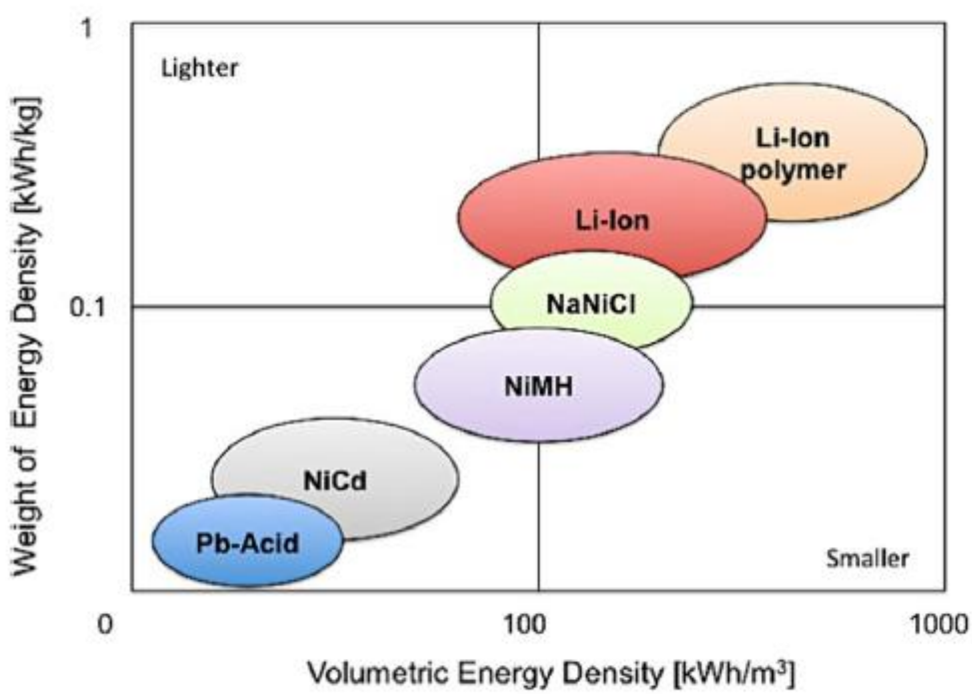

Figure 12 – Type of battery and energy density efficiency (weight / volume) [12]

Also, another factor is the battery lifetime, which directly influences the subsequent maintenance costs of purchasing an electric vehicle. Aging of lithium-ion cells, battery charge/discharge mode, electrolyte system, thermal and energy management system are inevitable phenomenon limiting the battery lifetime [12]. It is considered that undesirable side reactions during cycle or calendar aging affect directly the performance of all components of the lithium-ion cell. To improve the lifetime parameter, researches done were focused on nanotechnology application in development of anode and cathode material. This opens an avenue of research into green chemistry and green technologies for novel battery innovations.

2.2.1 Battery functioning - Simple Chemical and Electrochemical Reactions

First consider a simple *chemical reaction* between two metallic materials *A* and *B*, which react to form an electronically conducting product *AB*. This can be represented simply by the relation

$$A + B = AB \tag{2-3}$$

The driving force for this reaction is the difference in the values of the *standard Gibbs free energy* of the products - *AB* in this case, and the standard Gibbs free energies of the reactants, *A* and *B* [11].

If *A* and *B* are simple elements, this is called a *formation reaction*, and since the standard Gibbs free energy of formation of elements is zero, the value of the Gibbs free energy change that results per mol of the reaction is simply the *Gibbs free energy of formation* per mol of *AB*.

While the morphology of such a reaction can take a number of forms, consider a simple 1-dimensional case in which the reactants are placed in direct contact and the product phase *AB* forms between them. The time sequence of the *evolution of the microstructure* during such a reaction is shown schematically in Figure 13.

It is obvious that for the reaction product phase *AB* to grow, either *A* or *B* must move (diffuse) through it, to come into contact with the other reactant on the other side. If, for example, A moves through the *AB* phase to the *B* side, additional *AB* will form at the *AB/B* interface. Since some *B* is consumed, the *AB/B* interface will move to the right. As the amount of *A* on the *A* side has decreased, the *A/AB* interface will likewise move to the left. *AB* will grow in width in the middle. The action will be the same when species *B*, rather than species *A*, moves through the *AB* phase in this process.

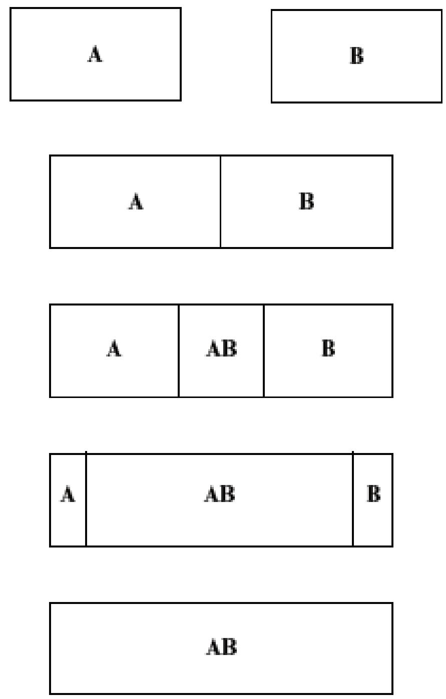

Figure 13 – Simple schematic model of chemical reaction of A and B to form AB, indication how the microstructure of the system varies with time [11]

In case this process occurs by an *electrochemical mechanism*, the time dependence of the microstructure is illustrated schematically in Figure 14. Like the chemical reaction case, product *AB* must form as the result of a reaction between the reactants *A* and *B*; but an additional phase is present in the system- an electrolyte.

The function of the electrolyte is to act as a filter for the passage of ionic, but not electronic species. The electrolyte must contain ions of either *A* or *B*, or both, and be an electronic insulator.

The reaction between *A* and *B* involves not just ions but electrically neutral atoms. Hence for the reaction to proceed there must be another path whereby electrons can also move through the system. This is typically an external electrical circuit connecting *A* and *B*. If A is transported in the system, and the electrolyte contains *A+* ions, negatively charged electrons, *e−*, must pass through the external circuit in equal numbers, or at an equal rate, to match the charge flux due to the passage of *A+* ions through the electrolyte to the other side.

For an electrochemical discharge reaction of the type illustrated in Figure 14 the reaction at the interface between the phase *A* and the electrolyte can be written as

$$A = A^{+} + e^{-} \tag{2-4}$$

with A^+ ions moving into the electrolyte phase and electrons entering the external circuit through a *current collector*. There will be a corresponding reaction on the other side of the electrolyte,

$$A^{+} + e^{-} = A \tag{2-5}$$

with ions arriving at the interface from the electrolyte and electrons from the external circuit through the electronic current collector. This results in the deposition of *A* atoms onto the adjacent solid phase *AB*. The *A*/electrolyte interface and the electrolyte/ *AB* interface move incrementally to the left in Figure 14. Inter-diffusion of *A* and *B* atoms within the phase *AB* is necessary to ensure that its surface does not have only *A* atoms. In addition, this phase must be an electronic conductor.

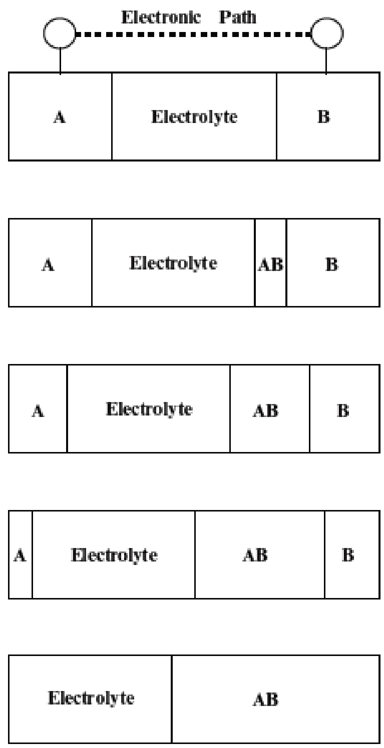

Figure 14 – Simple schematic model of time evolution of the microstructure during the electrochemical reaction [11]

When the electronic circuit is open, and there is no current flowing, there must be a force balance operating upon the electrically charged ions in the electrolyte. A *chemical driving force* upon the mobile ionic species within the electrolyte in one direction is simply balanced by an *electrostatic driving force* in the opposite direction.

It is interesting that, a chemical reaction between neutral species in the electrodes determines the forces on charged particles in the electrolyte in the interior of an electrochemical system.

If it is assumed that the electrodes on the two sides of the electrolyte are good electronic conductors, there is an externally measurable voltage *E* between the points where the external electronic circuit contacts the two electrodes. This voltage allows electrical work be done by the passage of electrons in an external electric circuit, if ionic current travels through the electrolyte inside the cell. This simple electrochemical cell acts as a transducer between chemical and electrical quantities; forces, fluxes and energy. Ideally chemical energy reduction due to the chemical reaction that takes place between *A* and *B* to form mixed-conducting *AB* is compensated by electrical energy transferred to the external electronic circuit. Flow of both internal ionic species and external electrons can be reversed if a voltage is imposed in the opposite direction in the electronic path that is larger than the voltage that is the result of the driving force of the chemical reaction. Since this causes current to flow in the reverse direction, electrical energy will be consumed and the chemical energy inside the system will increase; the electrochemical system is thus being recharged.

2.2.2 Electrochemical Cell

An electrochemical cell is a chemical device for generating or storing electric energy [13]. It consists of a positive electrode and a negative electrode, separated by electrolyte. The electrolyte is capable of conducting ions between the two electrodes, but is itself an electronic insulator. The positive and negative electrodes are immersed in the electrolyte and the reacting substances usually are stored within the electrodes, sometimes also in the electrolyte. The chemical reactions associated with the energy conversion take place at the two electrodes. During discharge (Figure 15.a), the negative electrode contains the substance that is oxidized (i.e. releases electrons), while the positive electrode contains the oxidizing substance that is reduced (i.e. accepts electrons). Those electrons pass through the external load, thereby doing useful work. When the battery is charged, this reaction is reversed and a corresponding amount of energy from an external source has to be supplied to the cell (Figure 15.b) [13].

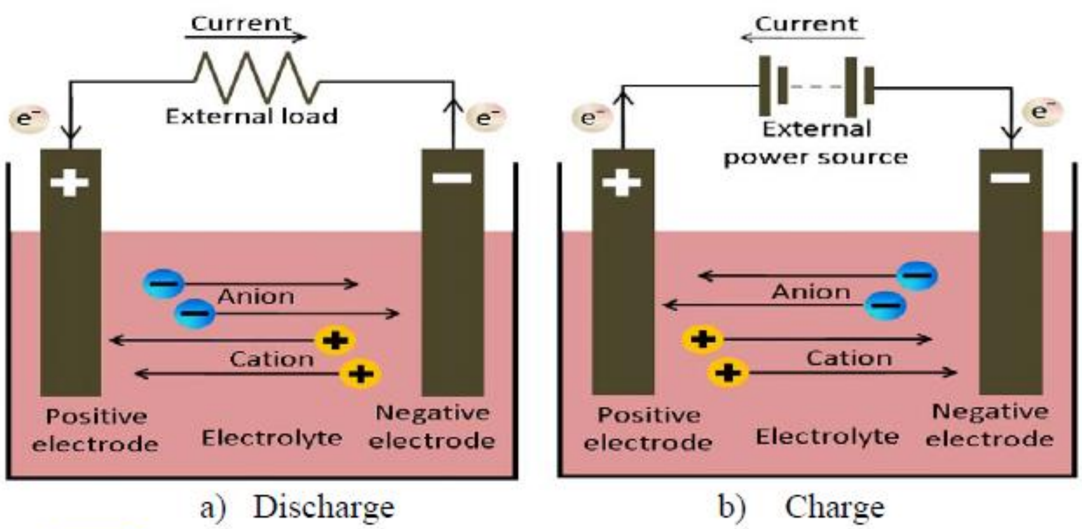

Figure 15 – Schematic representation of the operation of electrochemical cell [13]

As illustrated in [14], Figure 16 shows a Li-ion cell with previously described positive and negative electrodes and the electrolyte.

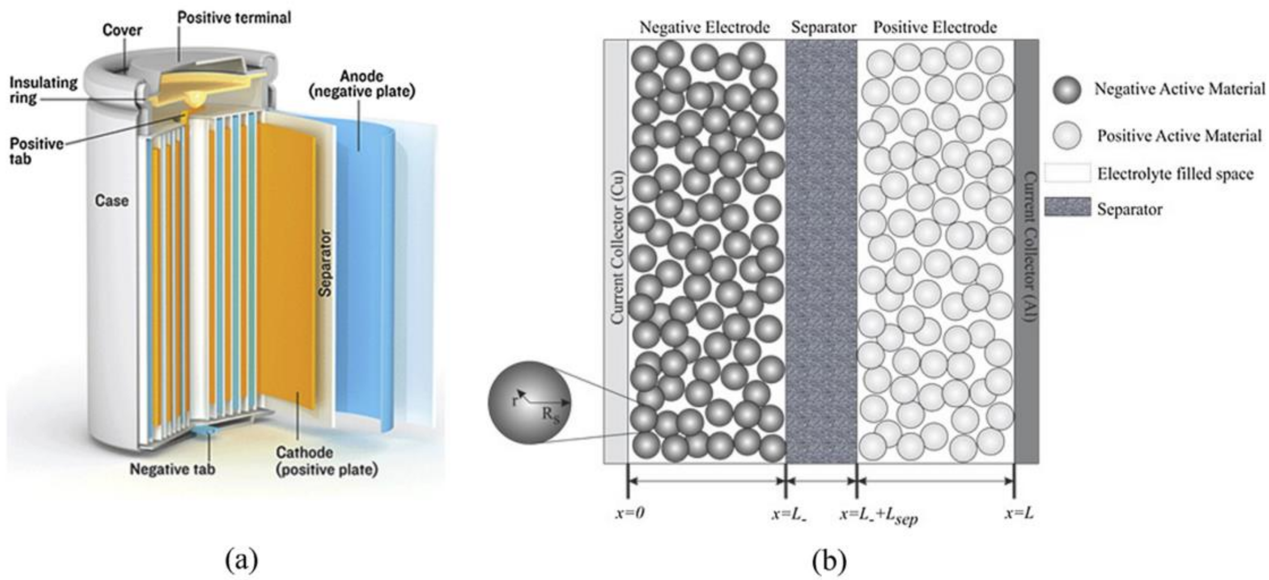

Figure 16 – (a) Cylindrical Li-ion cell, (b) Internal regions of Li-ion cell [14]

2.2.3 Important Practical Parameters

Batteries are characterized by their lifecycle, energy and power density and energy efficiency [15]. The lifecycle represents the number of charging and discharging cycles possible before it loses its ability to hold a useful charge (typically when the available capacity drops under 80% of the initial capacity). Lifecycle typically depends on the depth of discharge. When charging and discharging a battery, not all energy delivered by the battery, will be available due to battery losses, which are characterized by the battery efficiency.

The specific energy and power describe, respectively, the energy content (determining the vehicle range) and the maximum power (determining the vehicle acceleration performance) in function of the battery weight. A battery can be optimized to have a high energy content or it can be optimized to have a high-power capability. The first optimization is important for battery electric vehicles, while the second is mainly required for hybrid drive trains. Hybrid drive trains lead also to the consideration of a mixed energy-power capability.

A specific energy of at least 50Wh/kg and a specific power ranging from 100 W/kg, continuous, up to 200 or 300 W/kg intermittent pulse power is a must for a good electric vehicle design [15].

A battery for an electric vehicle consists of a combination in series, and possibly parallel, of individual battery cells. Minor differences in cell characteristics can be present. Consequently, a battery management system controlling the state of each cell is a key point for battery reliability and life duration.

When considering the use of electrochemical energy storage systems in various applications, one must be aware of the properties that might be relevant, since they are not always the same in every case.

Some rough values of the practical energy density (Wh/liter) and specific energy (Wh/kg) of several of the common rechargeable battery systems are listed in Table 1.

Table 1 – Approximate values of the practical specific energy and energy density of some common battery systems [11]

System	Specific energy Wh/kg	Energy density Wh/liter
Pb/PbO2	40	90
Cd/Ni	60	130
Hydride/Ni	80	215
Li-ion	135	320

The characteristics of batteries are often graphically illustrated through the use of *Ragone plots*, in which the specific power is plotted against the specific energy.

This type of presentation was named after D.V. Ragone, chairman of a governmental committee that wrote a report on the relative properties of different battery systems many years ago. Such a plot, showing approximate data on three current battery systems is shown in Figure 17.

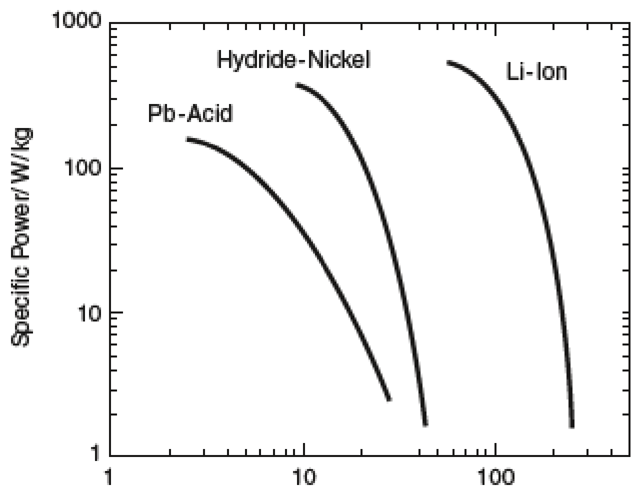

Figure 17 – Ragone plot showing approximate practical values of specific power and specific energy of 3 common battery systems [11]

2.2.3.1 The Charge Capacity

The energy (E) contained in an electrochemical system is the integral of the voltage (V) multiplied by the *charge capacity* (q), i.e., the amount of charge available. That is,

$$E = \int V dq \tag{2-6}$$

where V is the output voltage, which can vary with the state of charge as well as kinetic parameters, and q the amount of electronic charge that can be supplied to the external circuit.

Thus, it is important to know the maximum capacity, the amount of charge that can theoretically be stored in a battery. As in the case of voltage, the maximum amount of charge available under ideal conditions is a thermodynamic quantity, but of a different type. While voltage is an intensive quantity, independent of the amount of material present, charge capacity is an extensive quantity. The amount of charge that can be stored in an electrode depends on the amount of material in it. Capacity is always stated in terms of a measure such as the number of Coulombs per mol of material, per gram of electrode weight, or ml of electrode volume.

The state of charge is the current value of the fraction of the maximum capacity that is still available to be supplied.

2.2.3.2 Variation of the Voltage as Batteries are Discharged and Recharged

From the literature, it is seen that the voltage of most, but not all, electrochemical cells vary as their chemical energy is deleted as they are discharged. Likewise, it changes in the reverse direction when they are recharged. However, not only the voltage ranges, but also the characteristics of these state of charge – dependent changes vary widely between different electrochemical systems. It is important to understand what causes these variations.

On method of presenting this information is in terms of discharge curves and charge curves, in which the cell voltage is plotted as a function of the state of charge. There relationships can vary significantly, depending upon the rate at which the energy is extracted from, or added to the cell.

It is useful to consider the relation between the cell voltage and the state of charge under equilibrium or near-equilibrium conditions. In this case, a very important experimental technique, known as Coulometric titration, can provide a lot of information.

Some examples of discharge curves under low current, or near-equilibrium conditions are shown in Figure 18. They are presented here to show cell voltage as a function of the state of charge parameter. However, different battery systems have different capacities. Thus, care has to be taken not to compare energies stored in different systems in this manner.

The reason for presenting near-equilibrium properties of these different cells in this way is to show that there are significant differences in the types of their behavior, as indicated by the shapes of their curves. It is clear that some of the discharge curves are essentially flat, others have more than one flat region, and still others have a slanted and stretched S-shape, at times with an appreciable slope.

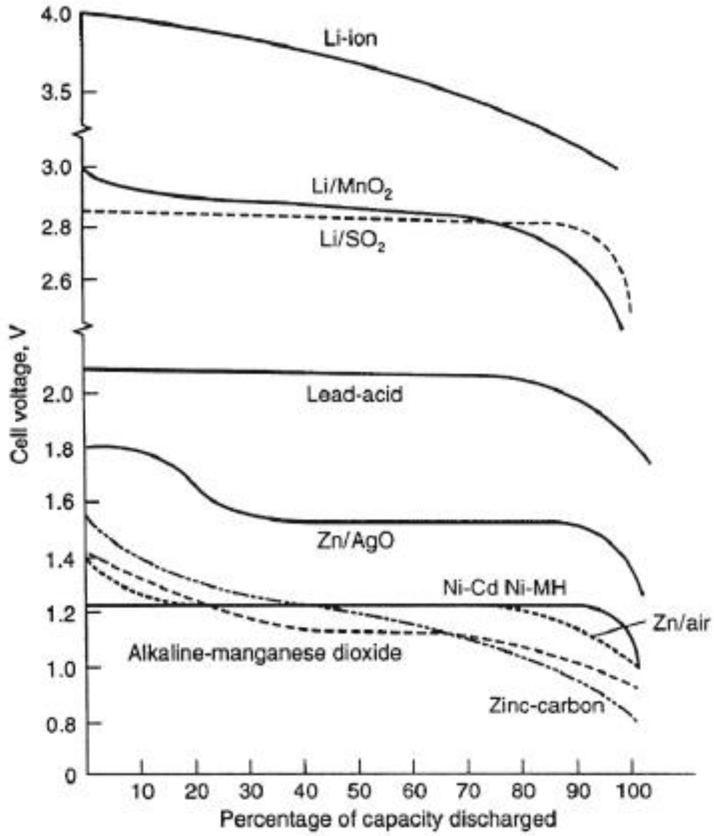

Figure 18 – Examples of battery discharge curves, showing variation of the voltage as function of available capacity [11]

2.2.3.3 Battery Lifetime

Due to the voltage variation over time, the battery has a lifetime and a prediction of it is important to warn the need for replacement or to recharge.

The two most important properties of a battery are its voltage (expressed in volts, V) and its capacity (mostly expressed in ampere-hour, Ah); the product of these two quantities is a measure for the energy stored in the battery [16]. For an ideal battery the voltage stays constant over time until the moment it is completely discharged, then the voltage drops to zero. The capacity in the ideal case is the same for every load for the battery. Reality is different, though: the voltage drops during discharge and the effectively perceived capacity is lower under a higher load. This phenomenon is termed the rate capacity effect.

In the ideal case it is easy to calculate the lifetime of a battery. The lifetime (*life*) in the case of a constant load is the capacity (K) over the load current (i)

$$life = \frac{K}{i} \tag{2-7}$$

Due to various non-linear effects this relation does not hold for real batteries. A simple approximation for the lifetime under constant load can be made with Peukert's law [16]

$$life = \frac{a}{i^b}$$

(2-8)

where *a* and *b* are constants which depend on the battery. For variable loads (*i(t)*) one can extend (2-8) by using the average current up until *t = life*

$$life = \frac{a}{\left(\left({}^{1}/_{life}\right)\int_0^{life} i(t)dt\right)^b}$$

(2-9)

Following (2-9), all load profiles with the same average current have the same lifetime. Experimentally it can be shown that this is not the case. One of the effects playing an important role here is the recovery effect of the battery, that is, the effect that the battery regains some of its ‘lost’ capacity during idle periods.

2.2.3.4 Cycling Behavior

In many applications a battery is expected to maintain its major properties over many discharge - charge cycles. This can be a serious practical challenge, and is often given a lot of attention during the development and optimization of batteries.

Figure 19 shows how the initial capacity is reduced during cycling, assuming three different values of the Coulombic efficiency – the fraction of the prior charge capacity that is available during the following discharge. This depends upon a number of factors, especially current and depth of discharge in each cycle.

It is seen that even minor inefficiency per cycle can have important consequences. For example, a half percent loss per cycle causes available capacity to drop to only 78% of the original value after 50 cycles. After 100 cycles, only 61% remains at that rate. The situation is worse if the Coulombic efficiency is lower.

Applications that involve many operation cycles require cells to be designed and constructed such that the capacity loss per cycle is extremely low. This means that compromises must be made in other properties.

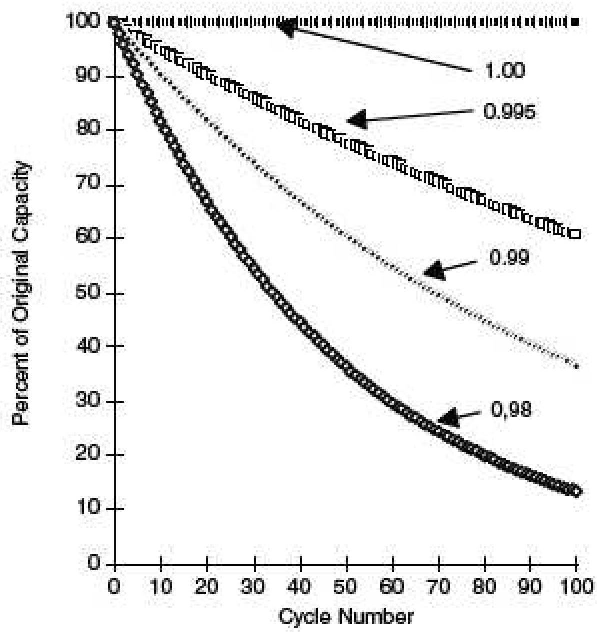

Figure 19 – Influence of Coulombic efficiency upon available capacity during cycling [11]

2.2.3.5 Self-Discharge

Another property of importance in practical cells is self-discharge. This implies a decrease in available capacity with time, even without energy being taken from the cell by the passage of current through the external circuit. This is a serious practical problem in some systems, but negligible in others. What needs to be understood at this juncture is that capacity is a property of the electrodes. Its value at any time is determined by the remaining extent of the chemical reaction between the neutral species in the electrodes. Any self-discharge mechanism that reduces the remaining capacity must involve either transport of neutral species, or concurrent transport of neutral combinations of charged species, through the cell. Since this latter process involves the transport of charged species, it is electrochemical self-discharge.

There are also several methods by which individual neutral species can move across a cell. These include transport through an adjacent vapor phase, cracks in a solid electrolyte, or as a dissolved gas in a liquid electrolyte. Since the transport of charged species is not involved, these processes produce chemical self-discharge.

It is also possible that impurities react with constituents in the electrodes or the electrolyte to reduce available capacity over time.

2.2.4 General Equivalent Circuit of an Electrochemical Cell

In general, the existing battery models can be classified into four categories: electrochemical models, analytical models, stochastic model, and electrical circuit models [17].

The electrochemical models use complex nonlinear differential equations to exactly describe chemical processes that take place in batteries cells. The electrochemical models are the most accurate models. However, establishing these models requires detailed knowledge of the battery chemical processes, which makes them difficult to configure [17]. Moreover, due to high complexity and intensive computation requirement, it is difficult to use these models for real-time battery power management and circuit simulation.

The analytical models are the simplified electrochemical models that can capture nonlinear capacity effects and predict runtime of the batteries with reduced order of equations. These models perform well for the SOC tracking and runtime prediction under specific discharge profiles. The simplest analytical model is the Peukert's law. It captures the nonlinear relationship between the runtime of the battery and the discharge rate, but the recovery effect is not taken into account.

As early as 1965, Shepherd [18] developed a mathematical equation, as in (2-10) to directly describe the electrochemical behavior of a battery in terms of a cell's potential V, no-load voltage and the potential drop due to the internal resistance R_i. No-load voltage is fitted by a constant voltage V_s, a reciprocal function and an exponential function.

$$V = V_s - \gamma\left(\frac{Q}{Q - it}\right)i + \alpha exp(-\beta Q^{-1}it) - R_i i \tag{2-10}$$

Where,
V = potential of a cell
V_s = no-load voltage
γ = polarization coefficient
Q = available amount of active material in coulombs
i = current density
t = time
α, β = empirical constants
R_i = internal resistance

The generic battery model provided by MATLAB/Simulink SimPowerSystems is based on this equation [18]. However, this model is too simple to reflect the performance of a battery under dynamic changing current load.

Another analytical model is the kinetic battery model (KiBaM) as informed in [18]. The KiBaM is an intuitive battery model, which was originally developed to model chemical processes of large lead-acid batteries by a kinetic process. The third analytical model is the diffusion model, which was developed to model lithium-ion batteries based on the diffusion of the ions in the electrolyte. The model describes the evolution of the concentration of the electroactive species in the electrolyte to predict the battery runtime under a given load profile. The KiBaM and the diffusion model take into account both the rate capacity effect and the recovery effect. However, they cannot describe the current–voltage (I-V) characteristics that are important for electrical circuit simulation and multicell battery design. The KiBaM is actually a first-order approximation of the diffusion model.

The stochastic model [18] focuses on modeling recovery effect and describes the battery behavior as a Markov process with probabilities in terms of parameters that are related to the physical characteristics of an electrochemical cell. However, the model does not handle arbitrary load profiles with varying discharge currents.

The electrical circuit models use equivalent electrical circuits to capture *I-V* characteristics of batteries by using the combination of voltage and current sources, capacitors, and resistors. Some of these models can also track the SOC and predict the runtime of the batteries by using sensed currents and/or voltages. The electrical circuit models are good for co-design and co-simulation with other electrical circuits and systems. However, the existing electrical circuit models do not integrate battery nonlinear capacity behaviors, leading to an inaccurate prediction of remaining battery capacity and operating time.

An electrochemical cell can be simply modeled as shown in Figure 20, and its basic equivalent circuit is shown in Figure 21, if there are no impedances or other loss mechanisms during the chemical reactions inside the battery, the externally measurable cell voltage V_{out} is simply equal to V_{th}.

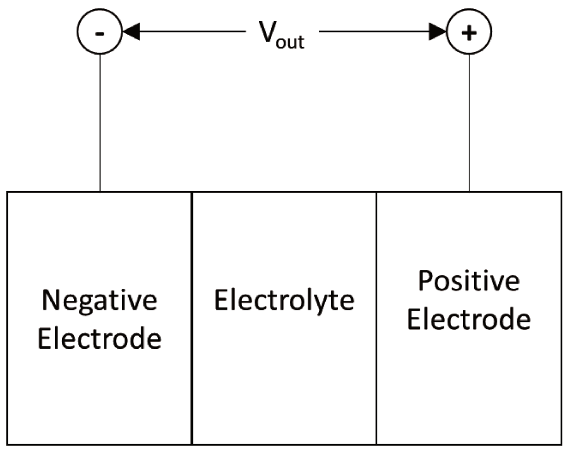

Figure 20 – Simplified physical model of electrochemical cell [11]

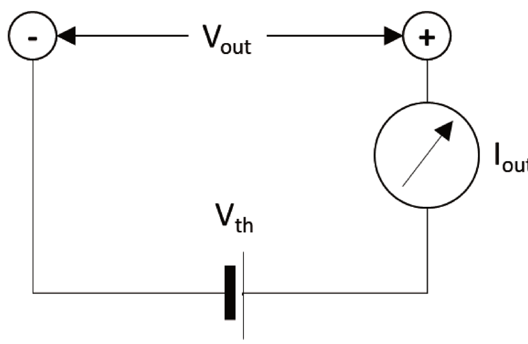

Figure 21 – Simple equivalent circuit model of an ideal electrochemical cell [11]

In practical electrochemical cells V_{out} is not always equal to V_{th}. There are several reasons for this disparity. Resistance always exist to the transport of electroactive ions and related atomic species across the cell e.g. resistance of electrolyte to ionic transport, or at one or both of the two electrolyte/electrode interfaces. Further, resistance to the progress of the cell reaction in some cases is related to the time-dependent solid-state diffusion of the atomic species into, or out of, the electrode microstructure.

It is important to note that the resistances used in this discussion can be time-dependent, since changes in structure or composition are occurring in the system. The *resistance* is an instantaneous ratio of the applied force (e.g. voltage) V_{appl} and the response (e.g. current) across any circuit element. As an example, if a voltage V_{appl} is imposed across a material that conducts electronic current i_e, the electronic resistance R_e is given by

$$R_e = \frac{V_{appl}}{i_e} \tag{2-11}$$

If current is flowing through the cell, there will be a voltage drop related to each impedance to the flow of ionic current within the cell. Thus, if the sum of these internal resistances is R_i the output voltage can be written as

$$V_{out} = V_{th} - i_{out}R_i \tag{2-12}$$

This relationship can be modeled by the simple circuit in Figure 22.

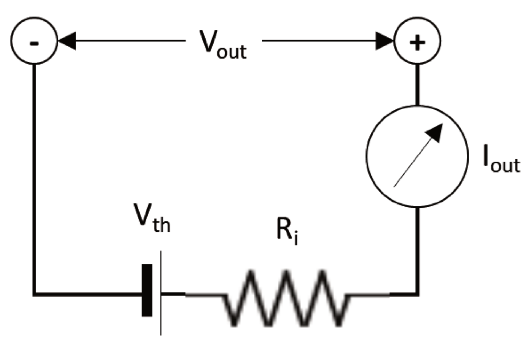

Figure 22 – Simple equivalent circuit for a battery or fuel cell indicating the effect of the internal ionic impedance [11]

Figure 22 represents the simplest equivalent circuit model for a battery system.

The output voltage V_{out} can also be different from the theoretical electrical equivalent of the thermodynamic driving force of the reaction between the neutral species in the electrodes V_{th} even if there is no external current i_{out} flowing. This can be the result of electronic leakage through the electrolyte that acts to short-circuit the cell.

This effect can be added to the previous equivalent circuit to give the circuit shown in Figure 23.

It is evident that, even with no external current, there is an internal current related to the transport of the electronic species through the electrolyte i_e. Since the current must be the same everywhere in the lower loop, there must be a current through the electrolyte i_i with the same magnitude as the electronic current. There must be charge flux balance so that there is no net charge buildup at the electrodes.

The current through the internal ionic resistance R_i generates a voltage drop, reducing the output voltage V_{out} by the product $i_i R_i$, which is equal to i_eR_e.

$$V_{out} = V_{th} - i_iR_i \tag{2-13}$$

In addition, the fact that both ionic and electronic species flow through the cell means that this is a mechanism of self-discharge. This topic, results in a decrease of the available charge capacity of the cell.

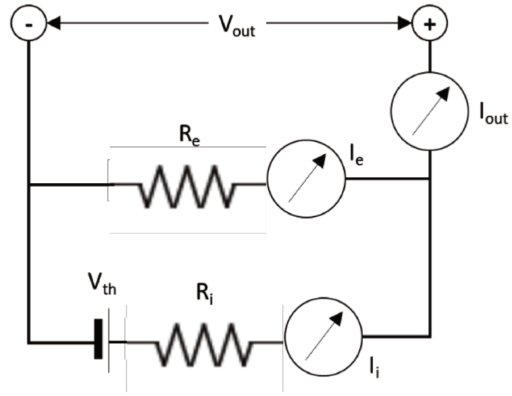

Figure 23 – Modified circuit including electronic leakage through the electrolyte [11]

Another basic circuit-based model is Thevenin model [19]. This model combines resistor, RC network, and voltage-controlled voltage source to capture battery response to various load cases. However, this model assumes that the open-circuit voltage keeps constant, which makes it infeasible for output voltage tracking and runtime estimation. Thevenin model works well only for a fixed state of charge (SOC) condition. Another circuit-based model which is developed originally from Thevenin model for signal cell battery is illustrated in Figure 24. On the left side, a capacitor and a current-controlled current source is used to represent capacity, SOC and runtime of the battery. The resistor R^T stands for self-discharging resistor, and captures self-discharge capacity loss during the period when battery is not connected to load. A voltage-controlled voltage source is used to bridge SOC to open circuit voltage. The internal resistance and discharging energy loss are emulated by the series resistance *R* on the right hand. The two *RC* networks are used to characterize the short-term and long-term transient response respectively.

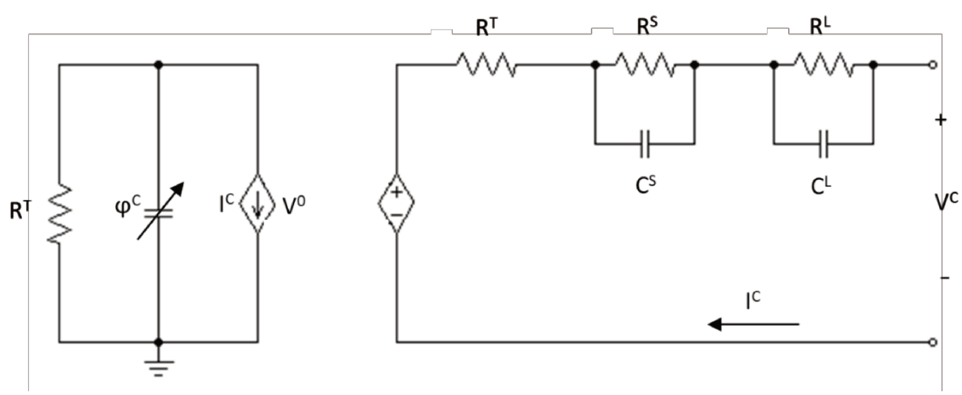

Figure 24 – Existing circuit-based Thevenin battery model [19]

Numerous previous works have shown that using two *RC* networks is the best tradeoff between computational complexity and accuracy [19]. Several other circuit-oriented models have been proposed based on this Thevenin's model, with some improvements in order to improve the current circuit, using non-linear equations. Such as [17], [20], [13], [21], [22], [23], but all of them are variations on this shown circuit and increases the complexity on the simulation.

It was not possible to find available parameters for the voltage that will be used for the simulations, therefore to determine all the battery parameters it is necessary to perform tests with the battery. Since studying the battery state-of-charge and its dynamics is not going to be the main purpose of this work, it will be considered the simplest battery model, which is a simple constant voltage source and the internal resistance as shown in Figure 22.

2.3 Electrochemical capacitors modelling

Capacitors which store the energy within the electrochemical-double-layer at the electrode/electrolyte interface were described for the first time in 1853 by the German physicist Hermman von Helmholtz [24]. Nowadays they are known under various names such as 'double-layer capacitors', 'supercapacitors', 'ultracapacitors', 'power capacitors', 'gold capacitors' or 'power cache'. 'Electrochemical double-layer capacitor' is the name that describes the fundamental charge storage principle of such capacitors. However, due to the fact that there are in general additional contributions to the capacitance other than double layer effects, it will be called in this text as electrochemical capacitors (EC) [25].

The electric load profile of automotive vehicles consists of high peaks and steep valleys due to repetitive acceleration and deceleration. An electric vehicle, which is constituted of a battery as main power source, the limited power release rate inherent in a battery, makes the battery- powered electric motor unable to follow rapid power demand spikes without drastically increasing battery size and cost [26], and it will still reduce the battery lifecycle. Rapid transients in power demand will be better handled by the use of high-power density EC. A typical EC is capable of releasing or storing energy roughly ten times faster than a battery of the same weight. The total energy which it can store, however, is typically ten times less than that same battery, meaning that an electrochemical capacitor provides an order of magnitude increase in power density at the cost of an order of magnitude of energy density.

EC is an energy storage device, which has the advantages of high power density (W/kg), long life of charging and discharging (typically 500,000 cycles [27]) and stable temperature characteristic. Electrochemical capacitors offer superior efficiency, longevity and are less temperature dependent as compared to batteries. By the synergic use of power battery and EC, the power battery is only supposed to provide the average power of the electric system, and the EC would compensate the exceeding power required. In other words, the EC will assist the battery during vehicle acceleration and hill climbing, and capture the regenerative braking energy [28] .

EC is an energy storage component between electrostatic capacitors and batteries, which combines higher energy density (Wh/kg) than traditional physical capacitor and higher power density than chemical batteries as shown in Figure 25, where typical energy storage and conversion devices are presented in the Ragone plot in terms of their specific energy and specific power. Therefore, it always acts as power source for short-time output [29].

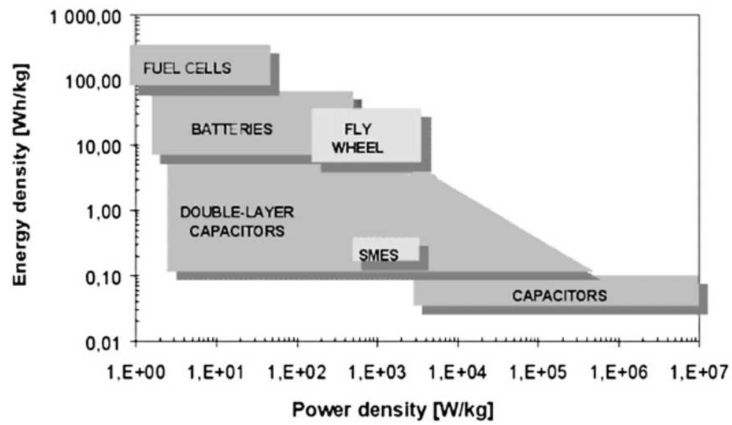

Figure 25 – Ragone plot: comparison between capacitors, SCs, batteries and FCs. [1]

Batteries and low temperature fuel cells are typical low power devices whereas conventional capacitors may have a power density of $>10^6$ watts per dm^3 at very low energy density. Thus, electrochemical capacitors may improve battery performance in terms of power density or may improve capacitor performance in terms of energy density when combined with the respective device. In addition, ECs are expected to have a much longer lifecycle than batteries because no or negligibly small chemical charge transfer reactions are involved.

The working temperature range is another feature to be pointed out. High power performance down to -40 °C can be achieved with ECs, which is not possible at the moment with batteries [30]. Besides, ECs are generally safer than batteries for high power-rating charging and discharging. Double layer capacitor cells do not rely on metals chemistries and do not thus run the risk of metal plating, which is an important battery degradation and failure mechanism as well as a safety concern that can lead to short circuits and uncontrollably energetic chemical reactions.

A comparative summary can be seen in Table 2 ad Table 3.

Table 2 – Comparison table among selected electrochemical energy storage technologies [30]

Characteristics	**Capacitor**	**Electrochemical capacitor**	**Battery**
Specific energy (Wh/kg)	< 0.1	1 – 10	10 – 100
Specific power (Wk/g)	> 10,000	500 – 10,000	< 1000
Discharge time	10^{-6} to 10^{-3}	sec to min	0.3 – 3h
Charge time	10^{-6} to 10^{-3}	sec to min	1 – 5h
Life cycle	Almost infinite	> 500,000	Approx. 1000

Table 3 – Comparison between batteries and electrochemical capacitors [30]

Comparison parameter	**Battery**	**EC**
Storage mechanism	Chemical	Physical
Power limitation	Reaction kinetics, mass transport	Electrolyte conductivity
Energy storage	High	Limited (surface area)
Charge rate	Kinetically limited	High, same as discharge
Life cycle limitations	Mechanical stability, chemical stability	Side reactions

Capacitors can be generally classified as follows:

- Electrostatic capacitors.
- Electrolytic capacitors.
- Electrochemical capacitors.

2.3.1 Electrostatic capacitors

As described in [24]**,** electrostatic capacitors are typically made of two metal electrodes (parallel plates) separated by a dielectric as shown in Figure 26. The dielectric is nothing, but is a non-conducting material that is inserted between the parallel plates of the metal electrode material. The dielectric increases the overall capacitance and the maximum operating voltage of the capacitor. The capacitance, measured in Farads (F), is defined as the ratio of total charge in coulombs (Q) in each electrode to the potential difference (V) between the plates (2-14). Dielectric material that is measured in volts per meter. The dielectric strength is the maximum electric field, which can exist in a dielectric without electrical breakdown.

$$C = \frac{Q}{V} \tag{2-14}$$

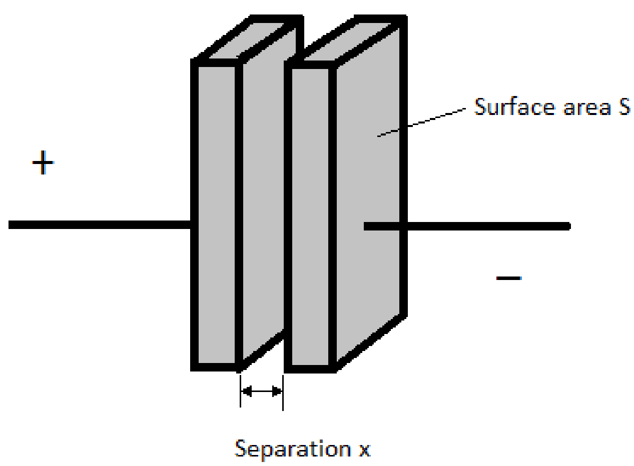

Figure 26 – Simplified parallel capacitor [24]

2.3.2 Electrolytic capacitors

An electrolytic capacitor is similar in construction to an electrostatic capacitor but has a conductive electrolyte salt in direct contact with the metal electrodes. Aluminum electrolytic capacitors, for example, are made up of two aluminum conducting foils (coated with an insulating oxide layer) and a paper spacer soaked in electrolyte [24]. The oxide layer serves as the dielectric and is very thin, which results in higher capacitance per unit volume than electrostatic capacitors. Electrolytic capacitors have plus and minus polarity due to the oxide layer, which is held in place by the electric field established during charge. If the polarity is reverse-biased, the oxide layer dissolves in the electrolyte and can become shorted and, in extreme cases, the electrolyte can heat up and explode.

2.3.3 Electrochemical capacitors

ECs also use electrolyte solutions but have even greater capacitance per unit volume due to their porous electrode structure compared to electrostatic and electrolytic capacitors. Electrochemical capacitors store the electric energy in an electrochemical double layer (Helmholtz Layer) formed at a solid/electrolyte interface. Positive and negative ionic charges within the electrolyte accumulate at the surface of the solid electrode and compensate for the electronic charge at the electrode surface. The thickness of the double layer depends on the concentration of the electrolyte and on the size of the ions and is in the order of 5–10 Å, for concentrated electrolytes [25]. The double layer capacitance is about 10–20 mF/cm^2 for a smooth electrode in concentrated electrolyte solution.

The corresponding electric field in the electrochemical double layer is very high and assumes values of up to 10^6 V/cm easily.

Compared to conventional capacitors where a total capacitance of pF and mF is typical, the capacitance of and the energy density stored in the electrochemical double layer is rather high per se and the idea to build a capacitor based on this effect is tempting.

In order to achieve a higher capacitance, the electrode surface area is additionally increased by using porous electrodes with an extremely large internal effective surface. Combination of two such electrodes gives an electrochemical capacitor of rather high capacitance.

Figure 27 (presented in [25])shows a schematic diagram of an electrochemical double-layer capacitor consisting of a single cell with a high surface-area electrode material, which is loaded with electrolyte. The electrodes are separated by a porous separator, containing the same electrolyte as the active material. The potential drop across the cell is also shown in Figure 27.

Generally, these devices work like capacitors, the capacitance, C, will depend on the dielectric constant of the electrolyte, ε_r, the effective thickness of the double layer, x (separation between charges), and the accessible surface, S, as follows:

$$C = \frac{\varepsilon_r \varepsilon_0 S}{x} \tag{2-15}$$

where ε_0 is the dielectric constant of the vacuum. The EC maximizes the (2-15) by having a very high electrode surface area (S) due to the porous electrodes and a very small separation (x) between the electronic and ionic charge at the electrode surface. Indeed, the surface-area of the porous electrodes has been recorded to be as large as 1000–2000 m^2/cm^3. The high-energy density of ECs is due to their greater capacitance per unit volume compared to conventional capacitors. The capacitance for an electric double layer on carbon surface varies usually from 5 to 20 μF/cm^2 depending on the electrolyte, although much higher values are sometimes reported for edge carbon atoms.

The capacitance of a single electrode can be estimated by assuming a high surface area carbon with 1000 m^2/g and a double layer capacitance of 10 μF/cm^2. This leads to a specific capacitance of 100 F/g for one electrode.

For a capacitor, two electrodes are needed with doubled weight and half the total capacitance ($1/C = 1/C1 + 1/C2$) resulting in 25 F/g of active capacitor mass for this example.

The energy (W) stored within an electrochemical capacitor is

$$W = \frac{1}{2} C V^2 \tag{2-16}$$

where V is the cell voltage. Equation (2-16 shows that the stored energy is proportional to both the capacitance of the device and the square of the cell voltage. Therefore, increasing both of them is a general strategy to increasing the energy density of the cell.

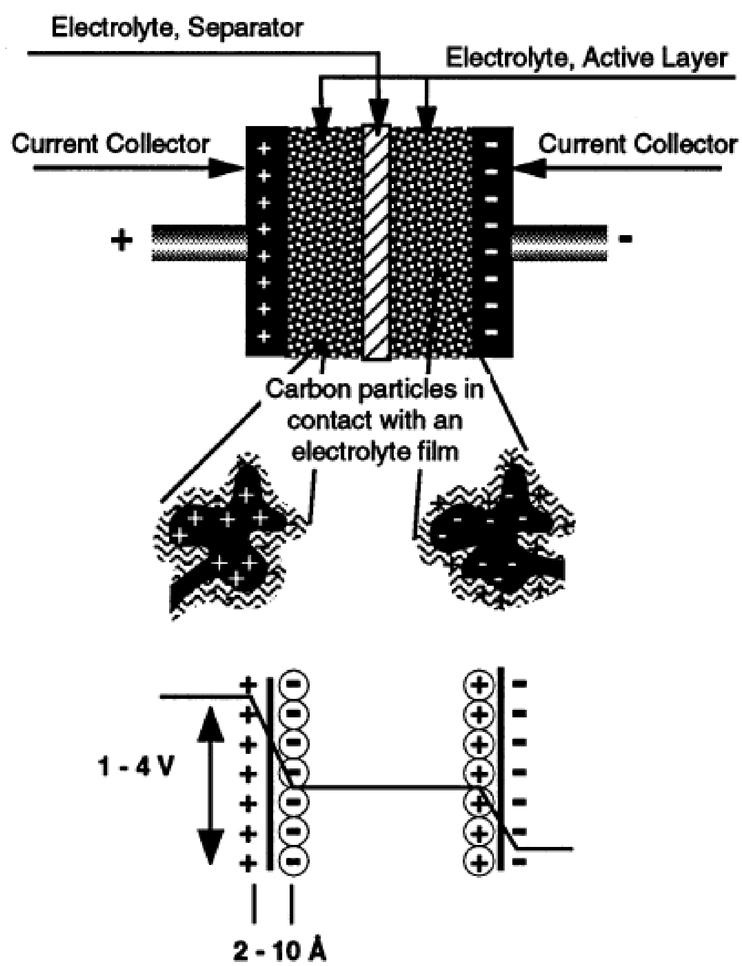

Figure 27 – Principle of a single-cell double-layer capacitor and illustration of the potential drop at the electrode/electrolyte interface [25]

With a cell voltage V of 1 V (aqueous electrolyte) one obtains a specific energy of about 3.5 Wh/kg of active mass. Using an organic electrolyte with a typical cell voltage of 2.3 V one obtains about 18 Wh/kg of active mass. These values are considerably lower than those obtained for available batteries but much higher than for conventional capacitors.

The maximum instantaneous power P_{max} that an EC is able to deliver, depends on the voltage and the internal resistance R as follows:

$$P_{max} = \frac{V^2}{4R}$$

(2-17)

Also, the current across the EC will be

$$i = C\frac{dv}{dt}$$

(2-18)

In industry [30], constant current tests are performed to determine the main characteristics of devices. This includes capacitance calculation (integral of the area contained during the discharge), and resistances associated to the cell such as equivalent series resistance (ESR) and equivalent distributed resistance (EDR), which represents ESR and the resistance in the pores (part of the discharge with curvature). These are calculated using the notation in Figure 28 with the following expressions:

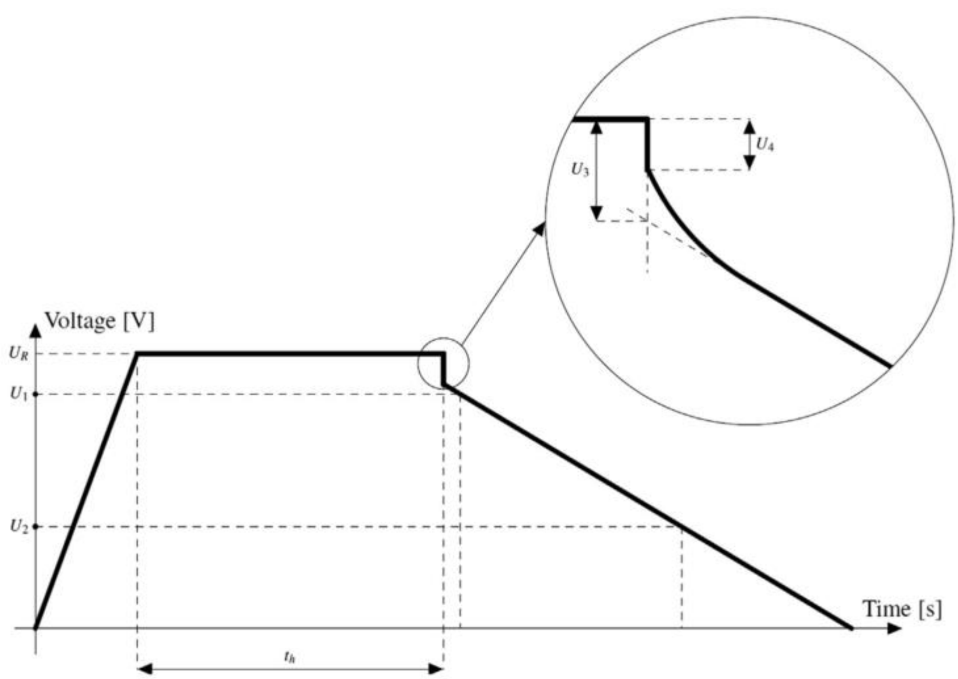

Figure 28 – Constant current discharge electrochemical capacitor cell test [30]

$$C = \frac{i_{discharge} t_{discharge}}{U_1 - U_2}$$

(2-19)

$$ESR = \frac{U_4}{i_{discharge}}$$

(2-20)

$$EDR = \frac{U_3}{i_{discharge}}$$

(2-21)

ECs themselves are grouped into two major categories: symmetric and asymmetric. Symmetric ECs (or SECs) use the same electrode material (usually carbon) for both the positive and negative electrodes. Asymmetric ECs (or AECs) use two different materials for the positive and negative electrodes. SECs get their electrostatic charge from the accumulation and separation of ions at the interface between the electrolyte and electrodes.

SECs can use aqueous or organic electrolyte solutions. The electrolyte solution comprises aqueous substances (such as potassium hydroxide or sulfuric acid) or organic substances (such as acetonitrile or propylene carbonate). A SEC using aqueous electrolyte is also known as a Type I SEC and an SEC using organic electrolyte is known as a Type II SEC. Similarly, an AEC using an aqueous electrolyte is known as a Type III AEC and one using organic electrolyte is known as a Type IV AEC. At the time of writing, there were no commercially available Type IV AEC devices [24].

2.3.4 Modeling of electrochemical capacitor

The process of storing charges in the double-layer capacitor is very different to those that occur in conventional capacitors. It should therefore be no surprise to find that traditional models used to describe capacitor behavior are inadequate in the case of electrochemical capacitors [24].

In recent years as ECs become used more widely, several different circuit models have been proposed in the literature. Three basic modeling approaches have been used: a mathematic model, an electric circuit model, and other non-electric circuit models (such as artificial neutral network modeling method). Each modeling approach has its own advantages and disadvantages respectively. The mathematical modeling approach includes complicated computations and requires too many parameters that must be experimentally identified. Additionally, the mathematical model does not usually have an explicit physical meaning and cannot readily be incorporated into a circuit diagram. Non-electric circuit models have similar shortcomings. In this work, we focus on electric circuit models, which are most commonly used by electrical engineers [31].

2.3.4.1 The classical equivalent circuit

The simplest EC circuit model, the RC model, has only one RC branch. Figure 29 is the electrochemical capacitor simple RC model. This model is composed of a resistor R, which models the EC's ohmic loss, usually called equivalent series resistor (ESR) and a capacitor C, which simulate the EC's capacitance during charging and discharging effects.

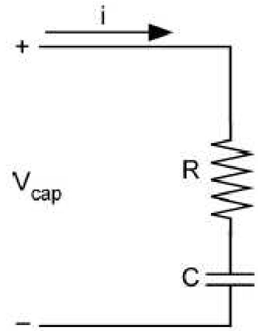

Figure 29 – Simple EC model [31]

By comparing the simulation result and the experimental results, it can be seen that the simple RC model has several advantages and disadvantages. The primary advantage is the simplicity of the model. It is easy to incorporate into a circuit and the simulation process is computationally straightforward. The primary disadvantage is that the simple RC model is not able to capture the nonlinear rise and fall of the EC voltage and the change in voltage after the charging and discharging stops. Therefore, more detailed models are required for better accuracy [31].

2.3.4.2 The three-branch model

Zubieta and Bonert observed that the classical circuit is insufficient when compared against experimentally observed behavior [24]. Therefore, a model consisting of three RC branches was suggested to achieve a better fit to the collected data. The basic objective of this model is to simulate the actual EC's behavior during charge and discharge.

When the EC is charged (discharged), the terminal voltage will increase (decrease) rapidly. If the charging (discharging) is stopped, the terminal voltage will continue to decrease (increase) gradually for several minutes and will ultimately become stable after tens of minutes. Thus, three different time constant RC branches are chosen to simulate the electrochemical capacitor's charge and discharge regions. Ideally, the number RC branches should be large. However, to simplify the modeling process and to ensure satisfactory accuracy, three or two branches are the typical choice for models. The three RC parallel branch model is shown in Figure 30. The three branches are called the fast-term branch composed of R_f and C_f, medium-term branch composed of R_m and C_m, and the long-term branch composed of R_s and C_s [31].

Each RC branch has a different time constant. The fast term branch dominates the charge and discharge behavior in the order of a few seconds. The medium-term branch dominates the behavior over the scale of minutes. Finally, the slow-term branch usually governs the long-term charge and discharge characteristics (longer than ten minutes).

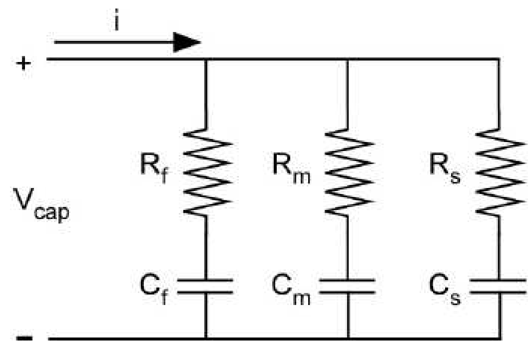

Figure 30 – RC parallel branch model [31]

The advantages of the RC parallel branch model are:

- The model reflects the internal charge distribution process very well within the considered time span and for voltages above 40% of the rated terminal voltage.
- There is good response of the EC's dynamic behavior during charging and discharging process.
- The parameters can be extracted from a relatively simple experimental test set-up.
- The accuracy is better than the simple RC model. However, at low voltages, the error between model and actual behavior may reach 10% of the rated voltage; this is due to several assumptions that have been made to simplify the model and the parameters' identification [31]

2.3.4.3 The RC transmission line model

The RC transmission line model is based on Porous Electrode Theory developed by de Levie [32]. This model is typically referred to as the transmission line model.

At the physical level, each pore in a porous electrode can be modeled as a transmission line. The transmission line model attempts to capture the distributed double-layer capacitance and the distributed electrolyte resistance that extends the pore depth. To achieve an estimation of the double-layer capacitive effects, straight, cylindrical pores of uniform diameter and a perfectly conducting electrode are assumed, leading to a ladder network with potentially many RC elements. A three-branch transmission line model is shown in Figure 31.

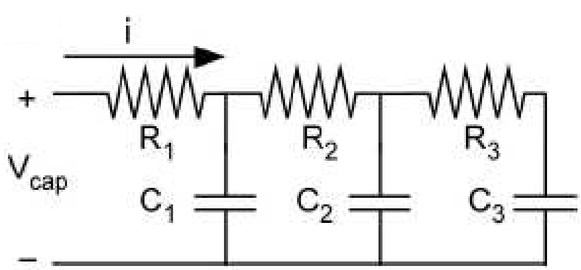

Figure 31 – RC transmission line model [31]

This model simulates the EC's physical structure and electromechanical characteristics directly. It has a clear physical meaning.

But the transmission line has a complex analytical expression which is not suitable for simulation.

2.3.4.4 RC series-parallel branch model

The RC series-parallel branch model is proposed in [31]. Figure 32 shows the principle circuit with three RC series-parallel branches.

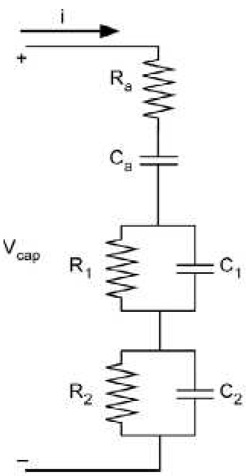

Figure 32 – RC branches series-parallel model [31]

R_a represents the equivalent series resistance, C_a and the other parallel RC branches represent the EC's pore impedance. For improved accuracy, the parameters can be dependent on the electrochemical capacitor temperature, voltage and operational frequency.

2.3.4.5 General RC network models

In some instances, it is not enough to simulate a real EC only by one of the RC models presented earlier. The above models can be expanded to a more general model. The number of branches can ideally be extended to infinity. Additionally, the EC has an inductance effect that should also be modeled, especially at high operating frequencies. Also, the effect of leakage current has been neglected in the earlier models. Figure 33 is a general RC parallel branch circuit model. The resistor R_p represents the leakage current losses and the series inductor L provides for the inductance effect at high frequencies.

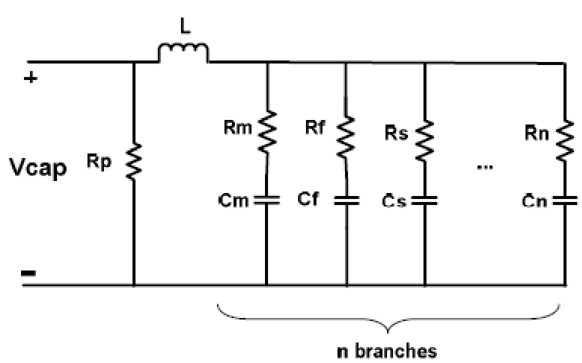

Figure 33 – General RC parallel branch model [31]

For EV applications, model robustness under transient and varying conditions is of utmost significance [33].

The three branch and classic models can better capture the dynamics of the tested EC in all the tests in comparison to the transmission line. Even though the classic model has a simpler structure and slightly better accuracy in the HPPC test, the dynamic model exhibits better robustness against varying loading conditions. [33]

In terms of model complexity, the classic model has the simplest structure. Only one ordinary differential equation (ODE) is sufficient to describe the state evolution during operation of the tested EC. Despite its desirable simplicity, it often fails to capture the highly dynamic voltage response of the tested EC. [33]

Since the aim of this work is to evaluate the electronics and the control structure to provide efficiently the energy available at battery and EC to the load and not precisely how the power sources behave, the classic model is going to be used.

2.4 Basic circuit

Once the battery and the EC models are defined, the basic circuit presented in Figure 34 is going to be used for the circuit modelling and later is going to get the interleaved portion and the 2-input power sources.

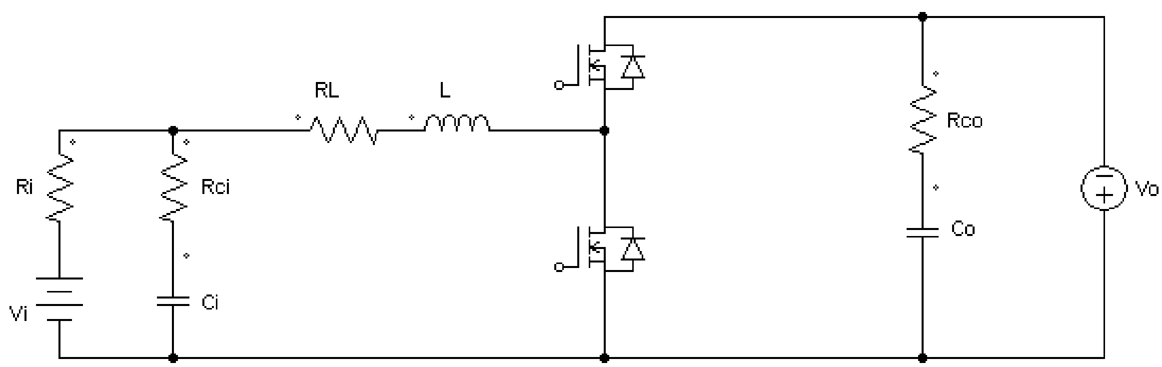

Figure 34 – Basic bi-directional DC-DC converter

Since the power demand for a bus is quite high, in each power source (battery and EC) is going to be applied a 3-phase interleaved bi-directional circuit. But both power sources are going to target the same rated voltage, therefore, one single circuit shall be calculated and replicated to the second.

2.5 Control strategy

The control strategy to be applied is described in [4], with the control diagram presented in Figure 35. The main strategy with this controlling system, is that blocks 1 and 2 are current controlled modes for the boost circuit from EC and battery respectively. Those control loops shall respond as quick as possible to new duty cycle demands. For that it is recommended to use a cutoff frequency one decade below the switching frequency.

The other block is the number 3, in which the output voltage V_o is controlled and this is mainly controlled by the EC. This control block shall be slower than the before mentioned controlling blocks, in order that the duty cycle is depending on the current demand (blocks 1 and 2) and the output voltage is dependent from the EC current (block 3). Therefore, the cutoff frequency for the block 3 controller shall be considered one decade below the cutoff frequency defined in blocks 1 and 2.

The last block is the number 4, which is the responsible for the battery control, which is going to supply the energy to the EC. This is the block, where the cutoff frequency defined by the load demand in frequency domain is applied. With that, it is possible to assure that the battery is going to act at low frequencies.

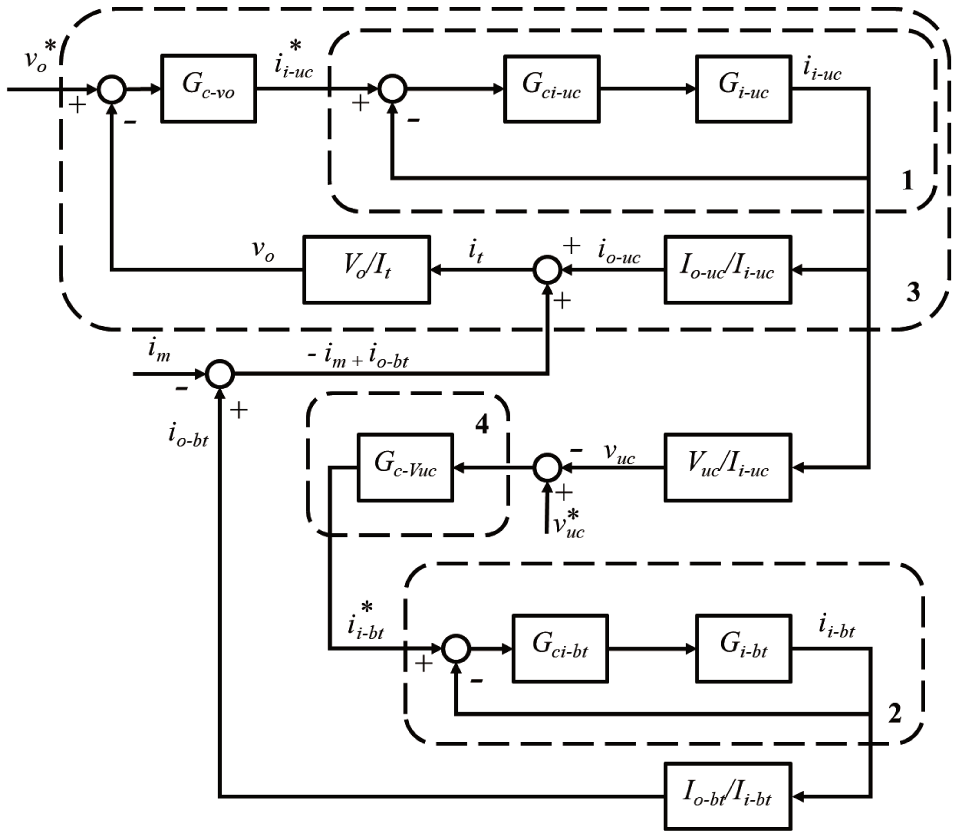

Figure 35 – Control diagram [4]

3 Dimensioning

3.1 Power demand analysis

The electric vehicle considered is a bus and the scope is focused on the DC-DC conversion and on the control system to manage the energy flow between the power sources and the drive train, which is considered a 3-phase asynchronous electric machine. The DC-AC converter is not part of this work, neither the electric machine. Therefore, the load considered is going to be a variable current source load.

In order to define the current demanded by the bus electric engine, it is necessary to define the bus torque demand in a defined cycle, thus derive the power necessary for the engine. Considering a DC constant voltage, it possible to derive the current consumption.

For the torque demand definition, it was primarily necessary to define the bus speed. The norm SAE J2711 – Recommended Practice for Measuring Fuel Economy and Emissions of Hybrid-Electric and Conventional Heavy-Duty Vehicles [34], defines several standard cycles for the measurement of fuel economy and emissions for heavy duty vehicles, which include buses. In this norm it is described three different driving cycles:

Manhattan cycle – the first recommended cycle, representing a lower speed operation, which is representative of transit bus operation in city service;

UUDS - heavy-duty Urban Dynamometer Driving Schedule, the second recommended cycle, representing higher speed operation, simulating operation in freeway;

Orange county – the third recommended cycle, representing a mid-speed operation.

One considered the Manhattan cycle, which represents an urban bus, more representative for electric vehicle buses, since the current driving range of an electric vehicle is not very high to apply it to long distances bus lines.

The Manhattan Cycle can be seen in Figure 36.

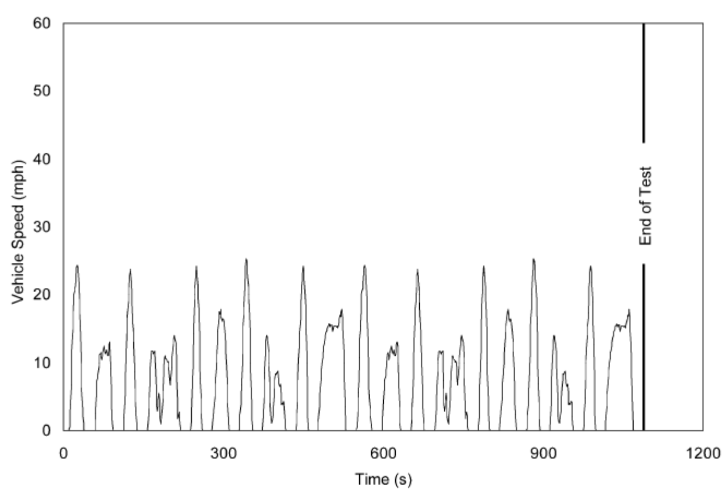

Figure 36 – Manhattan cycle [34]

In [35] it is described how to calculate the engine power demand, based on the speed profile.

It was defined in [35] that the required power for the vehicle according to the speed is:

$$P_{req} = \left[M_v \frac{dv}{dt} * v + 0{,}01 * \left(v + \frac{v^2}{100}\right) M_v \cdot g + \frac{1}{2} \cdot A_f \cdot C_d \cdot \rho \cdot v^3\right] \tag{3-1}$$

Where:

M_v: vehicle mass (it was 16 t, according to [36], however there is a significant difference between a fully loaded bus and an empty bus. It was considered in this case the empty bus weight, assuming that the electric bus is going to be smaller with a total weight of 16t, when fully loaded)
v: instant speed (defined by the Manhattan cycle)
g: gravity (9.81 m/s²)
A_f: front area (calculated 8.8m² as described below)

The bus front area was calculated based on the data available on [37]:

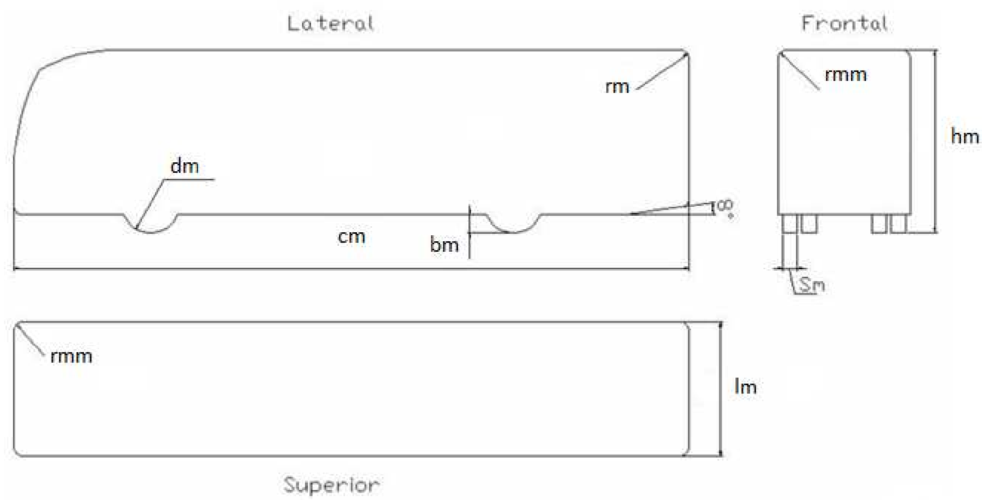

Figure 37 – Bus model dimensions [37]

Table 4 – Model dimensions with scale 1:17.5

Model dimensions [mm]	
Length (cm)	755
Height (hm)	208
Width (lm)	155
Distance to ground (bm)	22
Tire thickness (sm)	16
Front and rear radius (rm)	10
Lateral radius (rmm)	5

$h_{mf} = h_m - b_m$ = 186 mm x 17.5 = 3.255 m
l_m = 155 mm x 17.5 = 2.71 m
Front area $A_f = h_{mf} \times l_m$ = 8.8 m²

C_d: aerodynamic drag coefficient (conventional bus C_d = 0.6 – 0.7 according to [8]; it was defined 0.65 for this work)
ρ: air density (1.2258)

It was used the same Matlab program from [35] for this work (Appendix 1). However, it was adjusted the parameters as described before and also a new transmission relation, based on the data sheet [38] – Mercedes Bus OF-1721 was inserted. It is also important to mention that an efficiency of 94% was considered for the energy transfer from the bus wheels to the engine torque demand.

Simulating the power demand of a bus performing the Manhattan cycle, using the software Matlab from [35], the following graphs were obtained:

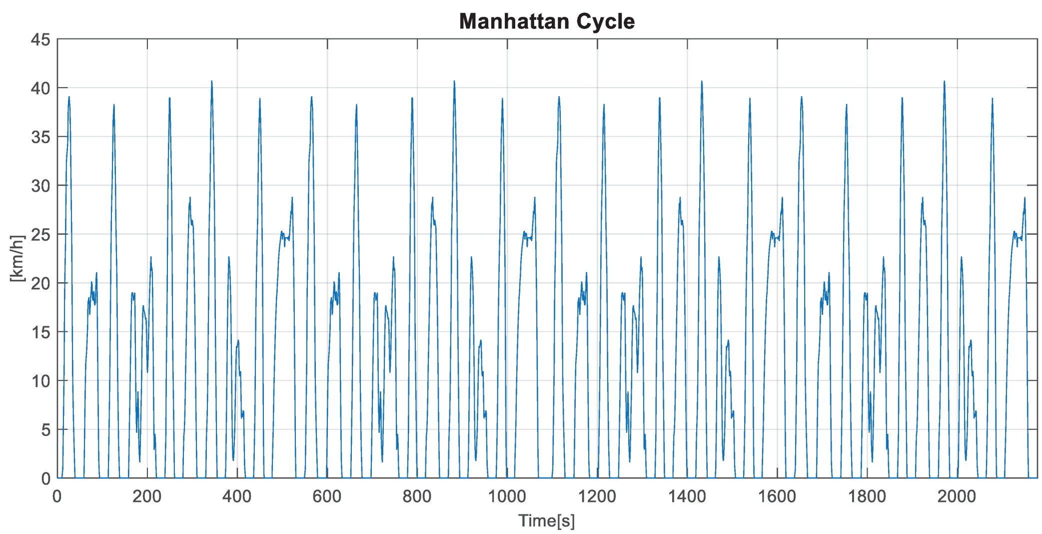

Figure 38 – Manhattan cycle (time vs. Speed)

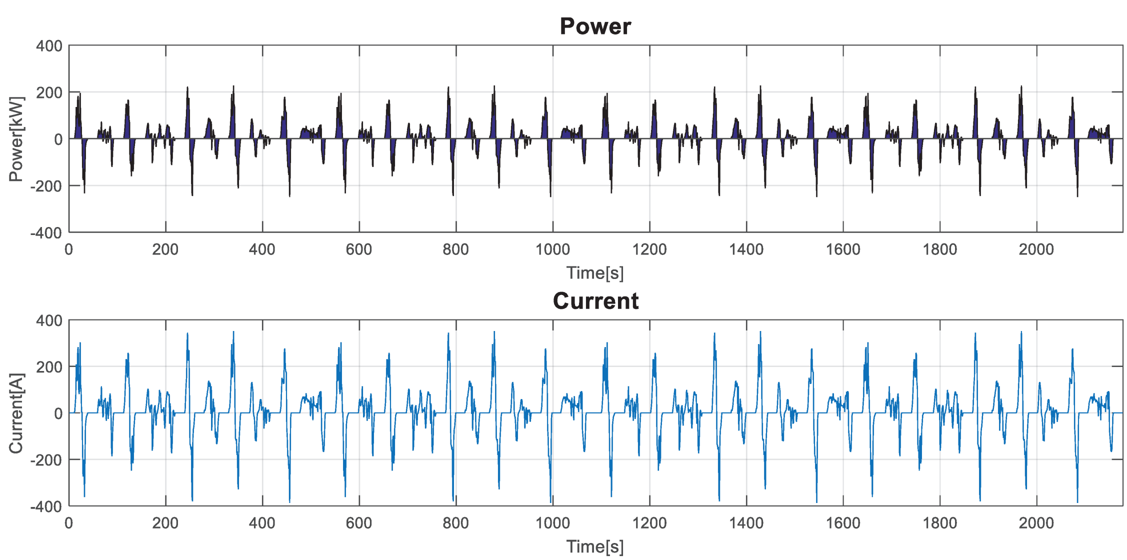

Figure 39 – Power and current demand

Maximal power required during traction in the Manhattan cycle is 226.71kW. While during regenerative braking power, the peak is 249.6 kW. It means that during the regeneration, the highest value will be found and the demand on the electronics should be considered at this point. On the other hand, the average power demand during the Manhattan cycle is 5.37 kW which is 50 times lower than the highest peak (249.6 kW).

It means that the battery and EC bank to be considered must be adequate to supply the power peaks and the electronics must be designed to accomplish this demand.

It is going to be considered a drive train electric machine as a 380V three-phase engine. For the definition of the DC link, it is necessary to determine the peak voltage for the rectifier.

$$V_{peak} = 380 \cdot \sqrt{2} = 537V$$

Considering 20% margin

$$V_{peak} = 645V = DC\ link\ voltage$$

Considering the converter output voltage constant, at 645V, the maximum current required will be 351.5 A for traction and 386.98 A during regenerative breaking.

Additionally, it is necessary to define the voltage sources. In order to work in CCM it is reasonable to define as a steady state duty cycle 50%. Thus, the battery and EC voltage should be considered 322V. Since batteries are commonly defined as modules of 48V, it will be defined the voltage sources at 336V.

$$V_i = 336V$$

3.2 Battery dimensioning

For the battery analysis, it was considered only the positive values from the consuming power, as no regenerative power could be recovered. The values can be seen on Figure 40.

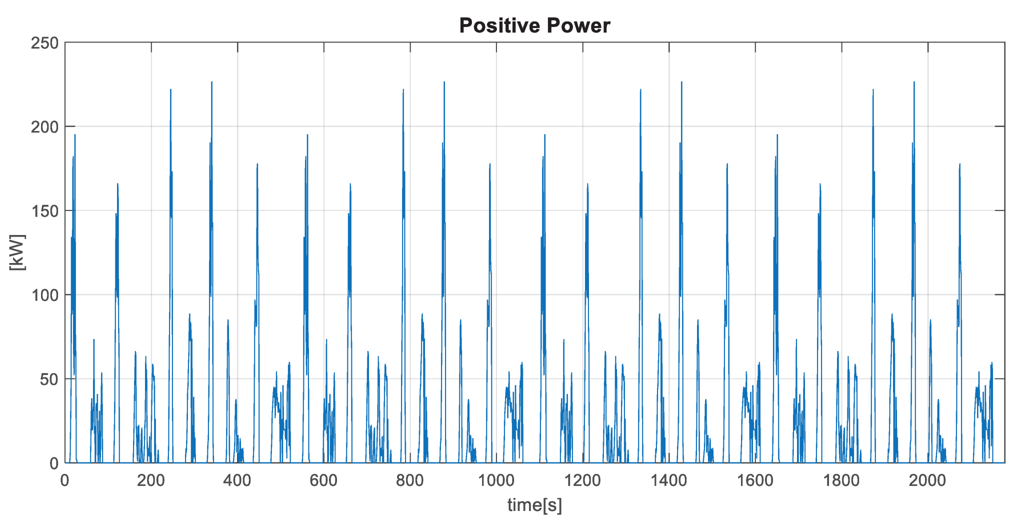

Figure 40 – Positive power values

The average value of the positive power is approximately 19.7 kW. The Manhattan cycle considers a total time of 2178s, which represents 36.3 minutes. This period of time can be considered the total time for the urban bus to complete its way from first bus station until the last bus station. This cycle can be considered to be traveled 8 times per day, which means that the battery energy should be calculated to supply for one day 290.4 minutes or 4.84h.

The energy required for the battery is then,

$$W = 19.7 \times 10^3 \times 4.84 = 95.35\ kWh$$

Therefore, the battery shall be a 336V with 96 kWh power.

Considering a li-ion battery and the values on Table 1, the specific energy is 135 Wh/kg, therefore, this battery is going to weight approximately 711kg.

3.3 EC dimensioning

It was used the power calculated previously from Figure 39, but considering the power modulus ($\sqrt{Power^2}$) in order to evaluate the total power demanded for the EC, independently if it is consuming of recovering energy. The values can be seen on Figure 41.

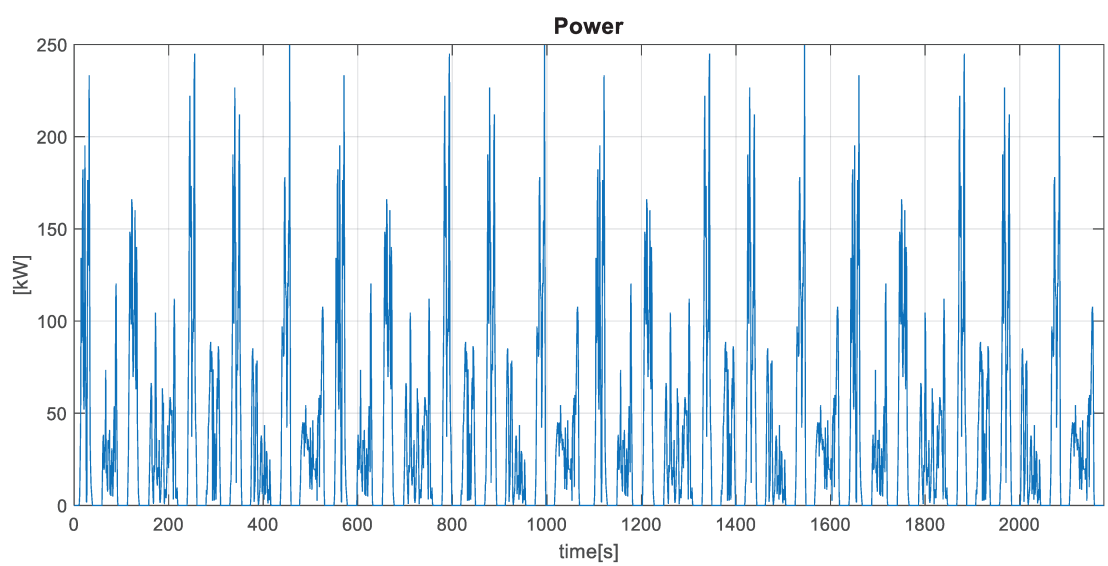

Figure 41 – Power Modulus

As observed in Figure 41, the average power is 34 kW and the power peak is 249.6 kW.

The EC nominal voltage is going to be the same as the battery voltage, thus 336V. But the EC should be able to absorb energy and release energy as required by the load demands. For this strategy, it is quite reasonable to define a working voltage range for the EC from 200V up to 400V. The capacitor energy is calculated by

$$W = \frac{1}{2}C(V_a^2 - V_b^2)$$

(3-2)

Where, V_a and V_b are the voltages in which the capacitor might vary. Therefore, the minimal capacitance value to be considered shall be at the minimal working voltage at maximal power consumption:

$$249.6 \times 10^3 = \frac{1}{2}C \cdot (400^2 - 200^2)$$

$$C_{EC} = 4.2F$$

Considering some safety factor on this capacitance value, it was adopted the capacitance of **5F**.

3.4 Cutoff frequency definition

As proposed by [8], in order to assure that the battery work as close as possible to a constant power supply for the enhancement of battery's lifetime, a frequency analysis is done. For this strategy it is suggested to divide the power into dissipative and conservative. In this way it is possible to determine more efficiently the control algorithm to optimize the use of battery and EC, based on their characteristics.

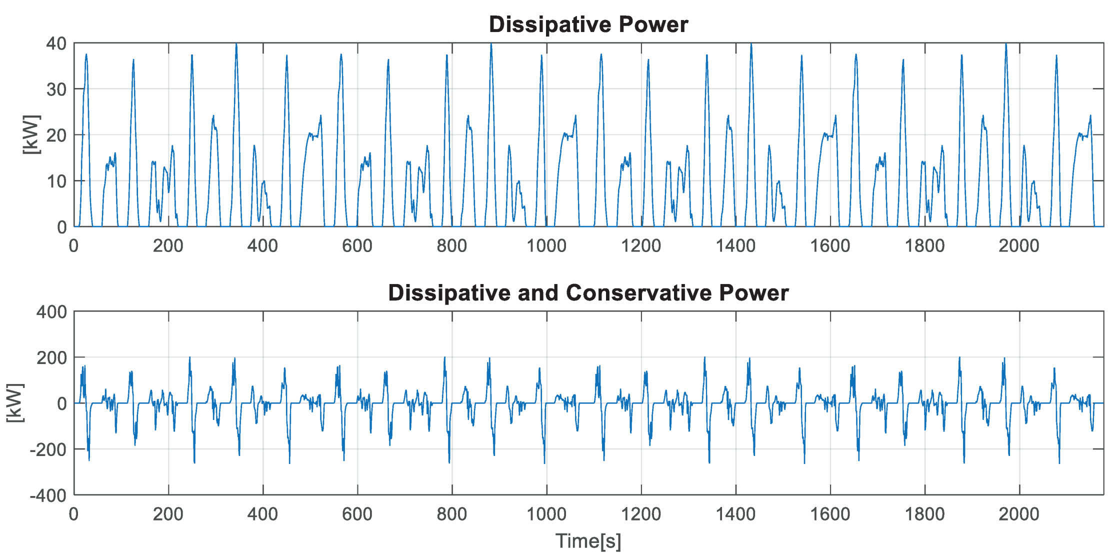

Figure 42 – Dissipative and conservative power

As observed in Figure 42, the dissipative power is the energy spent on dragging, friction and rolling forces, always positive and cannot be recovered. The conservative power is the energy provided to the vehicle kinetics, which can be recovered.

For the control strategy, it was used [4], [3] suggestion, creating the FFT from the conservative and dissipative power in order to define a cutoff frequency to determine when the battery and EC should actuate.

Using the Matlab FFT function it was created the Figure 43.

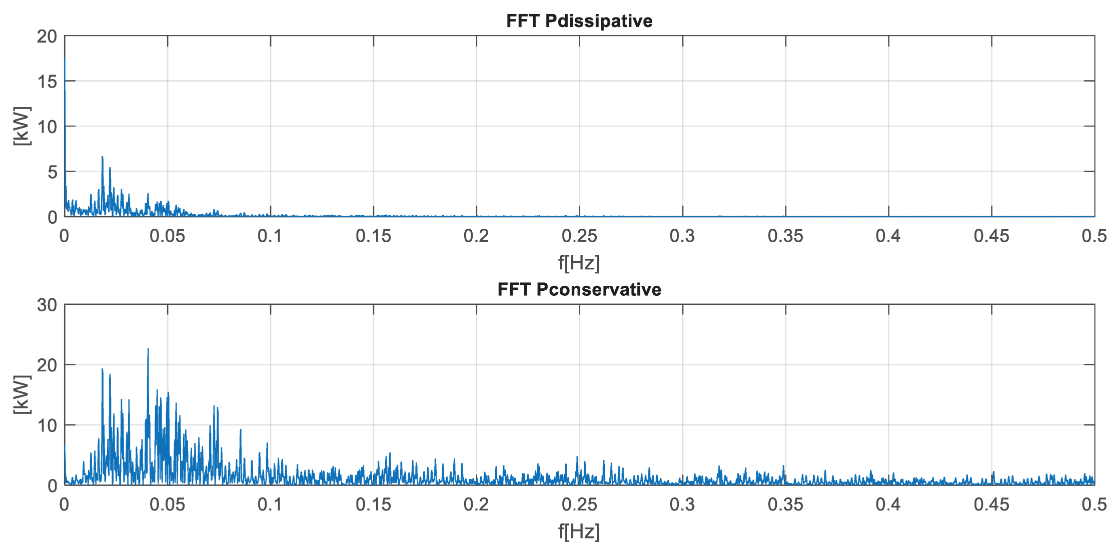

Figure 43 – FFT from dissipative and conservative power

It is possible to observe in Figure 43 that using the Manhattan cycle, the power demand is localized in frequencies below 500 mHz. The dissipative power is below 100 mHz.

In Figure 43, it can be observed that at 0.02 Hz there are still high conservative power peaks, which should be dealt by the EC. It was then created a new graph from 0 to 25 mHz as can be observed in the Figure 44.

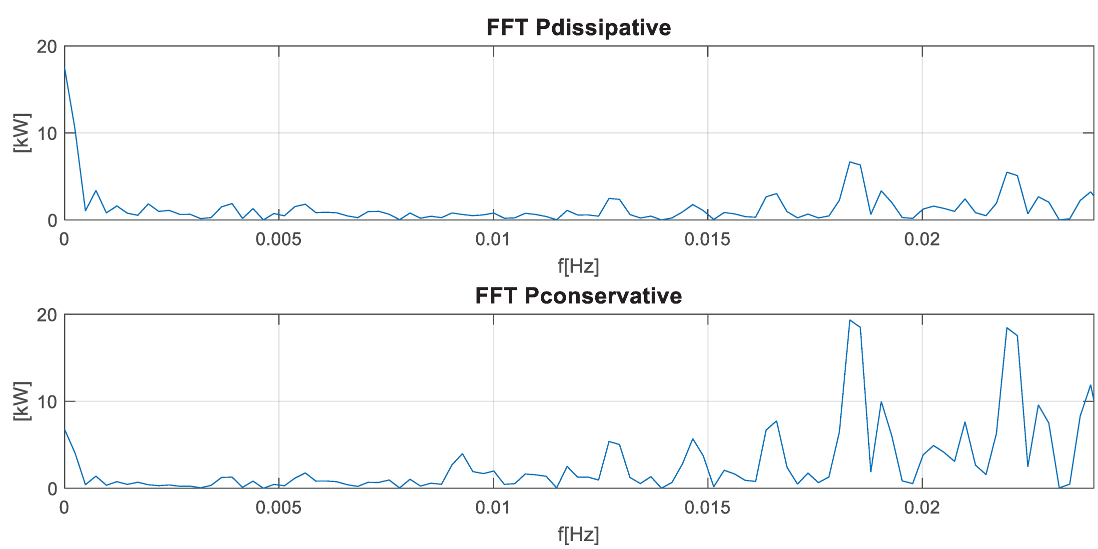

Figure 44 – FFT dissipative and conservative power from 0 to 18 mHz

Based on Figure 44, it was defined 0.01 Hz as a suitable cutoff frequency for the control strategy.

3.5 Thermal analysis

Before the rest of the circuit components is calculated, it is important to define the switching frequency and then if the transistors will be capable to switch in such frequency with the amount of current demanded.

In a first moment a suitable switching frequency to be adopted is 25 kHz, due to the fact that it minimizes the effect of parasitic capacitances, additionally, in such frequency there is no risk of sound noise issues that the human being is able to hear (generally the human ear, is capable to hear from 20Hz up to 20kHz).

As calculated in section 3.1, the maximal current draw demanded is 352A during power supply from power source to powertrain and 390A as regenerative energy (from powertrain to power source). Those values are related to the output current, but the input current in a boost converter is the output divided by the duty cycle. Considering a duty cycle of 50%, the input current which is going through the transistor is 780A in worst case.

For such high current and high frequency, it is necessary to use a SiC (silicon carbide) MOSFET, due to its properties of low power dissipation. It was searched for SiC transistors and it was found a 1200V, 200A SiC Mosfet from Infineon (FF11MR12W1M1_B11, [39]).

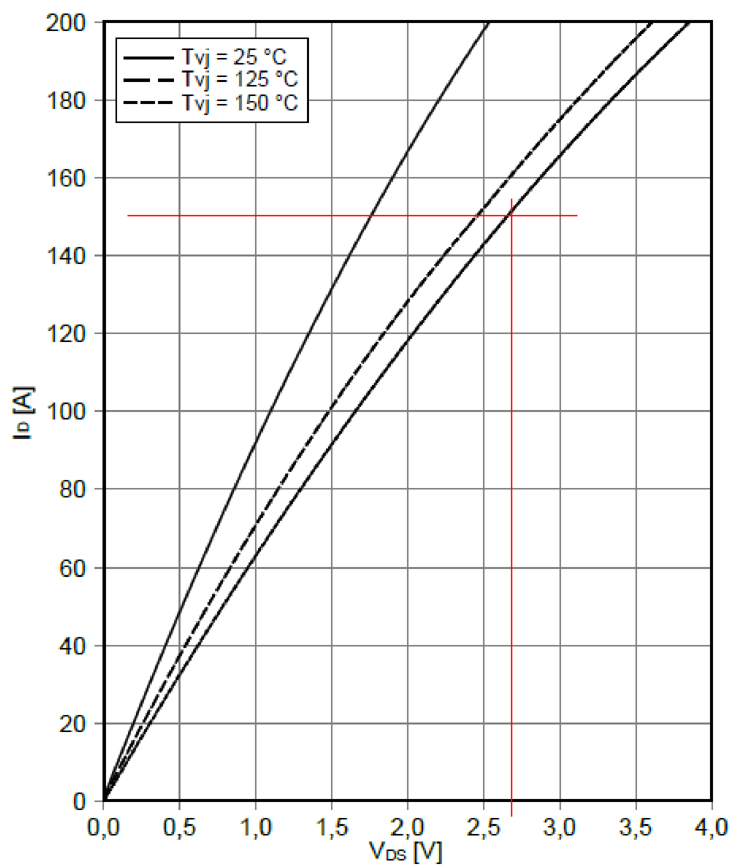

Figure 45 – MOSFET output characteristic [39]

In this case, since the rated current can reach 780A and the component maximal allowed current is 200A, it was considered a 3-phase interleaved circuit. When applying the interleaved topology, the RMS current is divided by $\sqrt{3}$ in each phase, therefore, the current in each transistor is:

$$\frac{780}{\sqrt{3}} = 450.35A$$

This current is still too high for the chosen transistor. Then, a suitable solution is to include parallel transistors in each interleaved phase. In this case, 3 parallel transistors are required for each interleaved phase. Thus,

$$\frac{450.35}{3} = 150.11A$$

Based on the transistor datasheet [39], considering the rated current in each transistor of 150A, in Figure 45 it can be observed the V_{DS} is approximately 2.5V. Thus, the power losses during conduction can be defined as

$$P_{ON} = I_D \cdot V_{DS} \cdot d \tag{3-3}$$

Where, *d* is the duty cycle, which can be considered 50%. Thus, the conduction losses (P_{ON}) is 187.5W.

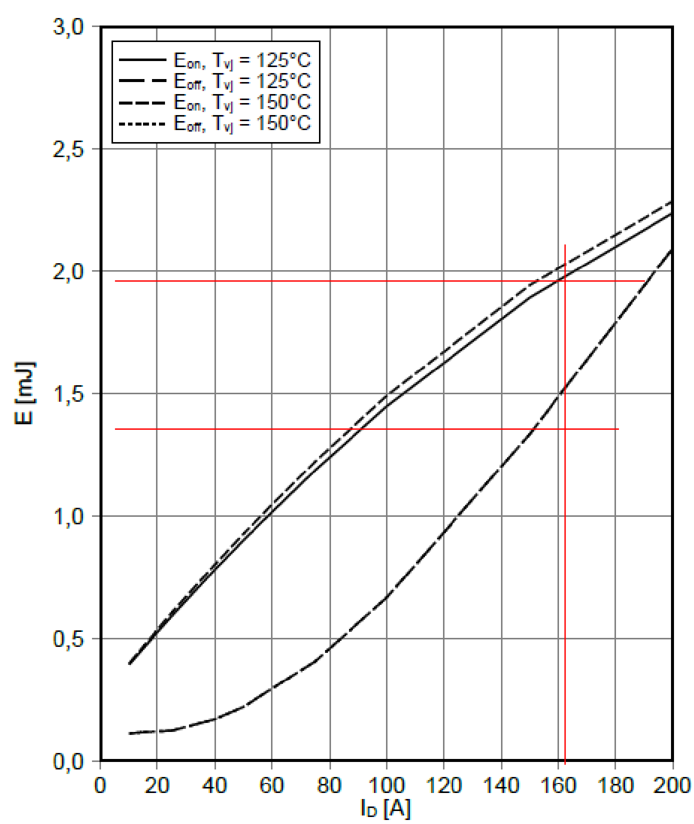

Figure 46 – MOSFET switching losses [39]

The switching losses are calculated in two different time slots, at the transistor switching ON time and at switching OFF time. From Figure 46, at rated current 150 A it is possible to obtain the ON and OFF energy, which are respectively E_{ON} = 1.9 mJ and E_{OFF} = 1.3 mJ.

It is known that power can be calculated as

$$P = E \cdot f \tag{3-4}$$

Where *P* is the power, *E* is the energy and *f* is the switching frequency.

$$P_{t-ON} = 1.9 \times 10^{-3} \cdot 25 \times 10^{3} = 47.5W$$

$$P_{t-OFF} = 1.3 \times 10^{-3} \cdot 25 \times 10^{3} = 32.5W$$

Therefore, the total power losses during one period is

$$P_{TOTAL} = 187.5 + 47.5 + 32.5$$

$$P_{TOTAL} = 267.5W$$

In order to evaluate the temperature at junction in the transistor, to see if the working conditions are adequate, it can be considered the circuit showed in Figure 47, where the resistor is the thermal resistance from junction to heatsink from datasheet.

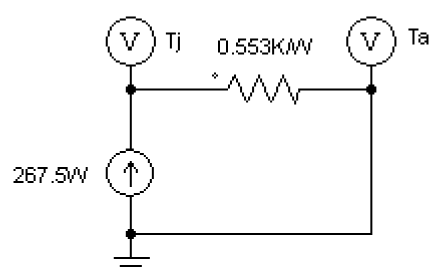

Figure 47 – Thermal circuit

Thus,

$$T_j - T_a = 267.5 \cdot 0.553$$

Considering that the maximal working temperature that the circuit will be working is 60ºC (*Ta*),

$$T_j = 208\ ^{\circ}\mathrm{C}$$

This temperature is above the maximal allowed working temperature for the chosen transistor (maximal value is 150ºC, according to datasheet).

For this reason, the switching frequency shall be reduced to allow the working conditions to be favorable for the transistors.

It was then defined a new switching frequency of 20 kHz. Just considering the switching frequency reduction, the junction temperature is going to reach 199°C, which still is above the transistor limit. Therefore, it was also considered an additional parallel transistor in each phase of the interleaved topology to divide even further the current in each phase. Thus, instead of 3, there is going to be 4 parallel transistors in each interleaved phase. In this case, each transistor is going to conduct in worst case condition 112.6A.

Based on the transistor datasheet [39], considering the rated current in each transistor of 112.6A, in Figure 45 it can be observed the V_{DS} as 1.6V. Thus, the power losses during conduction can be calculated as

$$P_{ON} = 112.6 \cdot 1.6 \cdot 0.5$$

P_{ON} is 90.1W.

From Figure 46, at rated current 112.6A the ON and OFF energy are respectively E_{ON} = 1.6 mJ and E_{OFF} = 0.8 mJ.

$$P_{t-ON} = 1.6 \times 10^{-3} \cdot 20 \times 10^{3} = 32W$$

$$P_{t-OFF} = 0.8 \times 10^{-3} \cdot 20 \times 10^{3} = 16W$$

Therefore, the total power losses during one period is

$$P_{TOTAL} = 90.1 + 32 + 16$$

$$P_{TOTAL} = 138.1W$$

Calculating the temperature at junction, based on Figure 47,

$$T_j - T_a = 138.1 \cdot 0.553$$

Considering that the maximal working temperature that the circuit will be working is 60ºC,

$$T_j = 136\ °\mathrm{C}$$

Therefore, in a worst-case condition (at maximal environmental temperature and at maximal engine power consumption) the junction temperature is below the maximal allowed junction temperature, with a safety factor of 10%.

3.6 Inductance definition

As described in [8], it is necessary to define ideal values for the inductor and capacitor which are going to be used in the converter, to assure that the converter is going to work on CCM in all conditions. Additionally, it is important to define the components in such a way that the current and voltage variation caused by the components are not going to disturb (or even damage) the input power source (in the case of the inductor) or the output voltage (in case of the capacitor).

In [6] it is defined the minimal inductance required in a boost or step-up converter to work on CCM:

$$L_{min} = \frac{V_i.\delta.(1-\delta).\tau}{2.I_{0(min)}} \tag{3-5}$$

Where,
V_i = input voltage
δ = duty cycle
τ = period
I_o = output current

Considering only the traction portion of the required current, and that at the standard operation mode the duty cycle is going to work at 50% to step up the battery or EC voltage from 336V to 645V, and the average output current from the traction portion (it means, only the positive values from current were considered), the output current is 73.15A. The switching frequency defined for this converter is 20 kHz a described previously.

Thus:

$$L_{min} = \frac{336 \times 0.5 \times (1-0.5) \times 50.10^{-6}}{2 \times 73.15}$$

$$L_{min} = 28.71\ \mu H$$

On the other hand, the inductor shall be designed to limit the input current oscillation in all loading conditions. The inductor current working in a step-up converter in the CCM, can be described according to the Figure 48:

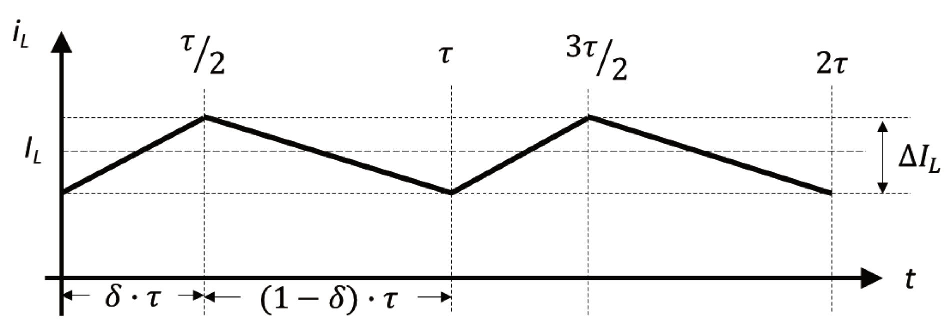

Figure 48 – Inductor current [8]

The design target is to limit the value of ΔI_L.

At the maximal power consumption, the output voltage is constant at 645V and the output current is 350A. Considering the input voltage as constant, 336V, and the converter has no losses, the input current at maximal power consumption can be defined as:

$$P_i = P_o$$

$$V_I \times I_i = V_0 \times I_0$$

$$I_i = 671.87\ A$$

At such conditions of maximal power demand, it is allowed to have a high oscillation on the current, because such conditions are so quite often. In this case it was considered 40% oscillation allowed, which will be later minimized by interleaved switches.

The inductance can be calculated as:

$$L \times \frac{\Delta I_i}{\Delta t} = V_i$$

$$\Delta I_i = 40\%\ I_i = 268.75\ A$$

Considering the duty cycle at 50% to step up from 336 to 645, Δt is going to be 25 µs. Therefore,

$$L = 31.26\ \mu H\ \rightarrow L = 32\ \mu H$$

Since this inductance is higher than the minimal inductance to work on CCM, this is the value to be considered in the circuit.

For the simulation, it was considered an equivalent series resistance (ESR) with a value observed in [40] of 9.8 mΩ.

3.7 Capacitance definition

For the capacitance definition, it is known that the capacitance equation is

$$C = \frac{\Delta Q}{\Delta V} \tag{3-6}$$

And,

$$\Delta Q = I \times \Delta t \tag{3-7}$$

Thus,

$$C = \frac{I \times \Delta t}{\Delta V} \tag{3-8}$$

The maximal current output as 350 A. It is desirable that the output voltage is constant and stable for the DC link, then it was decided that the voltage oscillation shall be around 1%. In this case the minimal capacitance shall be

$$C = 1.3566\ mF$$

For this work it was considered a capacitance of 2 mF and the ESR of the capacitor was used the value from [40] of 5 mΩ.

In summary, the inductors and capacitors used in this work are:

Table 5 – Inductor and capacitor values for the simulation

Inductor	*L* = 32 µH	*ESRL* = 9.8 mΩ
Capacitor	*C* = 2 mF	*ESRC* = 5 mΩ

3.8 Capacitive filter

To avoid ripple effect on the battery and on the EC output voltages it was defined a simple capacitive filter, as can be observed in Figure 49, where C_{in} is the capacitive filter for the input power source, battery or EC.

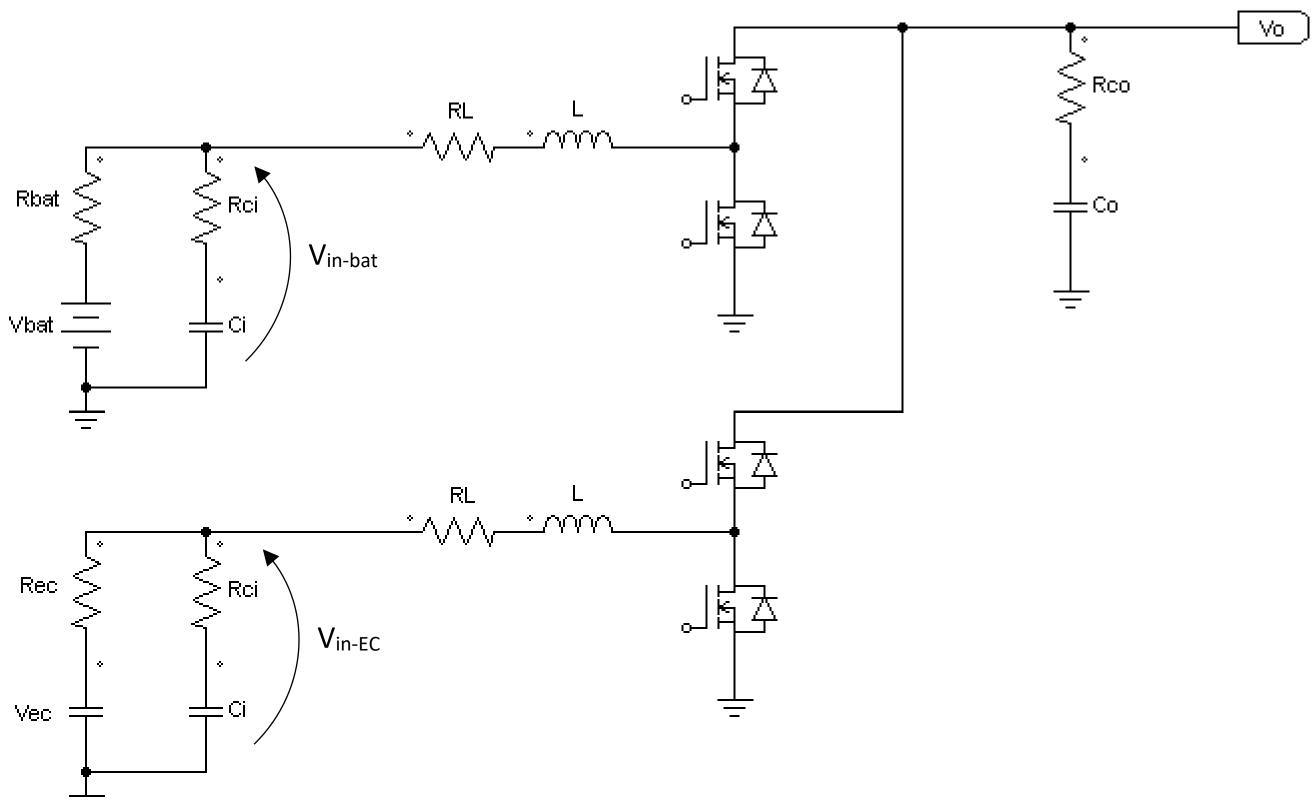

Figure 49 – Multiple input bi-directional converter

Considering that

$$\frac{V_{in}}{V_{bat}} = \frac{1 + sC_iR_{Ci}}{1 + sC_i(R_{bat} + R_{Ci})} \tag{3-9}$$

in this case,

R_{bat} = 0.013;
R_{Ci} = 0.074;
C_i = 0.001;

$$G = \frac{7.4 \cdot 10^{-5}\ \mathrm{s}\ +\ 1}{8.7 \cdot 10^{-5}\ \mathrm{s}\ +\ 1}$$

f_z = 2.1507e+03
f_p = 1.8294e+03

The Bode plot of the capacitive filter can be seen in Figure 50:

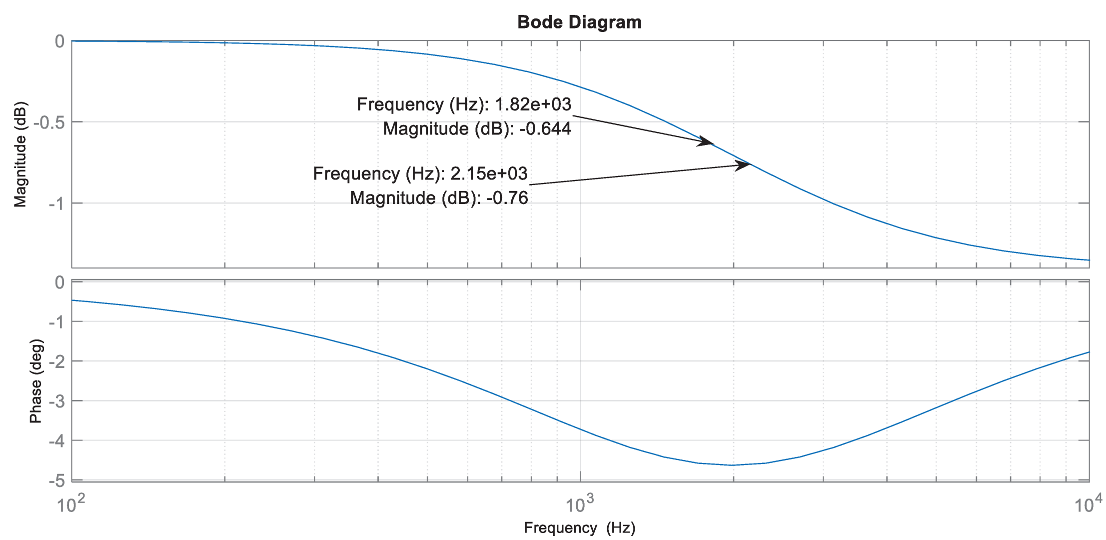

Figure 50 – Bode plot capacitive filter

Step response for the V_{bat} circuit portion can be observed in Figure 51:

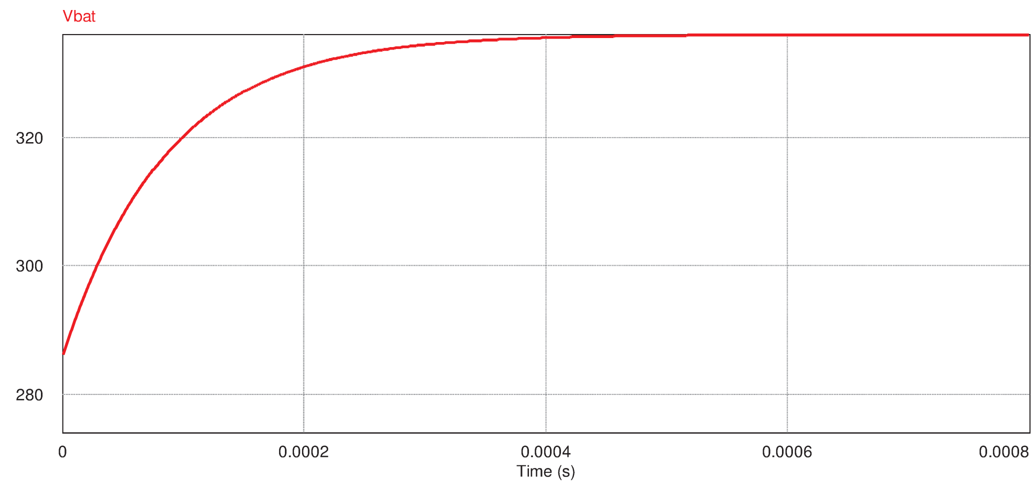

Figure 51 – Step response of the battery capacitive filter – PSIM simulation

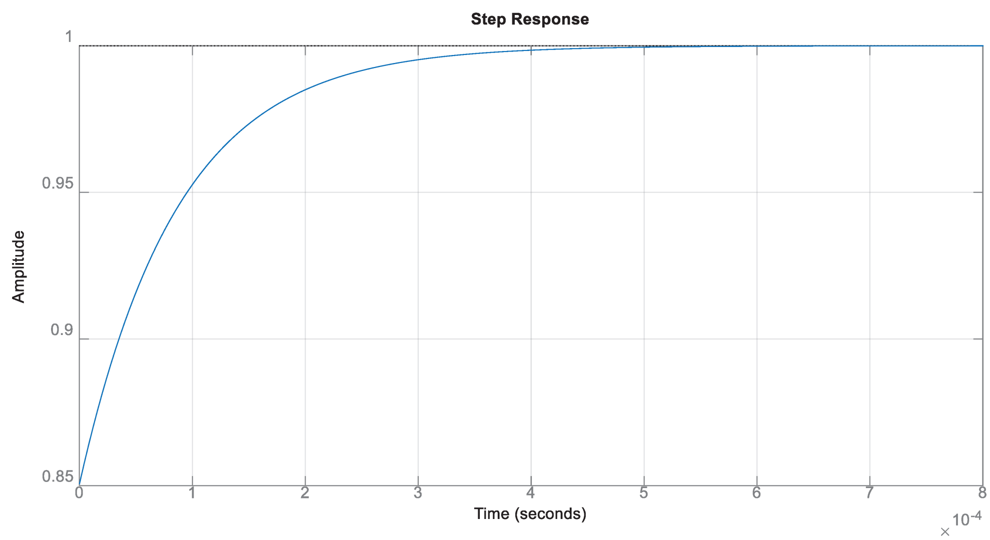

Figure 52 – Step response of capacitive filter transfer function in Matlab

Comparing Figure 51 and Figure 52 which are the step response from the circuit and the capacitive filter transfer function respectively, it is possible to observe that both simulations present similar results, thus the calculation is validated.

FFT of the V_{bat} step response can be seen below on Figure 53:

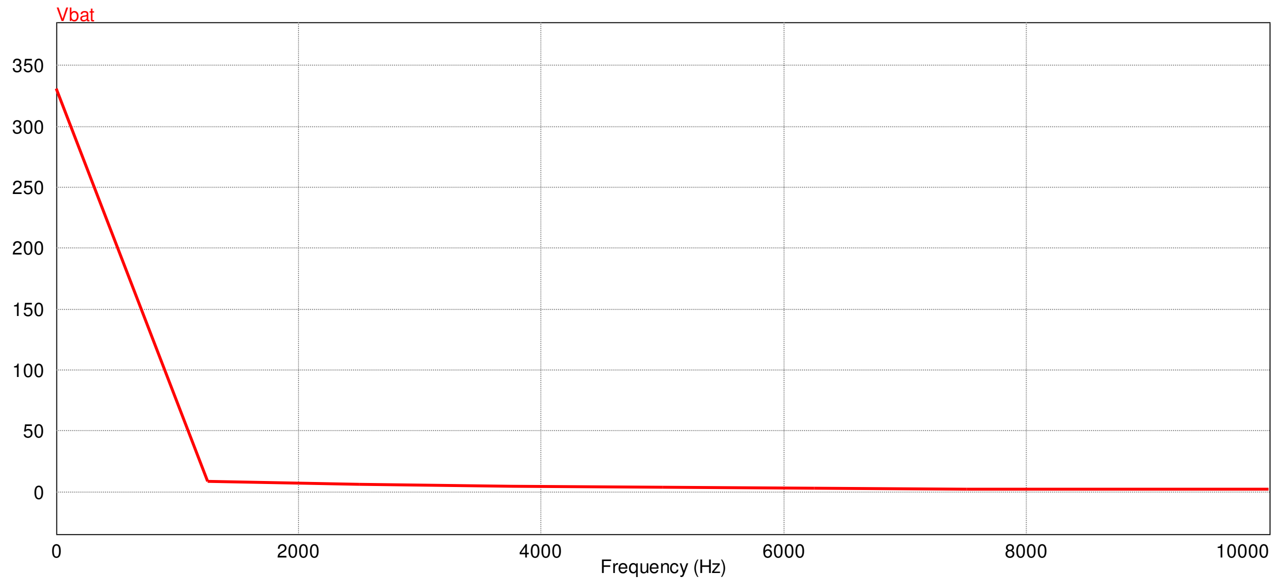

Figure 53 – FFT of step response of battery capacitive filter

Based on Figure 53 , it is possible to observe that the capacitive filter is acting as planned filtering frequencies above 2 kHz.

3.9 Circuit calculation

As described in chapter 4.7, the basic circuit used for the controlling analysis is the one considered in Figure 54:

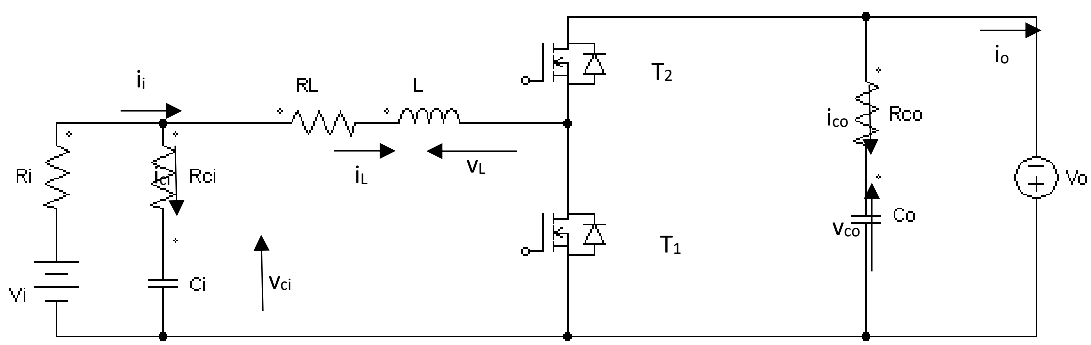

Figure 54 – Bi-directional DC-DC converter

Considering the state space variables:

$$x = \begin{bmatrix} v_{co} \\ v_{ci} \\ i_L \end{bmatrix} \tag{3-10}$$

It can be determined that at T_1 ON:

$$v'_{co} = \frac{-I_o}{C_o}$$

(3-11)

$$v'_{ci} = v_{ci}\left[\frac{-1}{C_i(R_i + R_{ci})}\right] + i_L\left[\frac{-R_i}{C_i(R_i + R_{ci})}\right] + V_i\left[\frac{1}{C_i(R_i + R_{ci})}\right]$$

(3-12)

$$i'_L = v_{ci}\left[\frac{R_i}{L(R_i + R_{ci})}\right] + i_L\left[-\frac{R_iR_L + R_iR_{ci} + R_LR_{ci}}{L(R_i + R_{ci})}\right] + V_i\left[\frac{R_{ci}}{L(R_i + R_{ci})}\right]$$

(3-13)

Therefore:

$$\dot{x} = A1\,x + B1\,U_i$$

(3-14)

$$\dot{x} = \begin{bmatrix} 0 & 0 & 0 \\ 0 & \frac{-1}{C_i(R_i + R_{ci})} & \frac{-R_i}{C_i(R_i + R_{ci})} \\ 0 & \frac{R_i}{L(R_i + R_{ci})} & -\frac{R_iR_L + R_iR_{ci} + R_LR_{ci}}{L(R_i + R_{ci})} \end{bmatrix} x + \begin{bmatrix} \frac{-1}{C_o} & 0 \\ 0 & \frac{1}{C_i(R_i + R_{ci})} \\ 0 & \frac{R_{ci}}{L(R_i + R_{ci})} \end{bmatrix} \begin{bmatrix} I_o \\ V_i \end{bmatrix}$$

(3-15)

At T_1 off:

$$v'_{co} = \frac{i_L}{C_o} - \frac{I_o}{C_o}$$

(3-16)

$$v'_{ci} = v_{ci}\left[\frac{-1}{C_i(R_i + R_{ci})}\right] + i_L\left[\frac{-R_i}{C_i(R_i + R_{ci})}\right] + V_i\left[\frac{1}{C_i(R_i + R_{ci})}\right]$$

(3-17)

$$i'_L = -\frac{v_{co}}{L} + v_{ci}\left[\frac{R_i}{L(R_i + R_{ci})}\right] + i_L\left[-\frac{R_iR_L + R_iR_{ci} + R_LR_{ci} + R_{co}(R_i + R_{ci})}{L(R_i + R_{ci})}\right] + V_i\left[\frac{R_{ci}}{L(R_i + R_{ci})}\right] + I_o\frac{R_{co}}{L}$$

(3-18)

Therefore:

$$\dot{x} = A2\,x + B2\,U_i$$

(3-19)

$$\dot{x} = \begin{bmatrix} 0 & 0 & \frac{1}{C_o} \\ 0 & \frac{-1}{C_i(R_i + R_{ci})} & \frac{-R_i}{C_i(R_i + R_{ci})} \\ \frac{-1}{L} & \frac{R_i}{L(R_i + R_{ci})} & -\frac{R_iR_L + R_iR_{ci} + R_LR_{ci} + R_{co}(R_i + R_{ci})}{L(R_i + R_{ci})} \end{bmatrix} x + \begin{bmatrix} \frac{-1}{C_o} & 0 \\ 0 & \frac{1}{C_i(R_i + R_{ci})} \\ \frac{R_{co}}{L} & \frac{R_{ci}}{L(R_i + R_{ci})} \end{bmatrix} \begin{bmatrix} I_o \\ V_i \end{bmatrix}$$

(3-20)

The output variable is considered V_o. Thus, at T_1 on:

$$V_o = C1\, x + E1\, U_i$$

(3-21)

$$V_o = \begin{bmatrix} 1 & 0 & 0 \end{bmatrix} x + \begin{bmatrix} -R_{co} & 0 \end{bmatrix} \begin{bmatrix} I_o \\ V_i \end{bmatrix}$$

(3-22)

At T_1 off:

$$V_o = C2\, x + E2\, U_i$$

(3-23)

$$V_o = \begin{bmatrix} 1 & 0 & R_{co} \end{bmatrix} x + \begin{bmatrix} -R_{co} & 0 \end{bmatrix} \begin{bmatrix} I_o \\ V_i \end{bmatrix}$$

(3-24)

As described in [41],

$$\frac{V_o(s)}{D(s)} = C \cdot [s \cdot I - A]^{-1} \cdot [(A_1 - A_2) \cdot x + (B_1 - B_2) \cdot U_i] + (C_1 - C_2) \cdot x$$

(3-25)

$$\frac{i_L(s)}{D(s)} = C \cdot [s \cdot I - A]^{-1} \cdot [(A_1 - A_2) \cdot x + (B_1 - B_2) \cdot U_i]$$

(3-26)

$$\frac{i_i(s)}{D(s)} = [C + G \cdot A] \cdot [s \cdot I - A]^{-1} \cdot [(A_1 - A_2) \cdot x + (B_1 - B_2) \cdot U_i] + G \cdot (A_1 - A_2) \cdot x + G \cdot (B_1 - B_2) \cdot U_i$$

(3-27)

Where *A1*, *A2*, *B1*, *B2*, *C1*, *C2*, *E1*, *E2* are described on the previous equations. *G1* and *G2* are zero, and *A* is

$$A = A_1 \cdot D + A_2 \cdot (1 - D)$$

(3-28)

Those equations were implemented in Matlab for the transfer functions calculations and the Bode plots creation (appendix 2). The implementing of the control system is going to be discussed in the next chapter.

3.10 Controllers calculation

3.10.1 Control blocks 1 and 2

The control strategy was explained in section 2.5. Considering that the switching frequency adopted was 20 kHz, it is reasonable to define the cutoff frequency for the blocks 1 and 2 (current control over duty cycle) at 2.0 kHz (one decade below the switching frequency).

The first step is to define the control of the inner control loop 1. The block $G_{i\text{-}uc}$ is the plant model that correlates the input current (i_L) with its control variable (duty cycle d).

As described in chapter 3.9, the transfer function that describes the input current with the duty cycle is equation (3-26):

$$\frac{i_L(s)}{D(s)} = C \cdot [s \cdot I - A]^{-1} \cdot [(A_1 - A_2) \cdot x + (B_1 - B_2) \cdot U_i]$$

(3-29)

Considering the values of inductors and capacitors defined previously, using the Matlab it was possible to get the transfer function:

$$\frac{i_L(s)}{d(s)} = \frac{1.9998 \cdot 10^7 (s + 274.6)}{(s^2 + 793.1s + 3.928 \cdot 10^6)}$$

(3-30)

The Bode plot of $G_{i\text{-}ec}$ is shown in Figure 55

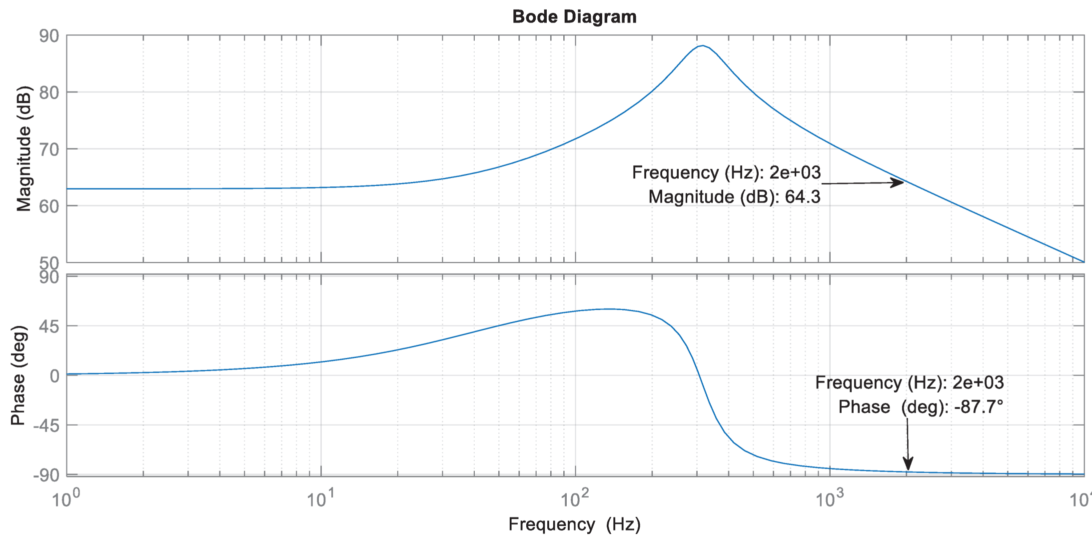

Figure 55 – $G_{i\text{-}uc}$ Bode plot

The cutoff frequency defined for the inner loop, which must be very fast, was defined as 2.0 kHz. At this point the magnitude is 64.3 dB and the phase is -87.7º.

Using the *K* factor calculation described in [42], considering that a type II controller is required and a phase margin of 60º was defined, it was calculated the controller $G_{ci\text{-}uc}$ as

$$G_{ci-uc} = \frac{0.0002748\ \mathrm{s}\ +\ 1}{1.039 \cdot 10^{-5}\, s^2 + 0.4508\ \mathrm{s}} \tag{3-31}$$

As it can be observed in the Bode plot in Figure 56, the controller is assuring 0 dB and 60º phase margin at the cutting frequency.

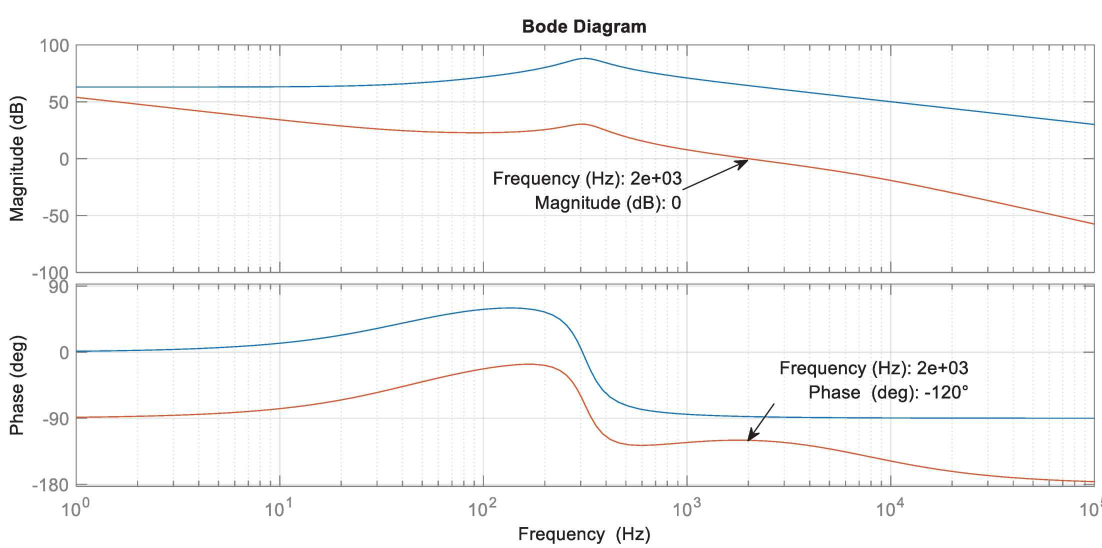

Figure 56 – $G_{ci\text{-}uc}$ Bode plot

Since the battery and the EC bi-directional DC-DC converter are considered with the same inductor and capacitor values and also the voltage at the EC is going to be controlled to be as close as possible to the battery voltage of 336V, it can be considered that both inner loop, current control 1 and 2 have the same plant and controller.

3.10.2 Control block 3

The block 3, in which the output voltage V_o is controlled mainly by the EC, it shall be slower than blocks 1 and 2, therefore the cutoff frequency is going to be 200 Hz (one decade below blocks 1 and 2).

For this step, it is required to define the controller $G_{c\text{-}vo}$, which is the transfer function $\frac{V_o(s)}{i_L(s)}$.

In chapter 3.9 it was determined the transfer functions $\frac{V_o(s)}{d(s)}$ and $\frac{i_L(s)}{d(s)}$. Thus, dividing one by the other, it is possible to get the transfer function

$$\frac{V_o(s)}{i_L(s)} = \frac{-0.017576(s - 1.347 \cdot 10^4)}{s + 274.6}$$

(3-32)

The Bode plot of this transfer function is shown in Figure 57

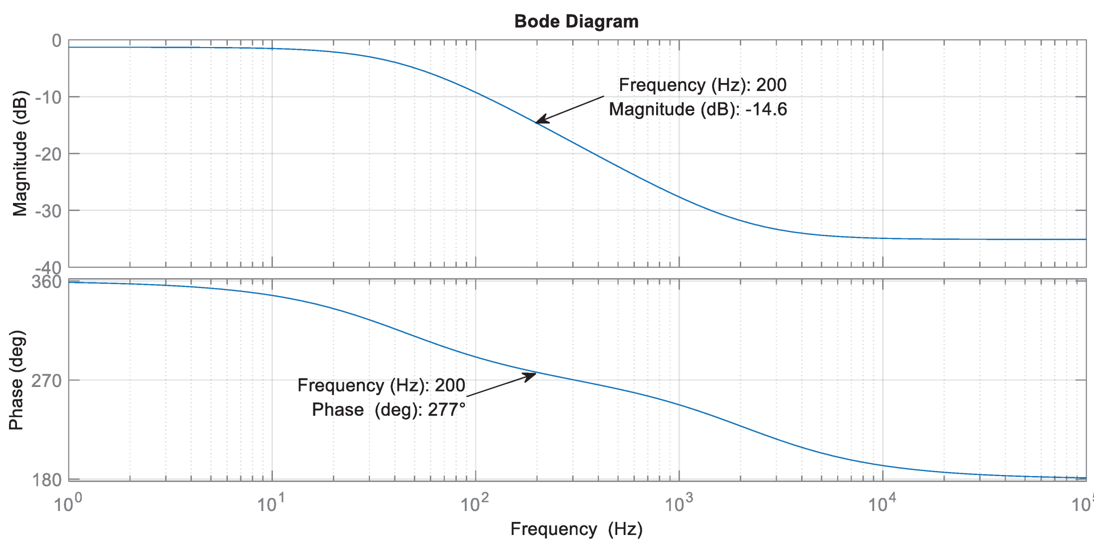

Figure 57 – $V_o(s)/i_L(s)$ Bode plot

Since this is the outer loop of the control diagram, and as described previously, the cutting frequency for the controller definition was defined at 200 Hz. At this frequency, the magnitude and phase are respectively -14.6 dB and 277°.

The controller calculation was again used the *K* factor, using a controller type 2. Then the controller transfer function is

$$G_{c-vo} = \frac{0.002378\ \mathrm{s}\ +\ 1}{1.179 \cdot 10^{-7}\mathrm{s}^2 + 0.0004429\ \mathrm{s}}$$

(3-33)

Evaluating if the controller if effectively acting at the defined cutting frequency with a desired phase margin of 60º, it can be observed in Bode plot in Figure 58.

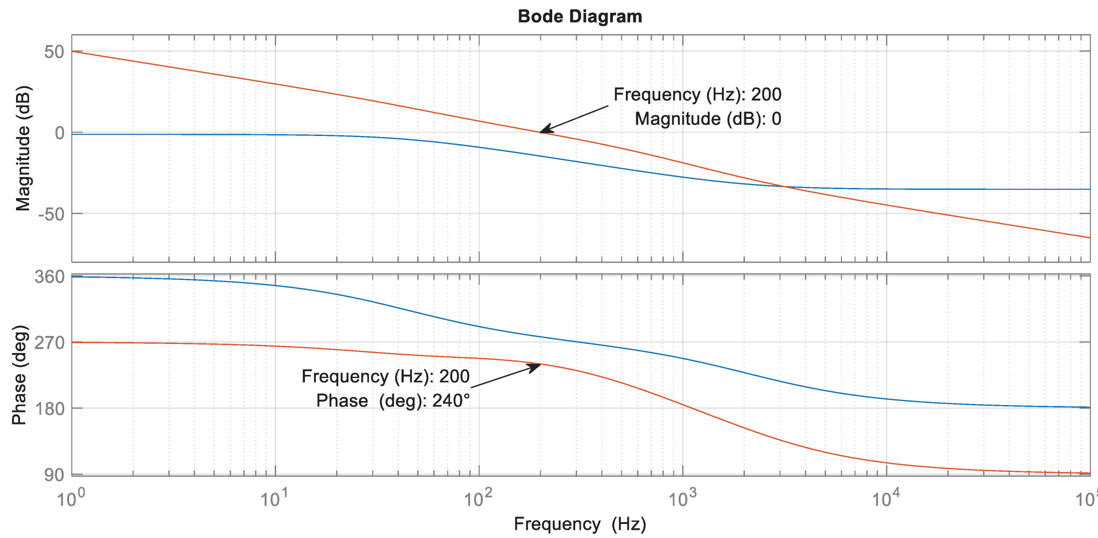

Figure 58 – $G_{c\text{-}vo}$ Bode plot

3.10.3 Control block 4

In the last block, number 4, which is the responsible for the battery control to supply the energy to the EC, the cutoff frequency was defined previously in chapter 3.4, thus it is going to be 0.01Hz. The transfer function of V_{uc} and I_{l_bat} is described in [4] that

$$\frac{V_{uc}}{I_{i-bt}} = \frac{V_{bt}}{V_o C_o C_{uc}} \frac{H_{i-bt} G_{c-vo} H_{i-uc}(1 + sC_{uc}R_{uc})}{s\left(s + \frac{G_{c-vo} H_{i-uc} V_{uc}}{C_o V_o}\right)} \tag{3-34}$$

Which in turn is

$$\frac{V_{uc}(s)}{i_{bt}(s)} = 2.5753 \cdot 10^{19} \cdot \frac{(s + 5.372 \cdot 10^4)^2 (s + 1.362 \cdot 10^4)(s + 9330)}{s(s + 2332)(s^2 + 1.075 \cdot 10^5 s + 2.89 \cdot 10^9)(s^2 + 7.765 \cdot 10^4 s + 1.507 \cdot 10^9)} \cdot \frac{(s + 4594)^2 (s + 420.5)(s + 5.128)}{(s^2 + 2046s + 1.102 \cdot 10^6)(s^2 + 1.719 \cdot 10^4 s + 7.444 \cdot 10^7)(s^2 + 1.519 \cdot 10^4 s + 6.982 \cdot 10^7)} \cdot \frac{1}{(s^2 + 1.56 \cdot 10^4 s + 8.403 \cdot 10^7)} \tag{3-35}$$

The Bode plot of this transfer function is in Figure 59.

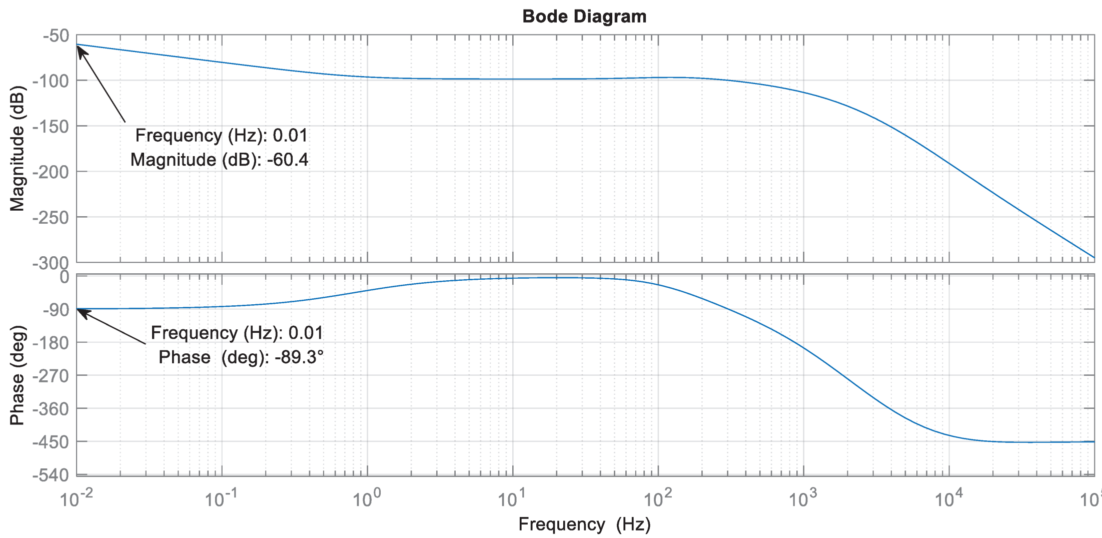

Figure 59 – $V_{uc}(s)/i_{i\text{-}bt}(s)$ Bode plot

As defined previously the cutting frequency is 0.01 Hz, to assure that the EC is going to act faster than the battery and to avoid high frequency demand at the battery. At this cutting frequency, the magnitude is -60.4 dB and the phase is -89.3º.

For the controller definition, it was considered a phase margin of 60º and a type 2 controller using the *K* factor.

Thus, the controller is

$$G_{c-V_{uc}} = \frac{57.98\,\mathrm{s} + 1}{0.2419\,\mathrm{s}^2 + 0.05537\,\mathrm{s}} \tag{3-36}$$

The Bode plot with the controller is then observed in Figure 60

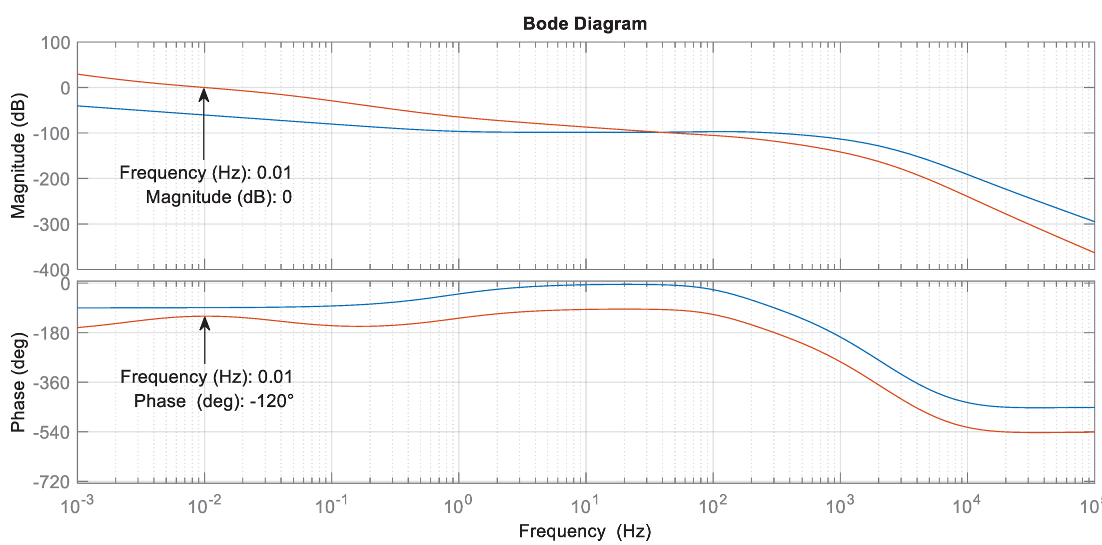

Figure 60 – $G_{c\text{-}vuc}$ Bode plot

4 *Simulation results*

4.1 Bi-directional boost model validation

In order to assure that the previous calculations were properly done, it is going to be shown the basic results from the calculated systems.

4.1.1 *$I_L(s)/d(s)$* analysis

It was implemented the basic circuit as a simple boost circuit, Figure 61. In this circuit it was connected the transfer function (block "H(s)" in Figure 61), described in (3-30), to simultaneously be able to compare the results.

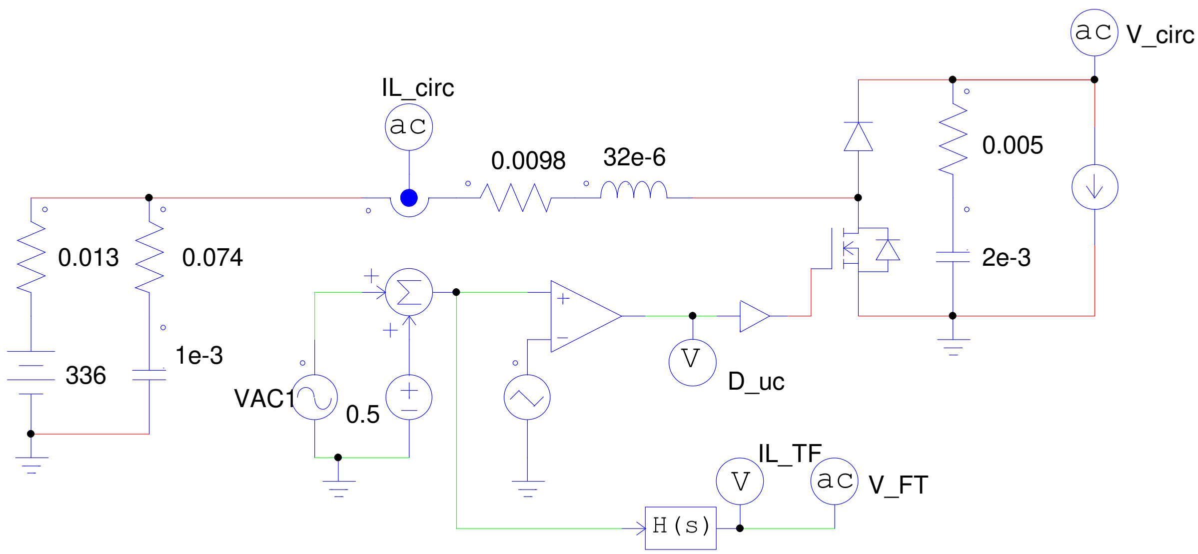

Figure 61 – Model validation $i_L(s)$

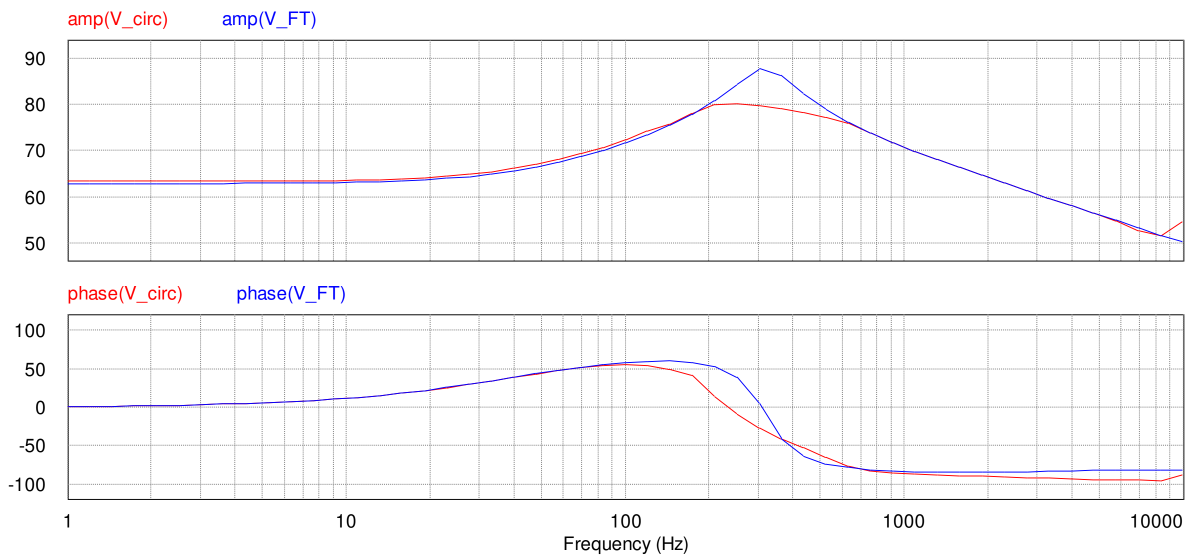

Figure 62 – Simulation results of $i_L(s)/d(s)$

In Figure 62 the simulation results are presented. The red line is the simulated circuit, while the blue line is the transfer function model result.

It is possible to observe that the curves are similar. The only difference is on the peak gain, which is lower on the simulation circuit.

4.1.2 *$V_o(s)/d(s)$* analysis

In a similar way, it was implemented the same basic boost circuit in PSIM software, as shown in Figure 63, and the respective transfer function was implemented in block diagram "H(s)".

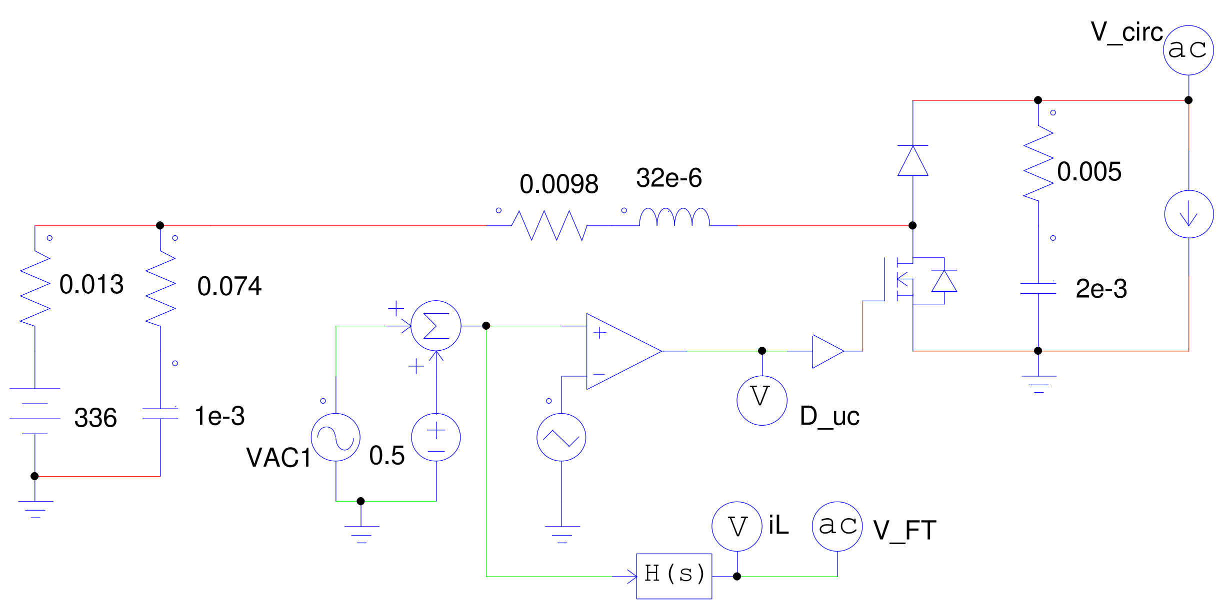

Figure 63 – Vo(s)/d(s) model validation

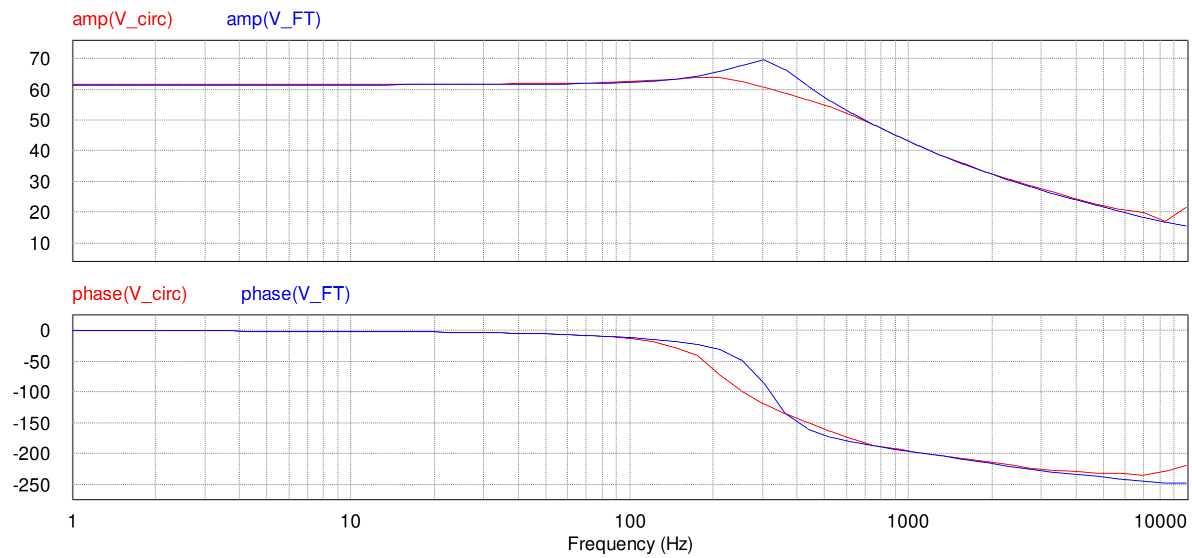

Figure 64 – Simulation results of Vo(s)/d(s)

The simulation results can be seen on Figure 64. The red line is the simulated circuit, while the blue line is the transfer function model result.

It is possible to observe that the curves are similar. The only difference is on the peak gain, which is lower on the simulation circuit.

At PSIM software it is not possible to run the AC Sweep using an AC current source. The software does not recognize it. Thus, the transfer function $V_o(s)/i_L(s)$ was not simulated and compared. The only way to do it, would be dividing the previous simulations $V_o(s)/d(s)$ and $i_L(s)/d(s)$ and having the desired transfer function, but the circuit behavior analysis based on the inductor current variation cannot be simulated, therefore an analysis based on calculation is not relevant and the complete model validation including the controlling system is going to be analyzed instead.

4.2 Controllers implementation at PSIM

Once the electrical circuit is defined and the controllers are calculated, it was implemented at PSIM. A simulation software for electrical circuits.

The type 2 controllers in PSIM are described in the following way:

$$G(s) = k \cdot \frac{1 + sT}{sT} \cdot \frac{1}{1 + sT_p} \tag{4-1}$$

Where,

k = controller gain

T = controller time constant

f_p = pole frequency in Hz,

$f_p = {}^{\omega_p}/_{2\pi}$

$T_p = {}^{1}/_{\omega_p}$

As described in section 3.10, equation (3-31):

$$G_{ci-uc} = \frac{0.0002748\ \mathrm{s}\ +\ 1}{1.039 \cdot 10^{-5}\ s^2 + 0.4508\ \mathrm{s}}$$

Which is equivalent to

$$G_{ci-uc} = \frac{0.0002748\mathrm{s}\ +\ 1}{\mathrm{s}} \cdot \frac{1}{1.039 \cdot 10^{-5}\ \mathrm{s} + 0.4508}$$

$$G_{ci-uc} = 0.0002748 \cdot \frac{0.0002748\mathrm{s}\ +\ 1}{0.0002748\mathrm{s}} \cdot \frac{1}{1.039 \cdot 10^{-5}\ \mathrm{s} + 0.4508} \cdot \frac{1/_{0.4508}}{1/_{0.4508}}$$

$$G_{ci-uc} = \frac{0.0002748}{0.4508} \cdot \frac{0.0002748\mathrm{s}\ +\ 1}{0.0002748\mathrm{s}} \cdot \frac{1}{\frac{1.039 \cdot 10^{-5}}{0.4508}\mathrm{s} + 1} \tag{4-2}$$

Thus,

$$k = 6.096 \cdot 10^{-4}$$

$$T = 2.748 \cdot 10^{-4}$$

$$T_p = 2.305 \cdot 10^{-5}$$

$$f_p = \frac{1}{T_p \cdot 2\pi} = 6.9 \cdot 10^3$$

Those parameters are included on the type 2 controller at PSIM for the inner control loops of battery current and EC current.

Using the same procedure for the other controllers,

$$G_{c-vo} = \frac{0.002378\ \mathrm{s}\ +\ 1}{1.179 \cdot 10^{-7}\mathrm{s}^2 + 0.0004429\ \mathrm{s}}$$

$$k = \frac{0.002378}{0.004429} = 5.369$$

$$T = 2.378 \cdot 10^{-3}$$

$$T_p = \frac{1.179 \cdot 10^{-7}}{4.429 \cdot 10^{-4}} = 2.662 \cdot 10^{-4}$$

$$f_p = \frac{1}{T_p \cdot 2\pi} = 600\ Hz$$

$$G_{c-Vuc} = \frac{57.98\ \mathrm{s}\ +\ 1}{0.2419\ \mathrm{s}^2 +\ 0.05537\ \mathrm{s}}$$

$$k = 1047.12$$

$$T = 57.98$$

$$T_p = 4.369$$

$$f_p = \frac{1}{T_p \cdot 2\pi} = 0.0364$$

It was then implemented in PSIM the electrical circuit in Figure 65 and the control circuit in Figure 66:

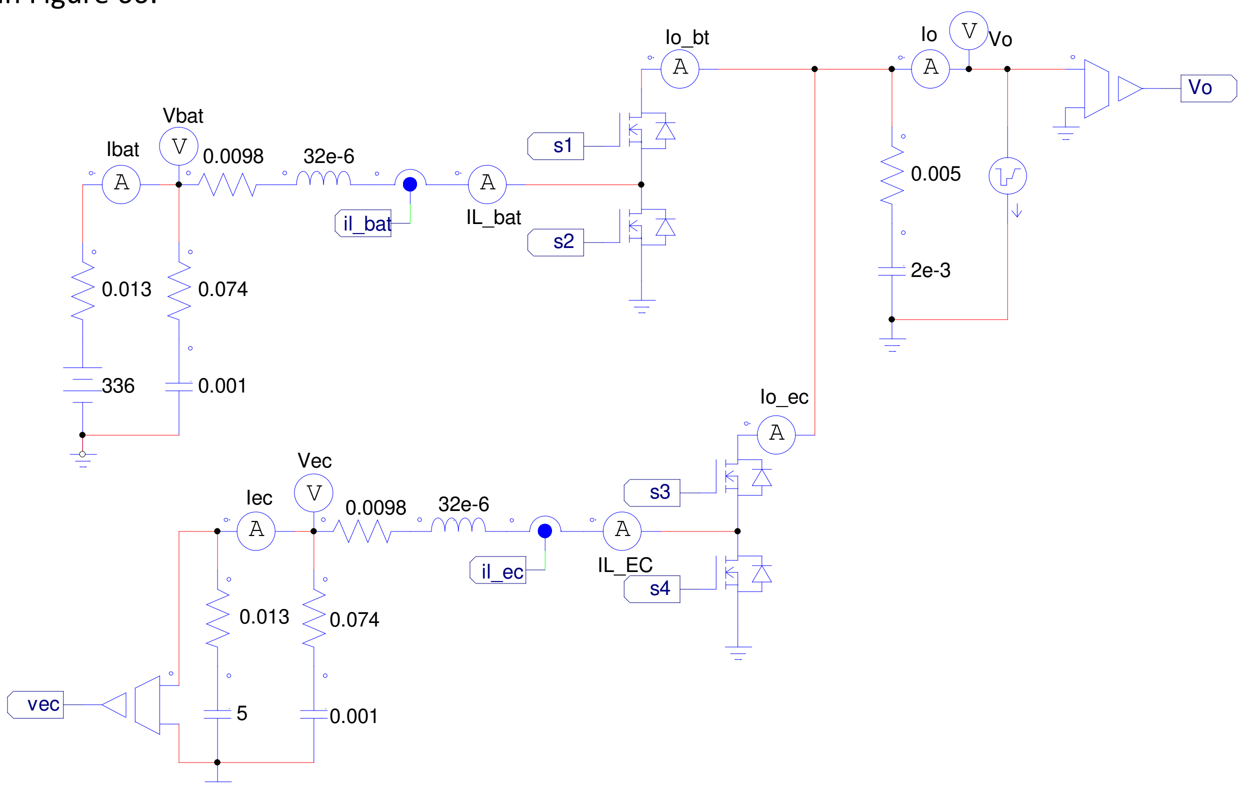

Figure 65 – Simulation circuit with multiple input

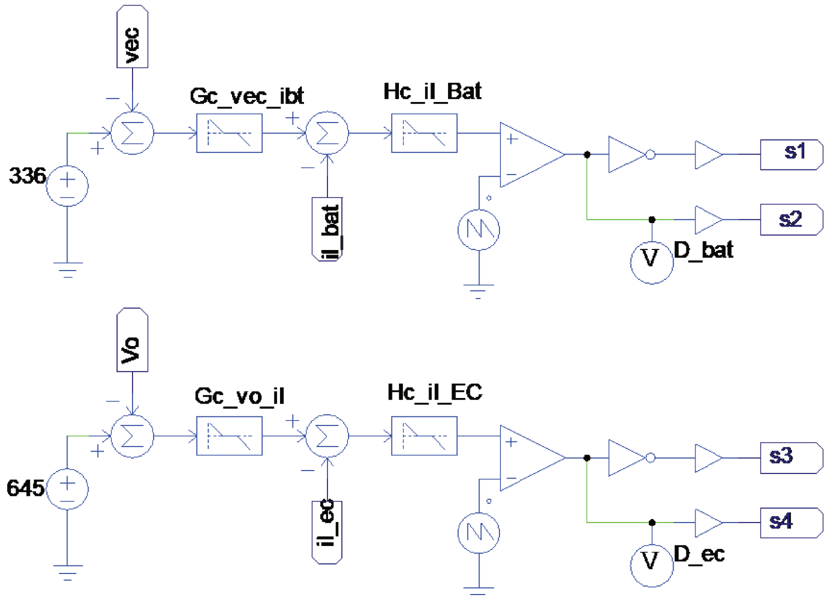

Figure 66 – Control circuit for multiple input simulation

4.3 Control strategy model validation

To complete the model validation, it was also implemented a different circuit based on transfer function blocks, which represents control strategy from Figure 35 and presented in Figure 67.

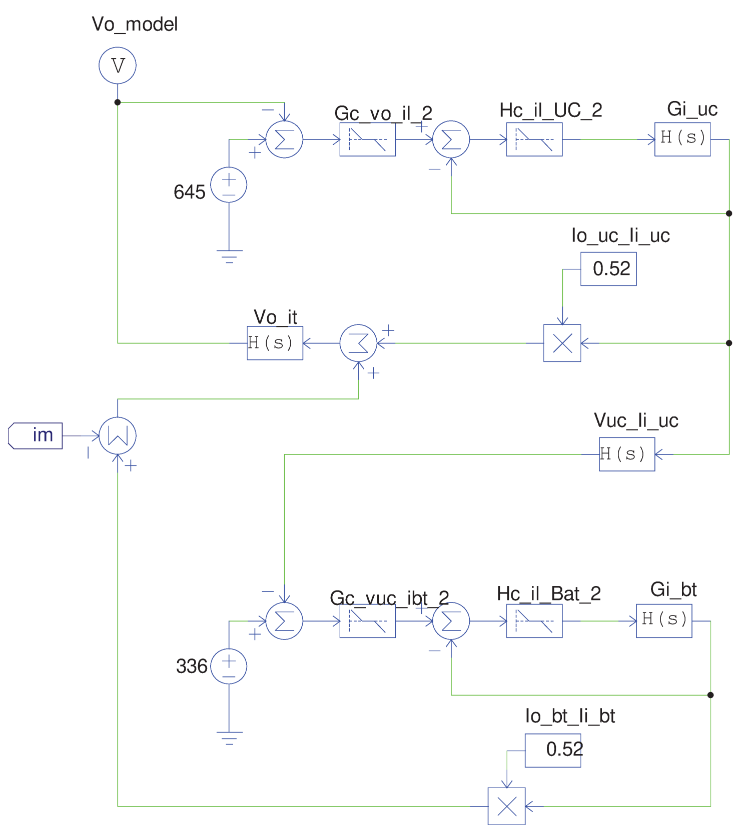

Figure 67 – Model validation in block diagram

For the circuit validation, it was implemented a load demand of 100A in the first 2 seconds, then a step to -100A and finally a ramp from -100A to 200A, as shown in Figure 68.

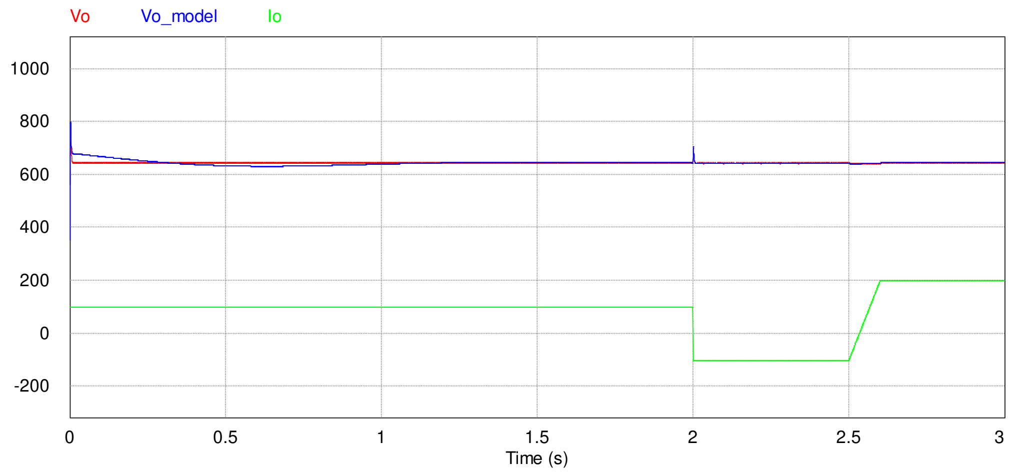

Figure 68 – Model validation simulation result

At initial conditions the model does not correspond properly, as observed in Figure 69. The block diagram is the blue line and it is possible to see that there is an oscillation on the output voltage, which does not appear at the circuit model.

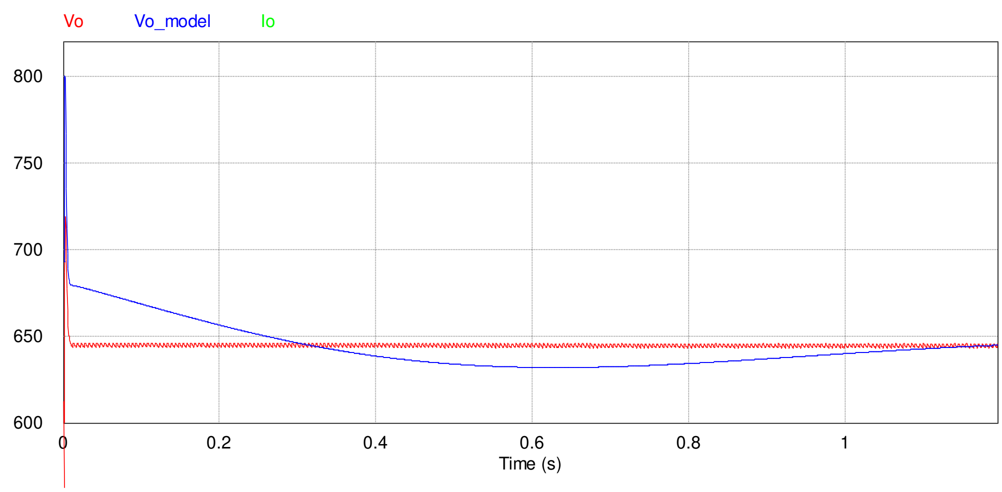

Figure 69 – Model valiation at initial conditions

Additionally, the voltage peak at zero second in the circuit is 720V, while at the block diagram this value is 800V. It represents a 10% difference. This variation is caused due to the fact that the circuit calculation is done considering the system at steady state condition.

After steady-state conditions, the model correspond quite similar, as observed in Figure 70.

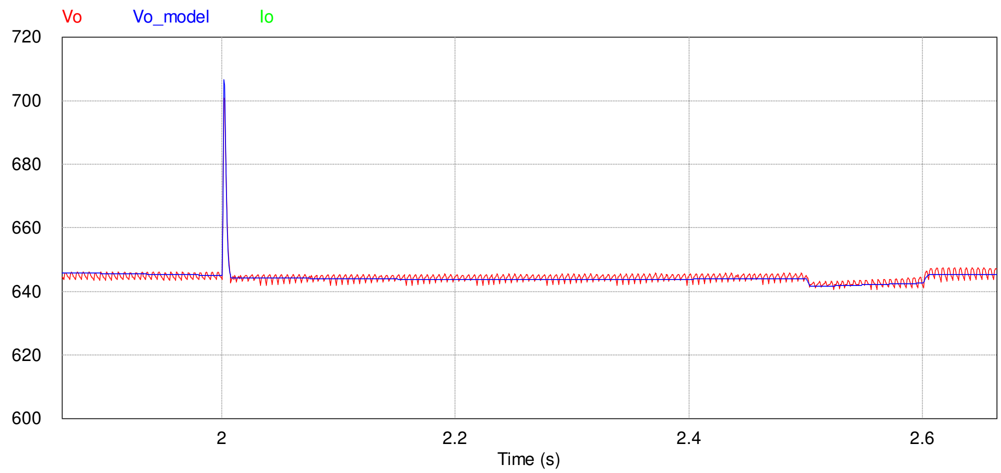

Figure 70 – Model validation results at steady state conditions

In Figure 71, it is possible to observe the step response and both models have a very similar behavior, with a slight variation on the peak.

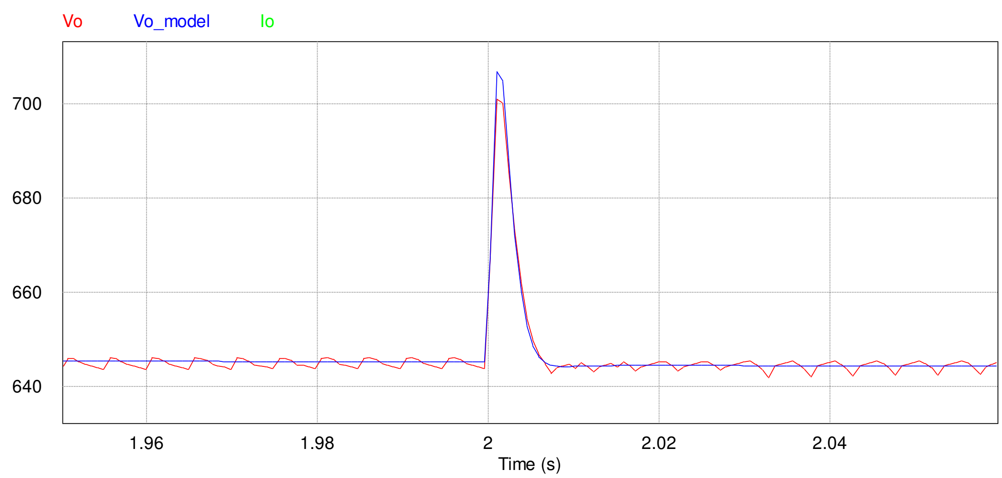

Figure 71 – Model validation step response

In Figure 72, it is possible to observe the ramp response and both models have a very similar behavior. The only observed difference is that the model (blue line) is a linear model, while the circuit (red line) is a switching circuit, therefore there is the slight oscillation on the output voltage, as expected.

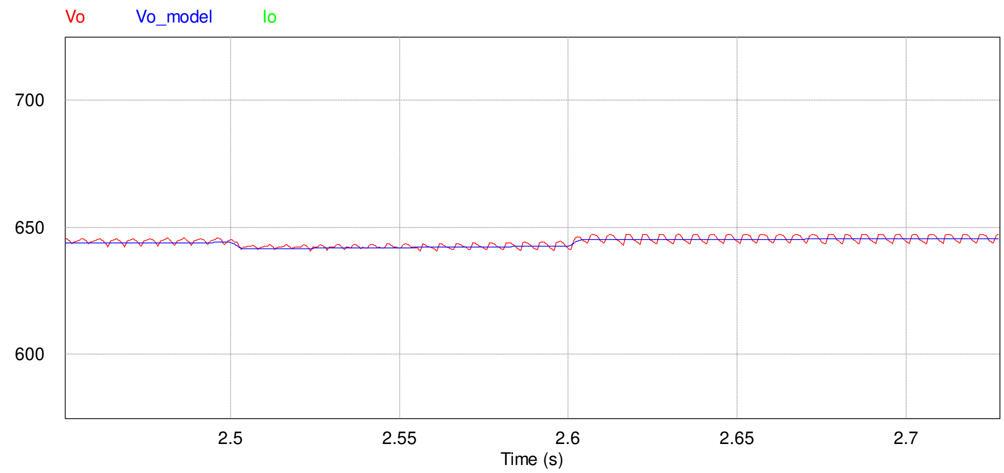

Figure 72 – Model valiation ramp response

4.4 Manhattan cycle simulation

The load was defined as a current source load, with the calculated Manhattan cycle current demand. Due to computer restrictions, it was simulated only the first 100 seconds of total cycle of 2178 seconds. It can be observed on the Figure 73 that the voltage V_0 was constant during the whole cycle.

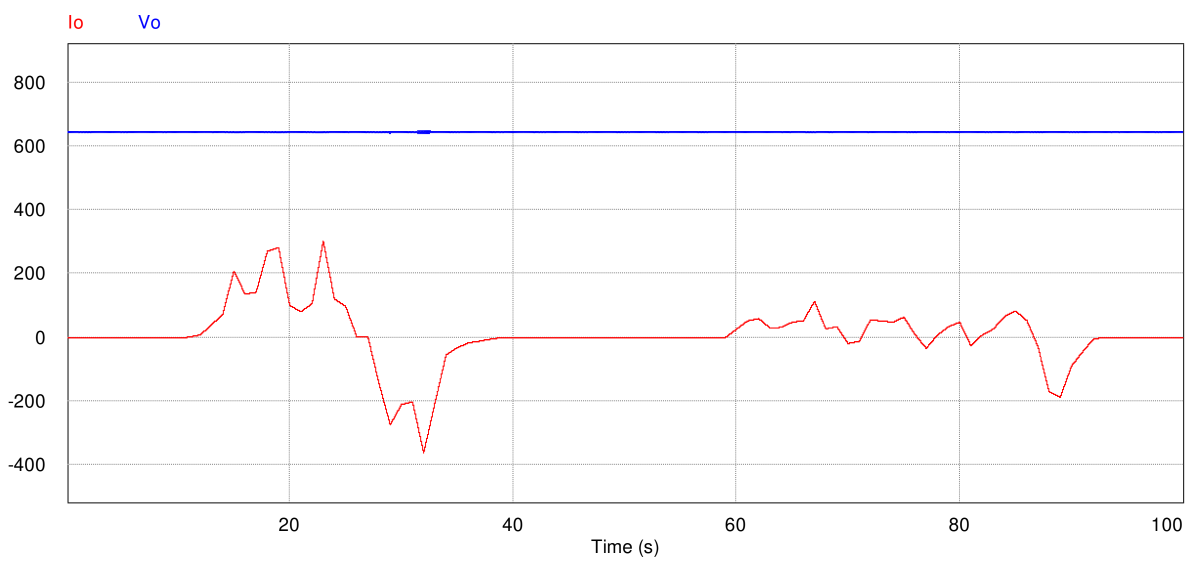

Figure 73 – Output voltage and current load simulation results (blue: V_o, red: I_o)

Where I_0 is the red curve and the blue line is the output voltage.

Zooming in the voltage behavior adjusting the voltage axis between 640V and 650V, it can be observed in Figure 74 that the voltage varied between 640V and 648V. The capacitance calculation was done considering 1% voltage variation, which defined a capacitance of 1.3566 mF.

But the adopted value was 2 mF. Using this value, the voltage variation reduces to 0.7%, which represents 4.5V (640V to 650V), very close to the variation observed.

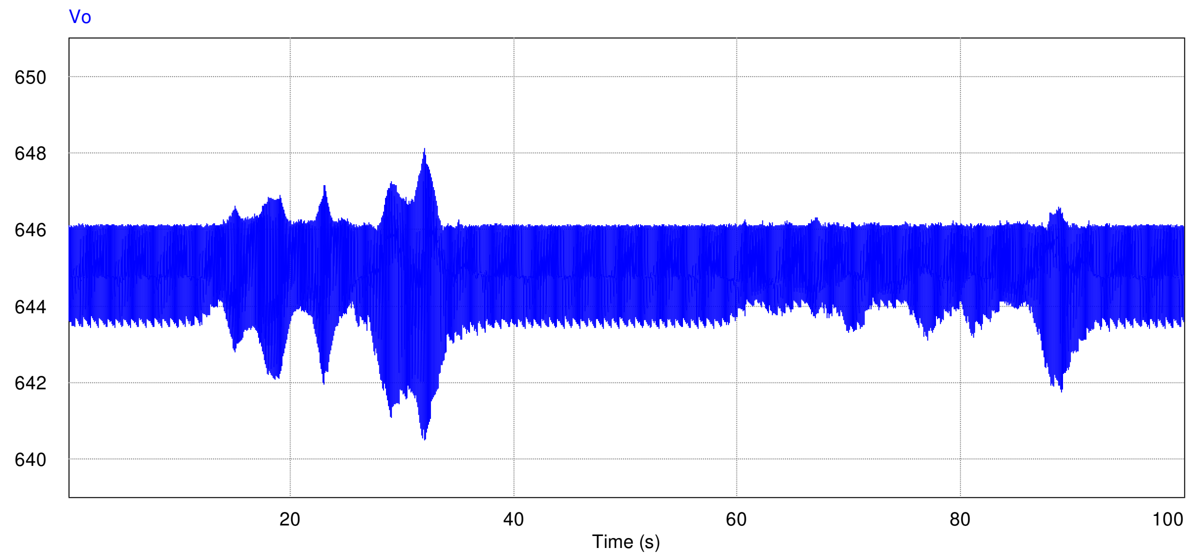

Figure 74 – Output voltage Vo zoom

Observing the current at the sources, in Figure 75 – 77, it can be observed that the battery current provides the power demand, while the EC is providing the current during the changes.

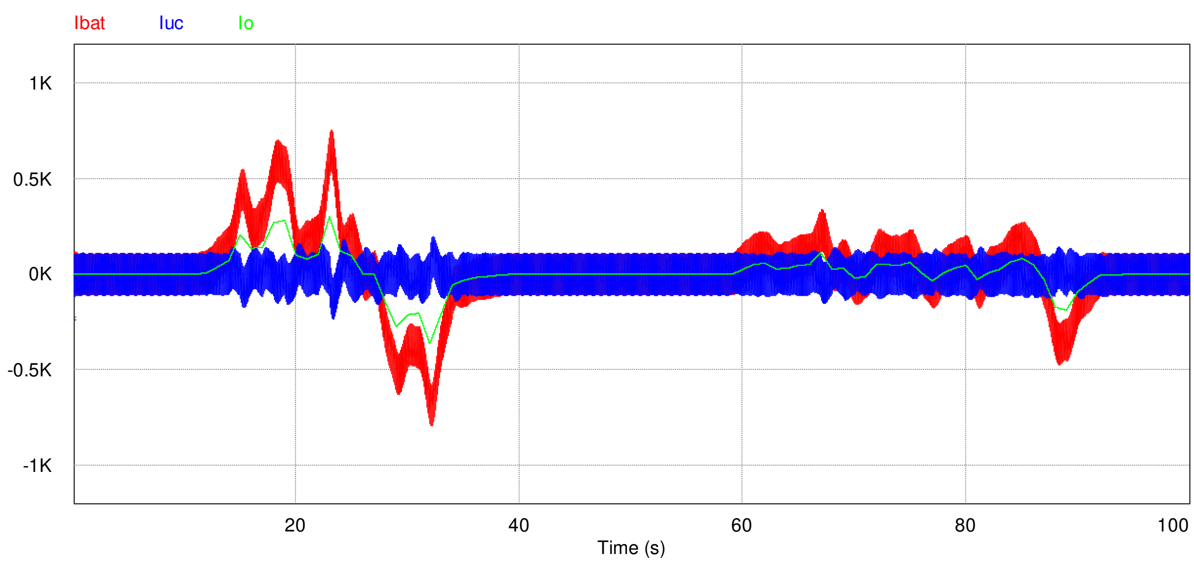

Figure 75 – Battery (red), EC (blue) and load (green) current

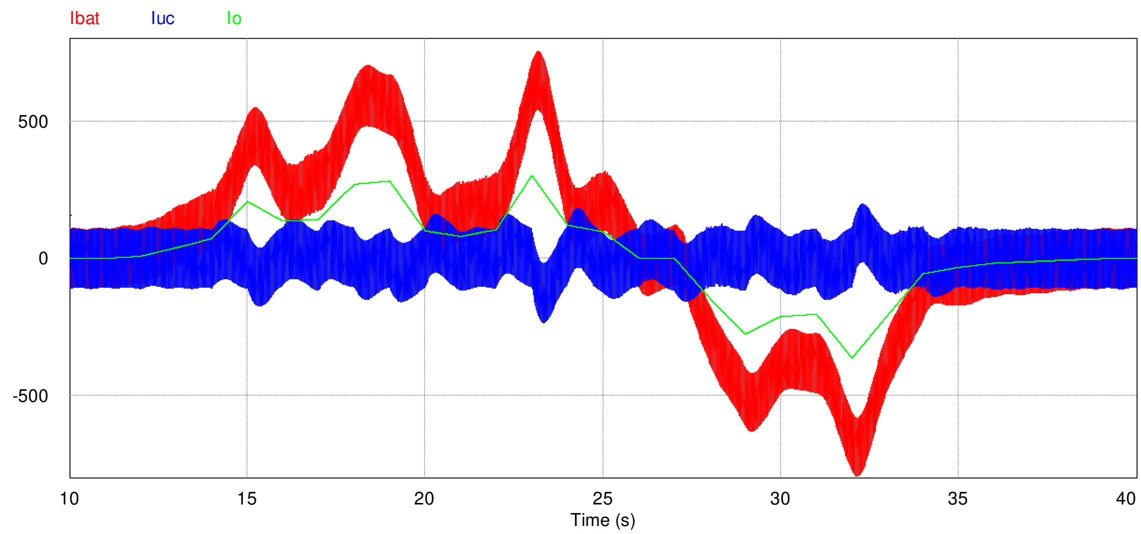

Figure 76 – Battery, EC and load currents from 10s to 40s

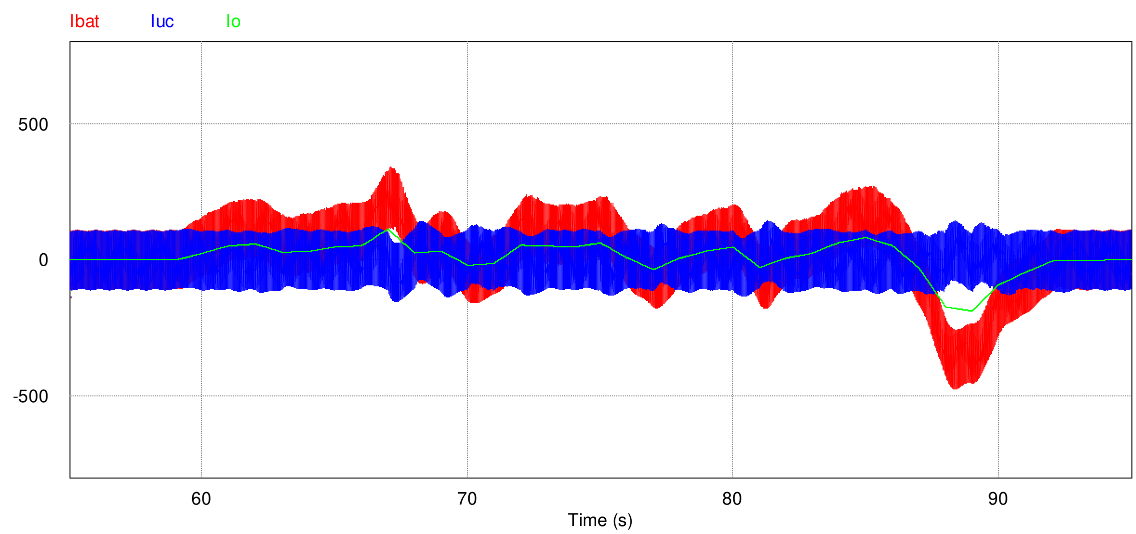

Figure 77 – Battery, EC and load current from 50s to 95s

Another evaluation to be considered is the driving current through the switch components. It can be observed in Figure 78 the switching behavior, since the values goes from zero to the peak, while on the Figure 75, the current at the power sources is delivering only the demand, not showing the ripple effect to zero. The capacitive filter supports it.

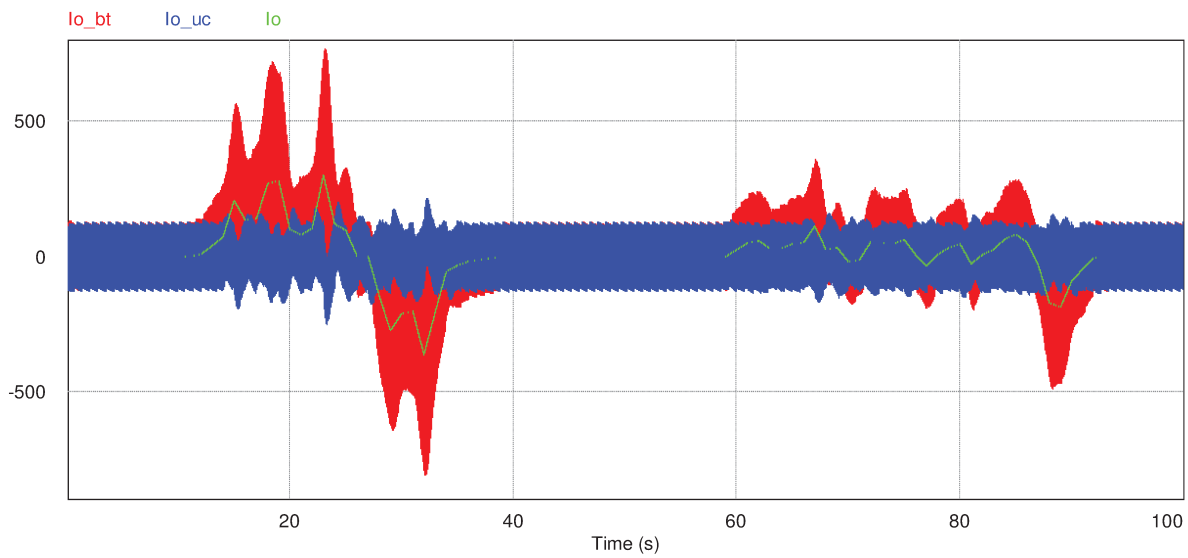

Figure 78 – Current at transistors (red: battery, blue: EC, green: I_o)

It is possible to observe that through the transistor and diode the current can reach 768A and -808A as peak values. Considering a voltage of 645V, the power is above 500 kW with a switching frequency of 20 kHz. Due to this fact the interleaved topology is required.

Implementing the interleaved topology, the circuit becomes more complex, but the controlling is the same, except by the fact that each transistor branch is going to be 120° shifted.

The electrical circuit is shown in Figure 79 and the controlling is shown in Figure 80:

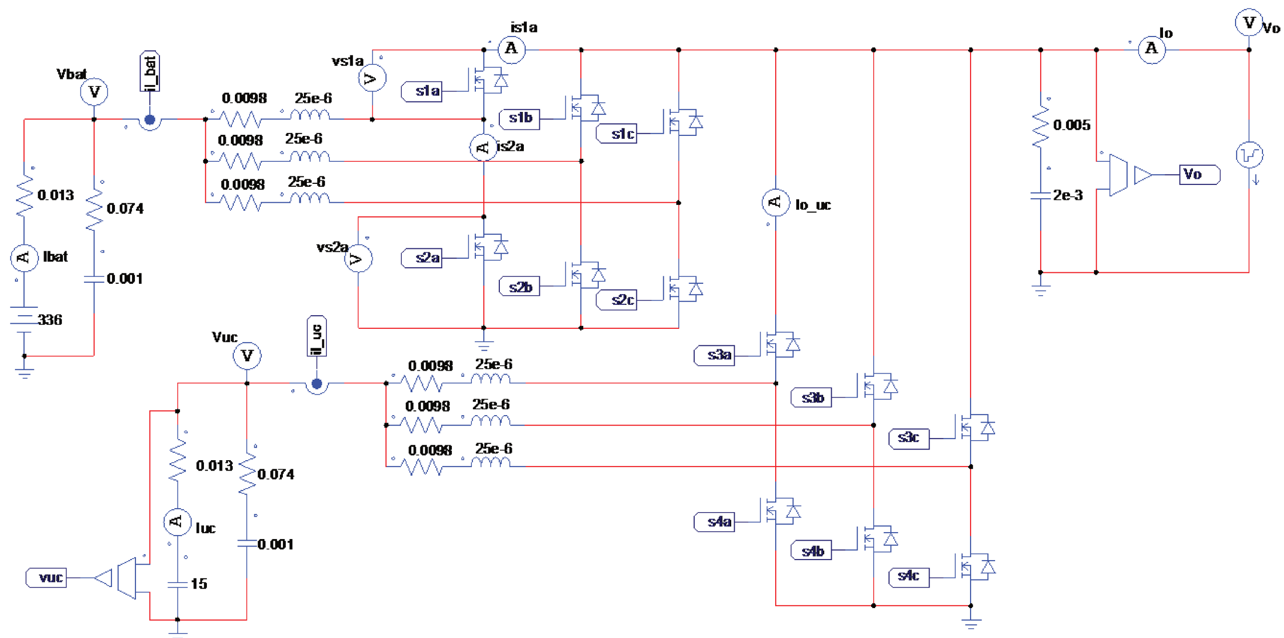

Figure 79 – Multiple input bi-directional interleaved DC-DC converter

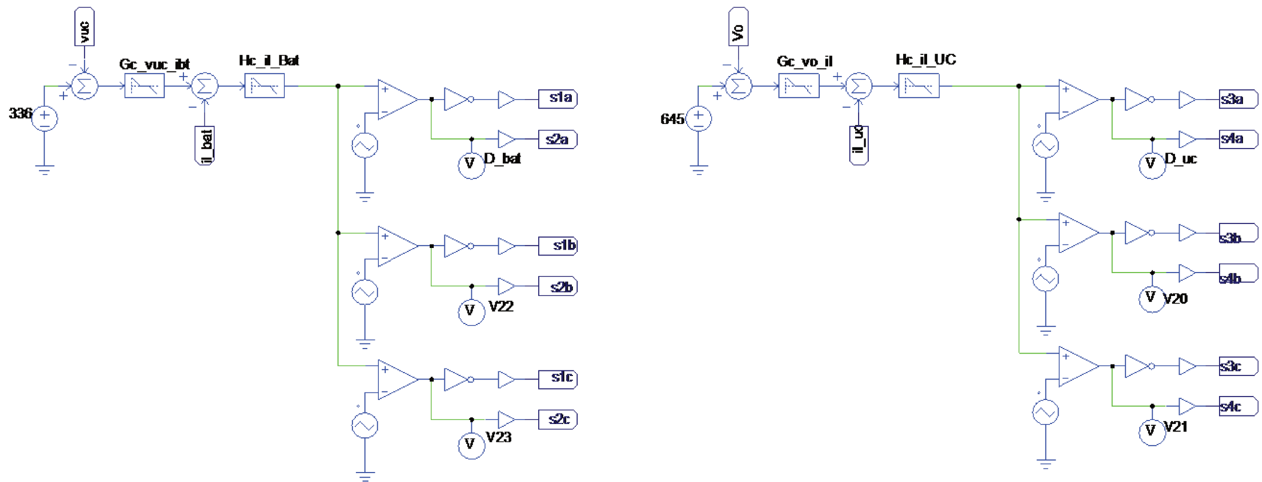

Figure 80 – Control circuit for the multiple input bi-directional interleaved DC-DC converter

On the Figure 81 it can be observed that the interleaved topology did not affect the voltage output.

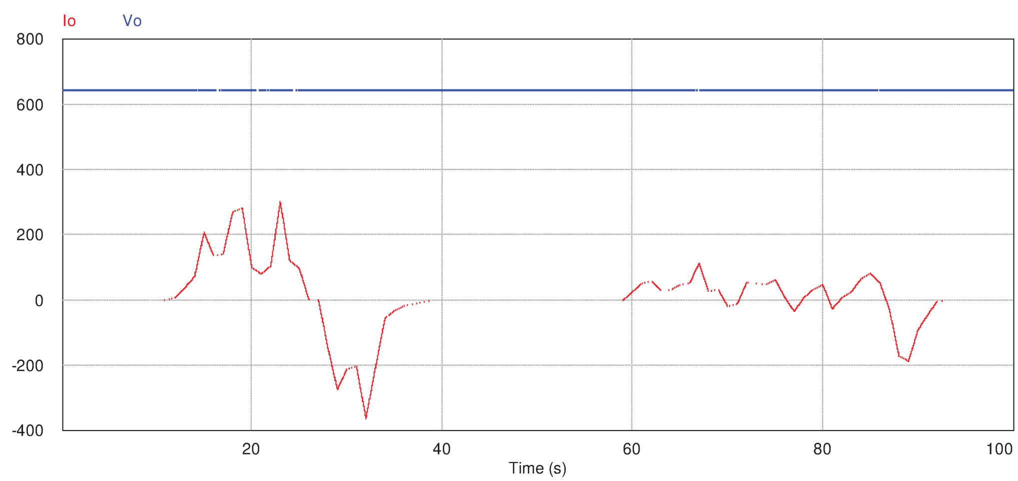

Figure 81 – Simulation results Vo (blue) and Io (red) for the interleaved topology

Zooming in the voltage, in Figure 82, it is possible to observe that in fact the interleaved topology improved the output voltage variation, reducing the maximal voltage to 646.3V and minimal voltage to 643.1V.

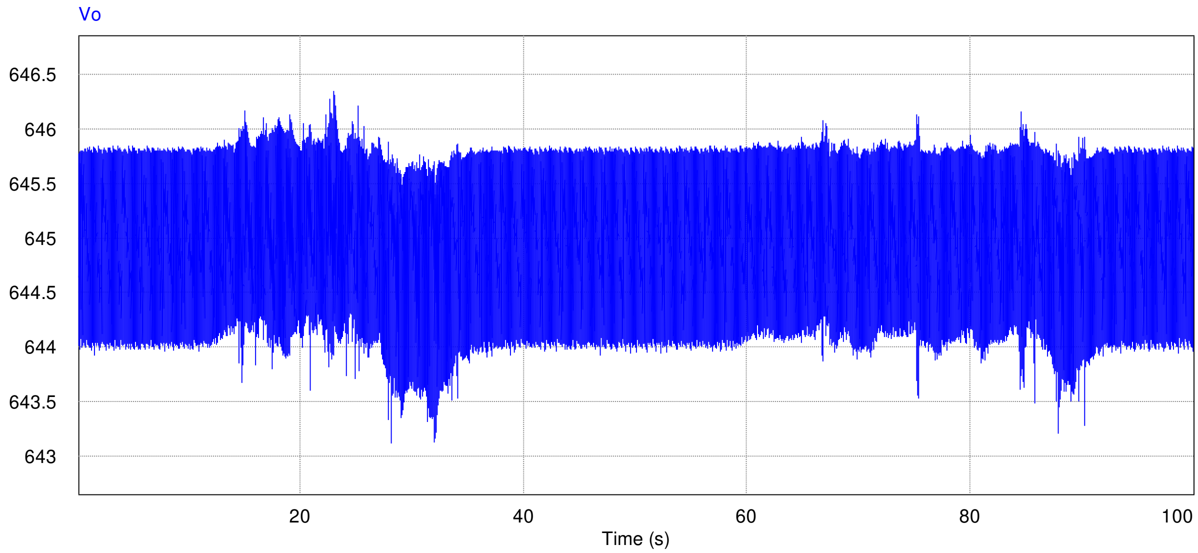

Figure 82 – Vo simulation result

Observing the current at the power sources, in Figure 83, that the interleaved helped to reduce the current ripple at the sources and also reduce the maximal current from 677A at the battery.

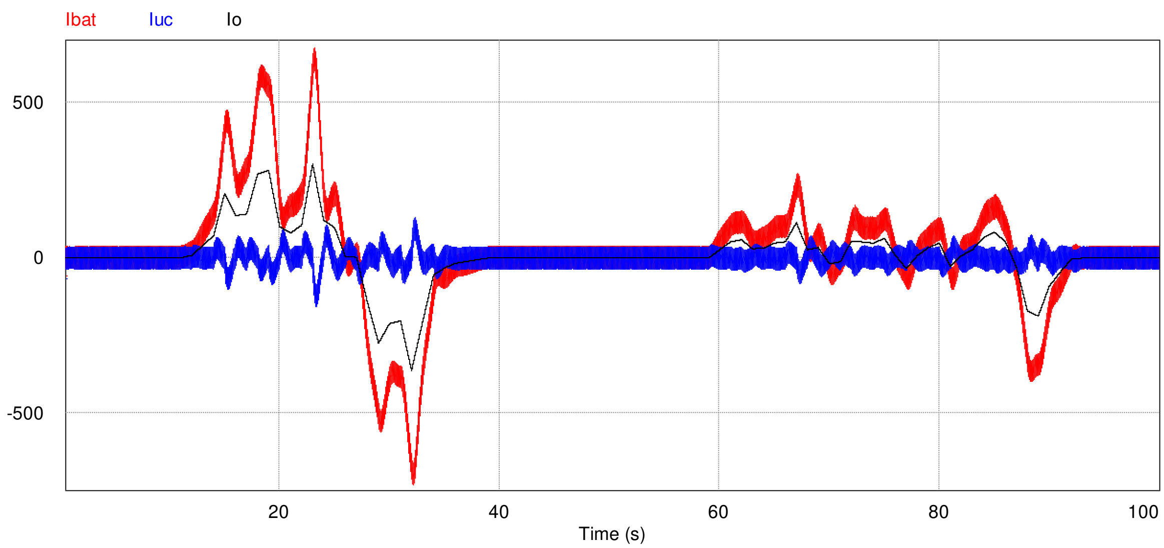

Figure 83 – Battery (red), EC (blue) and load (black) current results with interleaved topology

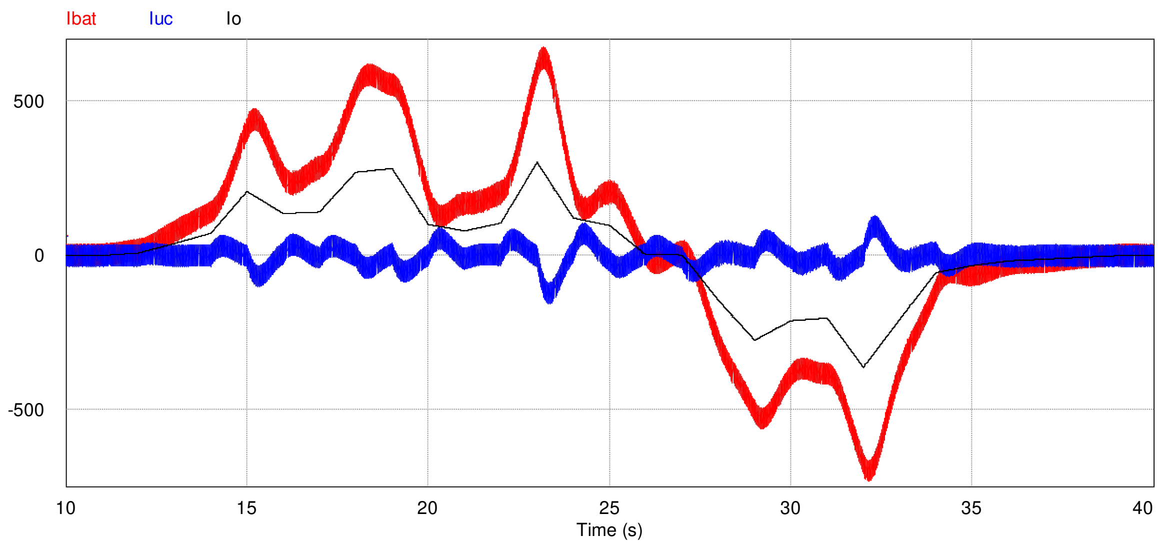

Figure 84 – Battery, EC and load currents from 10s to 40s (interleaved)

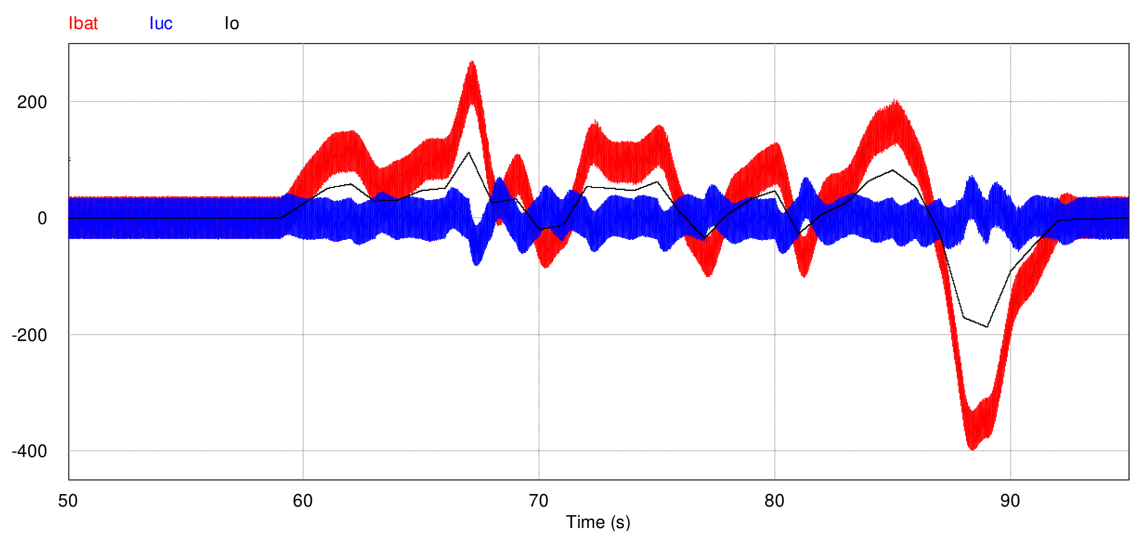

Figure 85 – Battery, EC and load currents from 50s to 95s (interleaved)

Analyzing the current at one inductor from the battery section, in Figure 86, the maximal value observed is 337A and the minimal value is -357A.

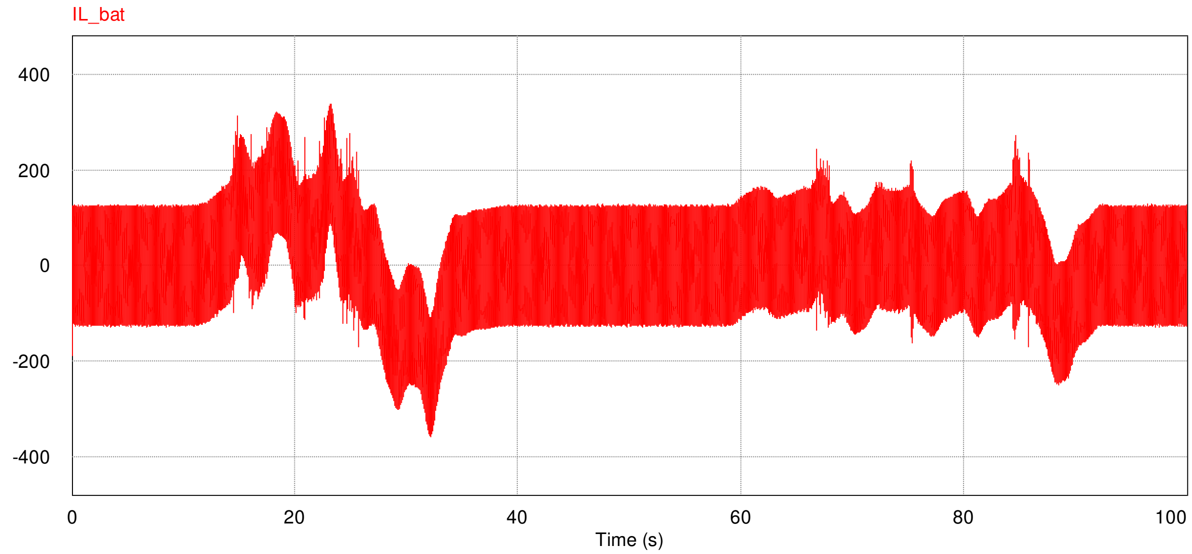

Figure 86 – Battery inductor current (interleaved)

At the EC, Figure 87, the inductor current maximal value is 200A and the minimal value is -203A.

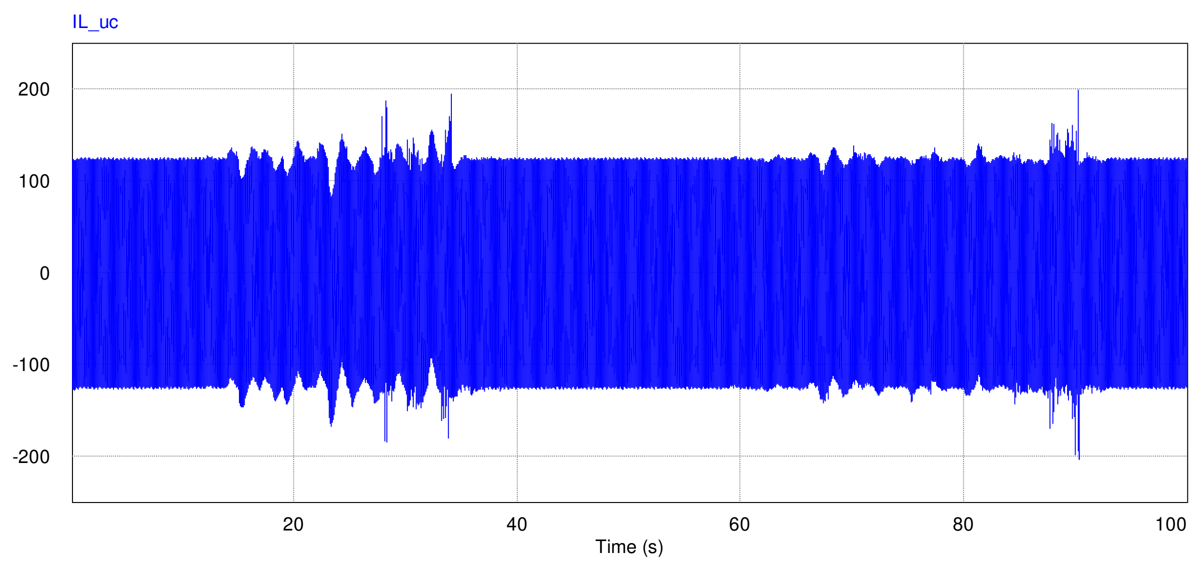

Figure 87 – EC inductor current (interleaved 20kHz)

Analyzing the battery inductor current during one duty cycle (while Io is zero), as shown in Figure 88, it is possible to see that the duty cycle is at 50% (23.7 µs) and the current variation is between +125A and - 123A.

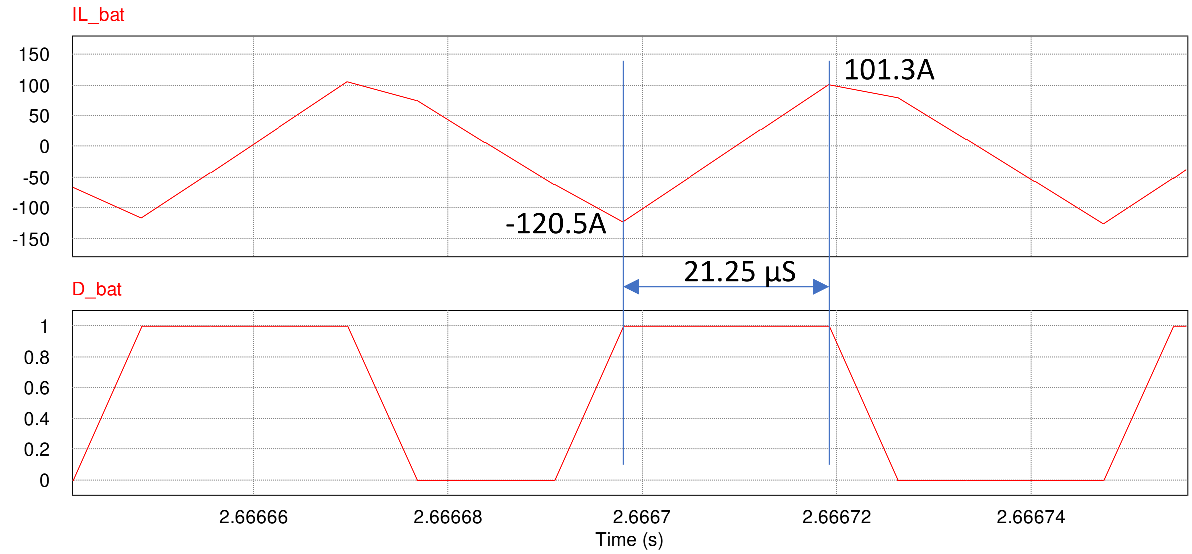

Figure 88 – Battery inductor current and duty cycle

Based on the values from Figure 88 (Δi = 221.8A), considering L = 32µH and Vi = 336V,

$$L \times \frac{\Delta I_i}{\Delta t} = V_i$$

$$\Delta t = 21.12\mu s$$

From simulation the value is 21.25µs, which is very close to the theoretical value.

Evaluating one transistor, it is possible to verify, in Figure 89, that the current flowing through it reduced, as needed and expected by using the interleaved topology.

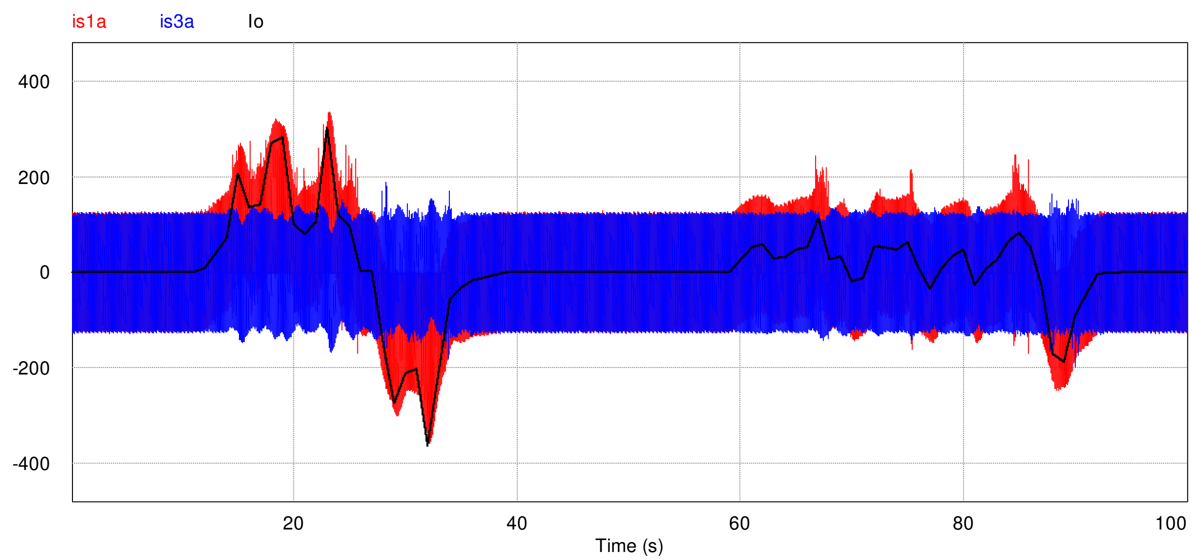

Figure 89 – Battery (red), EC (blue) transistor current results, load current (black)

The maximal value observed in the battery was 336A and -357A. In the EC switch, the maximal and minimal values observed were 188A and -197A. Considering that each transistor in this simulation represents 4 parallel transistors as described in section 3.5, the maximal current in each transistor is -89A. The value used for the thermal analysis was considered 112A, thus the transistors are going to work in all conditions.

Considering 4 parallel transistors in each interleaved phase, it is important to note that with the number of parallel transistors and the interleaved topology, using 20kHz of switching frequency, the parasitic inductances and capacitances from the circuit might have an influence and cause undesired oscillations, therefore, the circuit shall be constructed in such a way that it is as symmetrical as possible to avoid resonances.

Another behavior observed in Figure 83, when observing the different currents, is that basically the battery current is almost following the load current I_o. It happens because the I_o variation is at very low frequency, and it is difficult to observe the control actuating to attenuate the current variation at the battery. For this reason, it was created another simulation, varying rapidly the current I_o, in order to verify if the EC is going to act fast as designed.

As observed in Figure 90, it was defined a load current starting at 100A and after one second a step was applied switching the current to -100A. The output voltage V_o presented a short variation at initial conditions and at the step, but rapidly was back to the desired value of 645V.

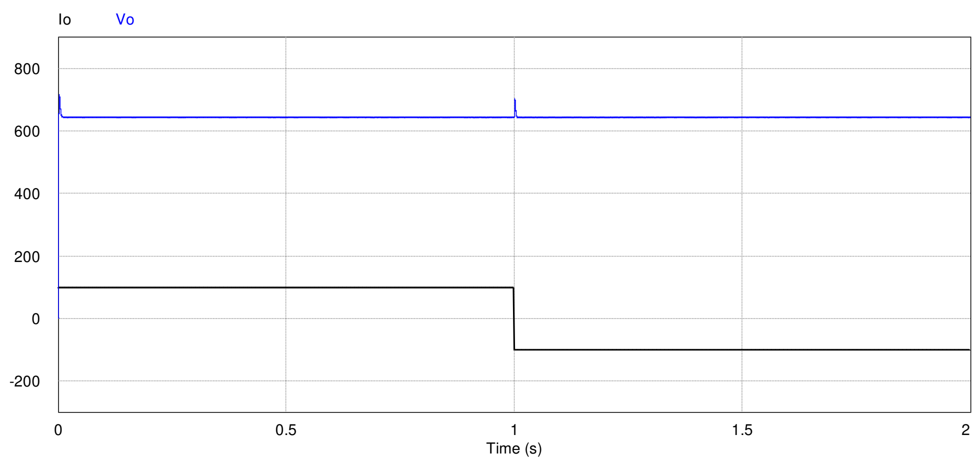

Figure 90 – output voltage V_o (blue), load current I_o (black)

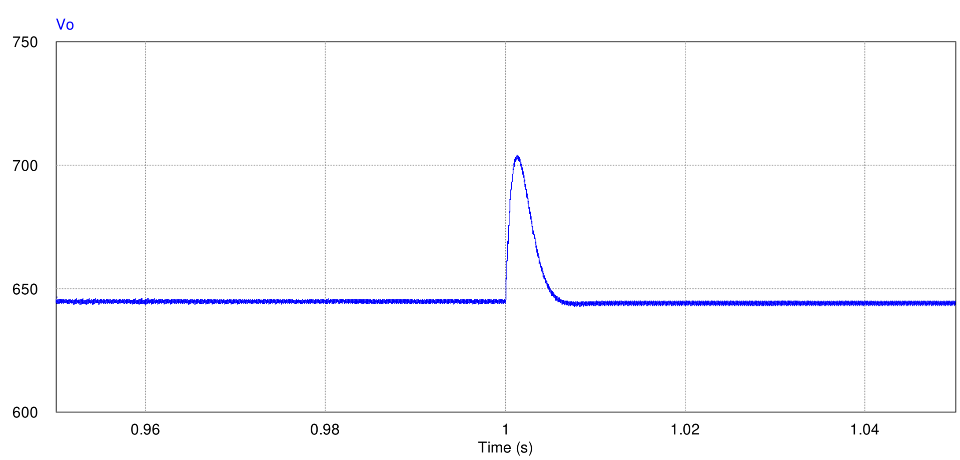

Figure 91 – output voltage V_o (blue) from 0.95ms to 1.05ms

In Figure 91 it is possible to observe the output voltage variation when the step was applied. In less than 8ms the voltage was regulated back to the setup value.

In Figure 92 is presented the battery and EC currents from the simulation. It is possible to observe that at initial conditions, the EC acts fast suppling the power demanded, while slowly the battery starts to provide the power demanded and the EC starts to be charged. Then at 1s time, the current changes and the EC acts rapidly absorbing the power, while the battery slowly reduces the current and starts to be recharged and the EC also send its charge to the battery. In Figure 93 there is a zoom at the step point for better visualization on the EC response.

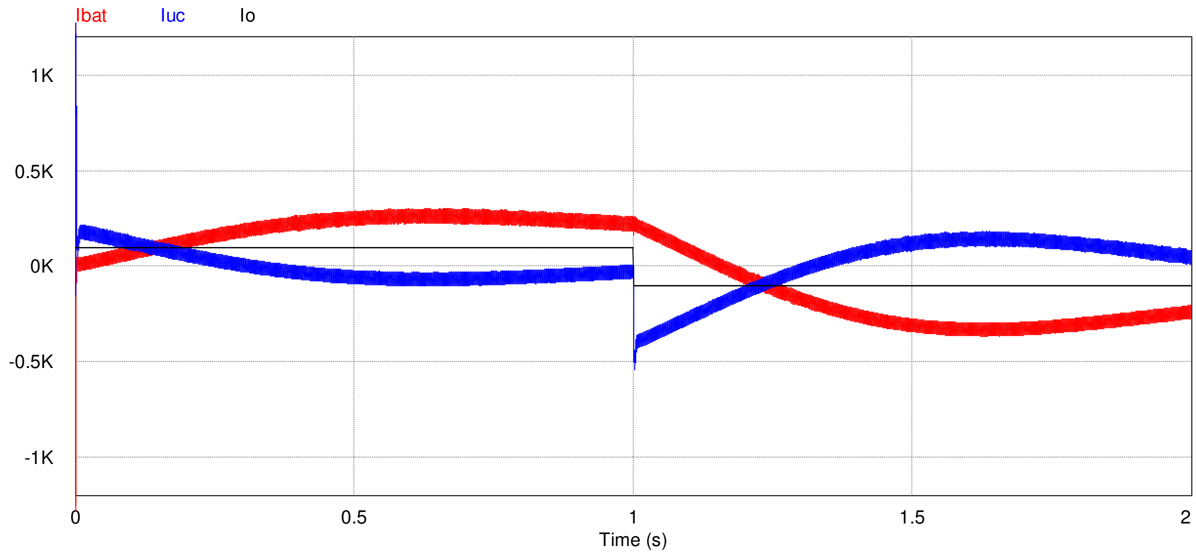

Figure 92 – battery current (red), EC current (blue), load current (black)

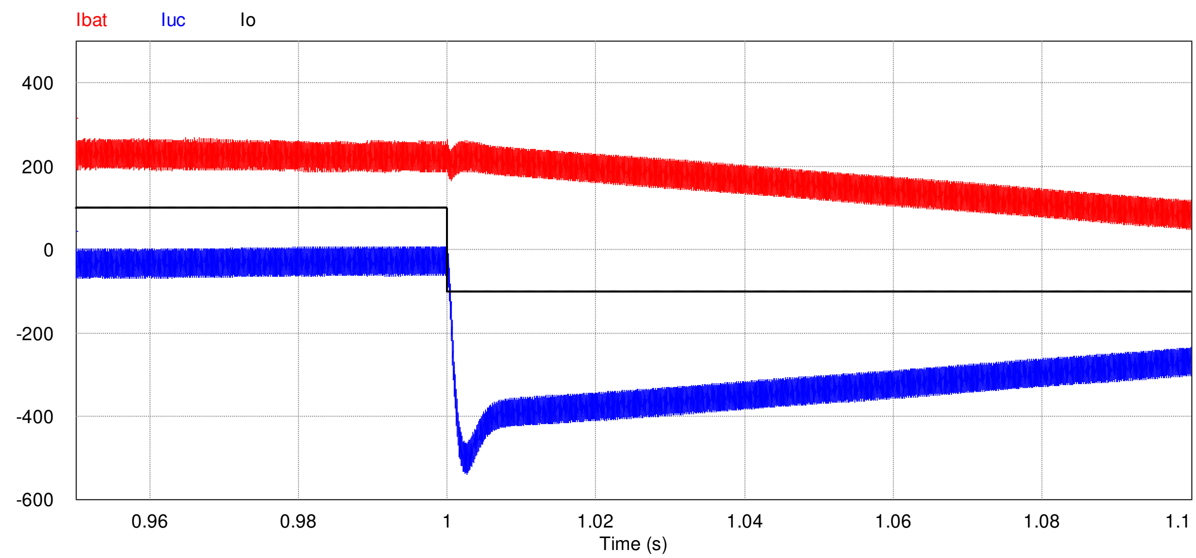

Figure 93 – battery current (red), EC current (blue), load current (black), time 0.95s to 1.1s

5 Conclusions

Considering the pollution problems observed currently, and the technological boundaries at the present moment, it is possible to create a system to be able to take the best profit of battery and electrochemical capacitors in order to optimize the battery lifetime and the vehicle driving range.

In this work a hybrid energy storage system (HESS) was created. The system is constituted of a multiple input bi-directional DC-DC converter, with a battery and electrochemical capacitors bank as the power sources for an electric bus. Due to engine demands, bus size and weight, it was necessary to create an interleaved topology on the DC-DC converter in order to reduce the amount of current in each transistor and also to reduce the current ripple in the power sources to improve specially the battery lifetime and also reduce the output voltage variation. Additionally, the demanded current is quite high and considering a high switching frequency to reduce parasitic losses, it is necessary to use SiC MOSFET transistors. In each phase of the interleaved converter it was necessary to use 4 transistors in parallel to divide the current and not to overload each transistor.

With the control strategy used, in which it was defined a cutoff frequency that determines when the battery and EC are going to act, it is possible to allow the battery to work as a constant power source, while the EC provides the load dynamics variation. Using this strategy, the battery lifetime is also enhanced.

For the circuit calculation and the transfer functions definitions, it was considered a simple bi-directional boost DC-DC converter. Once the transfer functions were determined, they were applied for the interleaved system as well. It is known that there is a variation on the resonance gain, but in this case, this was neglected and the system itself had no stability problems.

The system itself is complex, demanding several transistors, due to the load demanded by an electric urban bus. It is important to note that, when implementing the circuit, the positioning of each transistor shall be as symmetric as possible to avoid oscillations caused by eventual intrinsic inductances and capacitances in the circuit.

As future steps in this work, the inverter and the electric motor could be included in the system. A future research could also evaluate the battery state of charge and also implement an experimental system in order to confirm all the simulation results.

REFERENCES

[1] M. Y. Ayad, M. Becherif, and A. Henni, “Vehicle hybridization with fuel cell , supercapacitors and batteries by sliding mode control,” *Sci. Direct - Renew. Energy*, vol. 36, no. 10, pp. 2627–2634, 2011.

[2] A. Drolia, P. Jose, and N. Mohan, “An Approach to Connect Ultracapacitor to Fuel Cell Powered Electric Vehicle and Emulating Fuel Cell Electrical Characteristics using Switched Mode Converter,” *IECON Proc. (Industrial Electron. Conf.*, vol. 1, pp. 897–901, 2003.

[3] W. O. Avelino, F. S. Garcia, A. A. Ferreira, and J. A. Pomilio, “Electric Go-Kart with Battery-Ultracapacitor Hybrid Energy Storage System,” pp. 3–8.

[4] F. S. Garcia, A. A. Ferreira, and J. A. Pomilio, “Control Strategy for Battery-Ultracapacitor Hybrid Energy Storage System,” *Proc. 24th Annu. IEEE Appl. power Electron. Conf. Expo.*, pp. 826–832, 2009.

[5] J. Cao and A. Emadi, “A new battery/ultracapacitor hybrid energy storage system for electric, hybrid, and plug-in hybrid electric vehicles,” *IEEE Trans. Power Electron.*, vol. 27, no. 1, pp. 122–132, 2012.

[6] J. A. Pomilio, “Topologias básicas de conversores CC-CC,” in *Fontes Chaveadas*, 2016, pp. 1–19.

[7] R. W. Erickson, *Fundermentals of Power Electronics*, Second. 2000.

[8] W. de O. Avelino, “Sistema Híbrido de Armazenamento de Energia para Aplicação em Veículos Elétricos,” Universidade Estadual de Campinas - UNICAMP, 2014.

[9] A. Benrabah *et al.*, “FC / Battery Power Management for Electric Vehicle Based Interleaved DC-DC Boost Converter Topology To cite this version : FC / Battery Power Management for Electric Vehicle Based Interleaved dc-,” *HAL*, 2014.

[10] N. Jantharamin and L. Zhang, “Analysis of Multiphase Interleaved Converter by Using State-Space Averaging Technique,” *2009 6th Int. Conf. Electr. Eng. Comput. Telecommun. Inf. Technol.*, vol. 1, pp. 288–291, 2009.

[11] R. A. Huggins, *Advanced Batteries - Materials Science Aspects*. 2009.

[12] S. Manzetti and F. Mariasiu, “Electric vehicle battery technologies: From present state to future systems,” *Renew. Sustain. Energy Rev.*, vol. 51, pp. 1004–1012, 2015.

[13] S. Li and B. Ke, “Study of battery modeling using mathematical and circuit oriented approaches,” *IEEE Power Energy Soc. Gen. Meet.*, pp. 1–8, 2011.

[14] P. Amiribavandpour, W. Shen, D. Mu, and A. Kapoor, “An improved theoretical electrochemical-thermal modelling of lithium-ion battery packs in electric vehicles,” *J. Power Sources*, vol. 284, pp. 328–338, 2015.

[15] J. Van Mierlo, P. Van den Bossche, and G. Maggetto, “Models of energy sources for EV and HEV: Fuel cells, batteries, ultracapacitors, flywheels and engine-generators,” *J. Power Sources*, vol. 128, no. 1, pp. 76–89, 2004.

[16] M. R. Jongerden and B. R. Haverkort, “Which battery model to use?,” *IET Softw.*, vol. 3, no. 6, p. 445, 2009.

[17] T. Kim, “A Hybrid Battery Model Capable of Capturing Dynamic Circuit Characteristics and Nonlinear Capacity Effects,” vol. 26, no. 4, pp. 1172–1180, 2011.

[18] H. Zhang and M. Y. Chow, “Comprehensive dynamic battery modeling for PHEV applications,” *IEEE PES Gen. Meet. PES 2010*, pp. 1–6, 2010.

[19] N. Lin, S. Ci, and H. Li, "An enhanced circuit-based battery model with considerations of temperature effect," *2014 IEEE Energy Convers. Congr. Expo. ECCE 2014*, pp. 3985–3989, 2014.

[20] O. Tremblay, L. A. Dessaint, and A. I. Dekkiche, "A Generic Battery Model for the Dynamic Simulation of Hybrid Electric Vehicles," *IEEE Veh. Power Propuls. Conf.*, no. V, pp. 284–289, 2007.

[21] L. Yao, A. Aziz, P. Kong, and N. Idrus, "Modeling of lithium-ion battery using MATLAB/simulink," *IECON Proc. (Industrial Electron. Conf.*, pp. 1729–1734, 2013.

[22] B. Wu and B. Chen, "Study the performance of battery models for hybrid electric vehicles," *MESA 2014 - 10th IEEE/ASME Int. Conf. Mechatron. Embed. Syst. Appl. Conf. Proc.*, 2014.

[23] K. R.C., K. P.T., R. C. Kroeze, and P. T. Krein, "Electrical battery model for use in dynamic electric vehicle simulations," *Power Electron. Spec. Conf. 2008. PESC 2008. IEEE*, pp. 1336–1342, 2008.

[24] P. Sharma and T. S. Bhatti, "A review on electrochemical double-layer capacitors," *Energy Convers. Manag.*, vol. 51, no. 12, pp. 2901–2912, 2010.

[25] R. Kötz and M. Carlen, "Principles and applications of electrochemical capacitors," *Electrochim. Acta*, vol. 45, no. 15–16, pp. 2483–2498, 2000.

[26] D. Rotenberg, A. Vahidi, and I. Kolmanovsky, "Ultracapacitor assisted powertrains: Modeling, control, sizing, and the impact on fuel economy," *IEEE Trans. Control Syst. Technol.*, vol. 19, no. 3, pp. 576–589, 2011.

[27] A. F. Burke, "Batteries and Ultracapacitors for Electric, Hybrid, and Fuel Cell Vehicles," *Proc. IEEE*, vol. 95, no. 4, pp. 806–820, 2007.

[28] H. Sun, X. Pei, L. Xu, H. Wang, Y. Sheng, and Y. Yu, "Application of Battery-Ultracapacitor Hybrid System in the Hybrid Electric Vehicles," *SAE-China FISITA (eds.), Proc. FISITA 2012 World*, vol. 189, 2013.

[29] Y. Tao and Z. Li, "Study on Modeling and Application of Ultracapacitor," *IEEE Work. Adv. Res. Technol. Ind. Appl. Study*, pp. 847–857, 2014.

[30] A. González, E. Goikolea, J. A. Barrena, and R. Mysyk, "Review on supercapacitors: Technologies and materials," *Renew. Sustain. Energy Rev.*, vol. 58, pp. 1189–1206, 2016.

[31] L. Shi and M. L. Crow, "Comparison of ultracapacitor electric circuit models," *IEEE Power Energy Soc. 2008 Gen. Meet. Convers. Deliv. Electr. Energy 21st Century, PES*, pp. 1–6, 2008.

[32] R. de Levie, "On porous electrodes in electrolyte solutions. I. Capacitance effects," *Electrochim. Acta*, vol. 8, no. 10, pp. 751–780, 1963.

[33] L. Zhang, Z. Wang, X. Hu, F. Sun, and D. G. Dorrell, "A comparative study of equivalent circuit models of ultracapacitors for electric vehicles," *J. Power Sources*, vol. 274, pp. 899–906, 2015.

[34] SAE, "SAE J2711 - Recommended Practice for Measuring Fuel Economy and Emissions of Hybrid-Electric and Conventional Heavy Duty Vehicles." 2002.

[35] R. B. de Souza, "Uma visão sobre o balanço de energia e desempenho em veículos híbridos," Universidade Estadual de Campinas - UNICAMP, 2010.

[36] Volvo, "Classificação dos tipos de ônibus no Brasil," 2016. [Online]. Available: http://www.mobilidadevolvo.com.br/classificacao-dos-onibus-no-brasil/.

[37] A. L. Carregari, "Estudo do Escoamento de Ar sobre a Carroceria de um Ônibus usando um Programa de CFD e Comparação com Dados Experimentais," Universidade de São Paulo,

2006.

[38] "Datasheet Mercedes Bus OF-1721," *www.mercedes-benz.com.br*, 2014. .

[39] Infineon Technologies, "Datasheet Infineon FF11MR12W1M1 _ B11." pp. 1–7, 2017.

[40] L. Solero, A. Lidozzi, and J. A. Pomilio, "Design of multiple-input power converter for hybrid vehicles," *IEEE Trans. Power Electron.*, vol. 20, no. 5, pp. 1007–1016, 2005.

[41] a. Di Napoli, F. Crescimbini, S. Rodo, and L. Solero, "Multiple input DC-DC power converter for fuel-cell powered hybrid\nvehicles," *2002 IEEE 33rd Annu. IEEE Power Electron. Spec. Conf. Proc. (Cat. No.02CH37289)*, vol. 4, pp. 1685–1690, 2002.

[42] H. Venable, "The K factor: A new mathematical tool for stability analysis and synthesis," *Proc. of Powercon 10*. pp. 1–10, 1983.

APPENDIX 1 – Matlab program for vehicle power demand calculation

```
% Vehicle power demand calculation
clc; close all;
% Initial data
ro=1.2258;%air density
g=9.81;
% Bus data - informations from R.B. de Souza, A.L. Carregari and internet
Cd=0.65;
Af=8.8;%m^2
M=16000;%Kg
raio=0.98*0.506;%effective radius 0.98*r (Souza)
P=M*g;
% transmission relation - acc. to bus OF 1721
r1=6.70;r2=3.81;r3=2.29;r4=1.48;r5=1.00;D=5.87;re=6.29; %D = reduction; 6th
gear ignored
% Rotation at gears
wr1=V/3.6/raio*r1*D*60/2/pi;
wr2=V/3.6/raio*r2*D*60/2/pi;
wr3=V/3.6/raio*r3*D*60/2/pi;
wr4=V/3.6/raio*r4*D*60/2/pi;
wr5=V/3.6/raio*r5*D*60/2/pi;
%Resistance forces
idle=0;
nv=length(V);
for t=1:nv-1;
incl=0;% %
alfa=atan(incl);%pavement slope
% V=;%speed km/h
Vv=0;%air speed
a=(V(t+1)-V(t))/3.6;
ac(t)=a;
% Gear changes
if wr1(t)<3500
wmotor(t)=wr1(t);rt=r1;
elseif wr1(t)>3500 && wr2(t)<3500
wmotor(t)=wr2(t);rt=r2;
elseif wr2(t)>3500 && wr3(t)<3500
wmotor(t)=wr3(t);rt=r3;
elseif wr3(t)>3500 && wr4(t)<3500
wmotor(t)=wr4(t);rt=r4;
else
wmotor(t)=wr5(t);rt=r5;
end
if wmotor(t)<600 %idle
wmotor(t)=600;
end
% Mass factor
Mf=1+0.04+0.0025*rt*D; %Souza, depends on transmission releation
Meq=M*Mf;
% Rolling resistance
fr=0.013*(1+V(t)/100);%rolling resistance coeficient, aproximation for asphalt
and speed below 120km/h
Fr=P*fr*cos(alfa);
if V(t)==0;
Fr=0;
```

```
end
% Aerodinamic drag
Fa=1/2*Cd*Af*ro*((V(t)+Vv)/3.6)^2;
% Slope resistance
Fg=M*Mf*g*sin(alfa);
% Traction force
Ft=Meq*a+Fr+Fa+Fg;
Ftr(t)=Fr;
Fta(t)=Fa;
Fti(t)=Ft;
Vi(t)=V(t)/3.6;%m/s
ti(t)=t;
Pload(t)=Fti(t).*Vi(t);%Watts
Preq=Pload/0.94; %transmission efficiency (Souza,2014)
Pdis(t)=Ftr(t).*Vi(t)+Fta(t).*Vi(t);%dissipative power
Pdissip=Pdis/0.94;
Pcons(t)=Pload(t)-Pdis(t);%conservative power
Pconserv=Pcons/0.94;
Power(t)=sqrt(Preq(t)*Preq(t));%power as positive values for UC dimensioning
current(t)=Preq(t)/645;%current needed when constant voltage is applyed
(Vo=645V). Vector needed for the PSIM simulation
Ec(t)=0.5*M*Vi(t)^2;%kinetic energy
%power as positive values for battery dimensioning
if Preq(t)>0
Ppos(t)=Preq(t);
else
Ppos(t)=0;
end
if V(t)==0
idle=idle+1;
end
end
figure(1),plot(ti,Vi*3.6),grid,title('Manhattan
Cycle'),ylabel('[km/h]'),xlabel('Time[s]')
figure(2),area(ti,Preq/1000),grid,title('Power
demand'),ylabel('[kW]'),xlabel('Time[s]')
figure(3),subplot(3,1,1),plot(ti,Vi.*(60/(2*pi*raio))),grid,title('Wheel
Rotation'),ylabel('RPM')
subplot(3,1,2),plot(ti,Fti*raio),grid,title('Torque'),ylabel('Torque[N.m]')
subplot(3,1,3),area(ti,Preq/1000);title('Power'), grid, ylabel('Power[kW]'),
xlabel('Time[s]')
figure(4),subplot(2,1,1),area(ti,Preq/1000);title('Power'), grid,
ylabel('Power[kW]'), xlabel('Time[s]')
subplot(2,1,2),
plot(ti,current);title('Current'),grid,ylabel('Current[A]'),xlabel('Time[s]')
figure(5),title('Dissipative and Conservative
Power'),subplot(2,1,1),plot(ti,Pdissip/1000),grid,title('Dissipative
Power'),ylabel('[kW]')
subplot(2,1,2),plot(ti,Pconserv/1000),grid,title('Conservative
Power'),ylabel('[kW]'),xlabel('Time[s]')
%fft conservative and dissipative power
L = length(Preq);%signal length
NFFT = 2^nextpow2(L); % Next power of 2 from length of y
y = fft(Preq,NFFT)/L;
fs = 1 %one sample per second
f = fs/2*linspace(0,1,NFFT/2+1);
```

```
figure(6),plot(f,2*abs(y(1:NFFT/2+1))),grid,title('FFT
Preq'),ylabel('[W]'),xlabel('f[Hz]')%conforme exemplo do Matlab
fft_Pdiss=fft(Pdissip,NFFT)/L;
fft_Pconserv=fft(Pconserv,NFFT)/L;
figure(7),subplot(2,1,1),plot(f,2*abs(fft_Pdiss(1:NFFT/2+1))),grid,title('FFT
Pdissipative'),ylabel('[W]'),xlabel('f[Hz]'),
subplot(2,1,2),plot(f,2*abs(fft_Pconserv(1:NFFT/2+1))),grid,title('FFT
Pconservative'),ylabel('[W]'),xlabel('f[Hz]')
figure(8),subplot(2,1,1),plot(f(1:100),2*abs(fft_Pdiss(1:100))),grid,title('FF
T Pdissipative'),ylabel('[W]'),xlabel('f[Hz]'),
subplot(2,1,2),plot(f(1:100),2*abs(fft_Pconserv(1:100))),grid,title('FFT
Pconservative'),ylabel('[W]'),xlabel('f[Hz]')
figure(9),plot(ti,Power/1000),grid,title('Power'),ylabel('[kW]'),xlabel('time[
s]')
figure(10),plot(ti,Ppos/1000),grid,title('Positive
Power'),ylabel('[kW]'),xlabel('time[s]')
```

APPENDIX 2 – Matlab program for state space equations and transfer functions calculations

```
%state space equations - il(s)/d(s) and Vo(s)/il(s)
Vp = 336;
Io = 351.49; %considered Imax
D = 0.5; % considered as standard steady state duty cycle
Rp = 0.013;
Ri = 0.074;
Ci = 0.001;
Rl = 0.0098;
L = 25e-6;
Ro = 0.005;
Co = 0.002;
A1 = [0 0 0; 0 -1/(Ci*(Rp+Ri)) -Rp/(Ci*(Rp+Ri)); 0 Rp/(L*(Rp+Ri)) -
(Rp*Rl+Rp*Ri+Rl*Ri)/(L*(Rp+Ri))];
A2 = [0 0 1/Co; 0 -1/(Ci*(Rp+Ri)) -Rp/(Ci*(Rp+Ri)); -1/L Rp/(L*(Rp+Ri)) -
(Rp*Rl+Rp*Ri+Rl*Ri+Ro*(Rp+Ri))/(L*(Rp+Ri))];
B1 = [-1/Co 0; 0 1/(Ci*(Rp+Ri)); 0 Ri/(L*(Rp+Ri))];
B2 = [-1/Co 0; 0 1/(Ci*(Rp+Ri)); Ro/L Ri/(L*(Rp+Ri))];
C1 = [0 0 1];
C2 = C1;
E1 = [0 0];
E2 = E1;
G1 = [0 0 0];
G2 = G1;
A = A1*D+A2*(1-D);
B = B1*D+B2*(1-D);
C = C1*D+C2*(1-D);
E = E1*D+E2*(1-D);
G = G1*D+G2*(1-D);
Ui = [Io; Vp];
X = -inv(A)*B*Ui;
Vout = C*X+E1*Ui
I = eye(3);
s = tf('s');
Aux_1 = inv(s*I-A);
Aux_2 = (A1-A2)*X+(B1-B2)*Ui;
Aux_3 = (C1-C2)*X;
H = Aux_1*Aux_2;
vo_s = [1 0 0] * H
vi_s = [0 1 0] * H
il_s = [0 0 1] * H
FT_il = C*Aux_1*Aux_2
vo_il_s = vo_s/il_s;
figure(1),bode(FT_il)
figure(2),bode(vo_il_s)

%Type 2 controller Hc_il(s)
fc = 2500; %Hz
mag = 64.4; %dB
phase = -87.4; %°
phase_rad = phase/(180/pi);
ganho = 10^(-mag/20);
margem = 60;
alpha = margem - phase - 90;
alpha_rad = alpha/(180/pi);
```

```
k = tan(alpha_rad/2 + pi/4);
R1 = 10e6;
C2 = 1/(2*pi*fc*ganho*k*R1);
C1 = C2*(k^2-1);
R2 = k/(2*pi*fc*C1);
AV = ganho; %R2/R1;
fz = 1/(2*pi*R2*C1);
wz = 2*pi*fz;
fp = (C1+C2)/(2*pi*R2*C1*C2);
wp = 2*pi*fp;
s = tf('s');
Hc_il = (1+s*C1*R2)/(s*R1*(C1+C2+s*R2*C1*C2))

%Type 2 controller Gc_Vo_il(s)
fc = 250; %Hz
mag = -16.5; %dB
phase = -85; %°
phase_rad = phase/(180/pi);
ganho = 10^(-mag/20);
margem = 60;
alpha = margem - phase - 90;
alpha_rad = alpha/(180/pi);
k = tan(alpha_rad/2 + pi/4);
R1 = 10e6;
C2 = 1/(2*pi*fc*ganho*k*R1);
C1 = C2*(k^2-1);
R2 = k/(2*pi*fc*C1);
AV = ganho; %R2/R1;
fz = 1/(2*pi*R2*C1);
wz = 2*pi*fz;
fp = (C1+C2)/(2*pi*R2*C1*C2);
wp = 2*pi*fp;
s = tf('s');
Gc_vo_il = (1+s*C1*R2)/(s*R1*(C1+C2+s*R2*C1*C2))

%FT Vuc/Ii-bt(s)
Vco = 645;
Co = 2e-3;
Ro = 5e-3;
Cuc = 15;
Ruc = 0.013;
Vuc = 336;
Vbt = Vuc;
Gi_uc = il_s;
Gi_bt = il_s;
Gc_i_uc = Hc_il;
Gc_i_bt = Hc_il;
Gc_vo = Gc_vo_il;
Hi_uc = (Gc_i_uc*Gi_uc)/(1+(Gc_i_uc*Gi_uc));
Hi_bt = (Gc_i_bt*Gi_bt)/(1+(Gc_i_bt*Gi_bt));
s = tf('s');
FT_vuc_ibt =
(Vbt/Vco*Co*Cuc)*(Hi_bt*Gc_vo*Hi_uc*(1+s*Co*Ro)*(1+s*Cuc*Ruc))/(s*(s+((1+s*Co*
Ro)*Gc_vo*Hi_uc*Vuc)/(Co*Vco)))
bode(FT_vuc_ibt)
```